May 2021

Two Counting Problems in Geometric Triangulations and Pseudoline Arrangements

Ritankar Mandal
University of Wisconsin-Milwaukee

TWO COUNTING PROBLEMS IN GEOMETRIC TRIANGULATIONS AND PSEUDOLINE ARRANGEMENTS

by
Ritankar Mandal

A Dissertation Submitted in
Partial Fulfillment of the
Requirements for the Degree of

Doctor of Philosophy
in Engineering

at
The University of Wisconsin-Milwaukee
May 2021

ABSTRACT

TWO COUNTING PROBLEMS IN GEOMETRIC TRIANGULATIONS AND PSEUDOLINE ARRANGEMENTS

by

Ritankar Mandal

The University of Wisconsin-Milwaukee, 2021
Under the Supervision of Professor Adrian Dumitrescu

The purpose of this dissertation is to study two problems in combinatorial geometry in regard to obtaining better bounds on the number of geometric objects of interest: (i) monotone paths in geometric triangulations and (ii) pseudoline arrangements.

(i) A directed path in a graph is monotone in direction of $\mathbf{u}$ if every edge in the path has a positive inner product with $\mathbf{u}$. A path is monotone if it is monotone in some direction. Monotone paths are studied in optimization problems, specially in classical simplex algorithm in linear programming. We prove that the (maximum) number of monotone paths in a geometric triangulation of n points in the plane is $O(1.7864^n)$. This improves an earlier upper bound of $O(1.8393^n)$; the current best lower bound is $\Omega(1.7003^n)$ (Dumitrescu et al., 2016).

(ii) Arrangements of lines and pseudolines are fundamental objects in discrete and computational geometry. They also appear in other areas of computer science, for instance in the study of sorting networks. Let B_n be the number of nonisomorphic arrangements of n pseudolines and let $b_n = \log_2 B_n$. The problem of estimating B_n was posed by Knuth in 1992. Knuth conjectured that $b_n \leq \binom{n}{2} + o(n^2)$ and also derived the first upper and lower bounds: $b_n \leq 0.7924(n^2+n)$ and $b_n \geq n^2/6 - O(n)$. The upper bound underwent several improvements, $b_n \leq 0.6974\, n^2$ (Felsner, 1997), and $b_n \leq 0.6571\, n^2$ (Felsner and Valtr, 2011), for large n. Here we show that $b_n \geq cn^2 - O(n \log n)$ for some constant $c > 0.2083$. In particular, $b_n \geq 0.2083\, n^2$ for large n. This improves the previous best lower bound, $b_n \geq 0.1887\, n^2$, due to Felsner and Valtr (2011). Our arguments are elementary and geometric in nature. Further, our constructions are likely to spur new developments and improved lower bounds for related problems, such as in topological graph drawings.

Developing efficient algorithms and computer search were key to verifying the validity of both results.

TABLE OF CONTENTS

LIST OF FIGURES

LIST OF TABLES

ACKNOWLEDGEMENTS

I would like to express my deep respect and gratitude to my doctoral advisor Prof. Adrian Dumitrescu. I have always appreciated his knowledge on my research topics. I am thankful to have the possibility of pursuing a doctoral degree in a topic I was passionate about. My exposure to the various topics in Geometry and Computer Science has shaped me as a researcher and a professional.

I am thankful to my parents for always inspiring me in every moment of my life, especially during my doctoral journey. I would like to convey my sincere regards to my colleagues and friends for supporting me during these years.

I am grateful to all my doctoral committee members – Prof. Christine Cheng, Prof. Guangwu Xu, Prof. Craig Guilbault and Prof. Jun Zhang for rendering their valuable inputs and suggestions in my research work.

Finally, my appreciation goes to the Department of Computer Science at the University of Wisconsin-Milwaukee for supporting my research.

1. Introduction

The purpose of this dissertation is to study two problems in combinatorial geometry in regard to obtaining better bounds on the number of geometric objects of interest: (i) monotone paths in geometric triangulations and (ii) pseudoline arrangements.

1.1. Monotone paths in geometric triangulations

In Chapter 2 we obtain a new lower bound on the maximum number of monotone paths in plane geometric graphs (also referred to as *plane straight-line graphs*) with n vertices. A directed path in a graph is *monotone in direction of* $\mathbf{u}$ ($\mathbf{u}$-monotone) if every edge in the path has a positive inner product with $\mathbf{u}$. A path is *monotone* if it is monotone in some direction. Examples of monotone and non-monotone paths are depicted in Fig. 1.1. Study of monotone paths is used in optimization specially in classical simplex algorithm in linear programming.

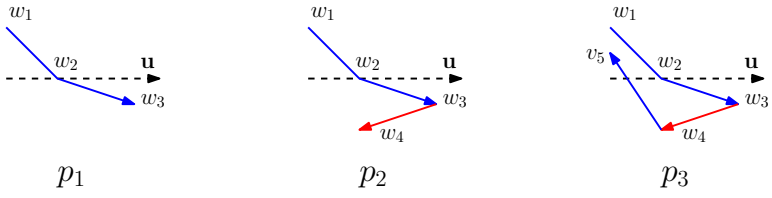

Figure 1.1.: Left: p_1 is $\mathbf{u}$-monotone path. Center: p_2 is not $\mathbf{u}$-monotone path since $w_3\,w_4$ has a negative inner product with $\mathbf{u}$. Right: p_3 is non-monotone path.

A graph is a *plane geometric graph* where the vertices are points in the plane and the edges are line segments between these points where no two edges intersect except at the vertices. In extremal graph theory, we study the minimum or maximum number of certain subgraphs, e.g., perfect matchings, spanning trees, spanning cycles contained in

a graph. The monotonicity of a path is defined geometrically, i.e., membership in the class depends on the coordinates of the vertices. Since adding edges only increase the number of monotone paths, we consider only fully triangulated graphs [18, Lemma 3.1]. A triangulation of ten points is shown in Fig. 1.2. Two paths $w_1\, w_2\, w_3\, w_4\, w_5\, w_6\, w_7\, w_8\, w_9\, w_{10}$ and $w_1\, w_3\, w_5\, w_4\, w_2$ are monotone with respect to the positive direction of the x-axis and y-axis, respectively.

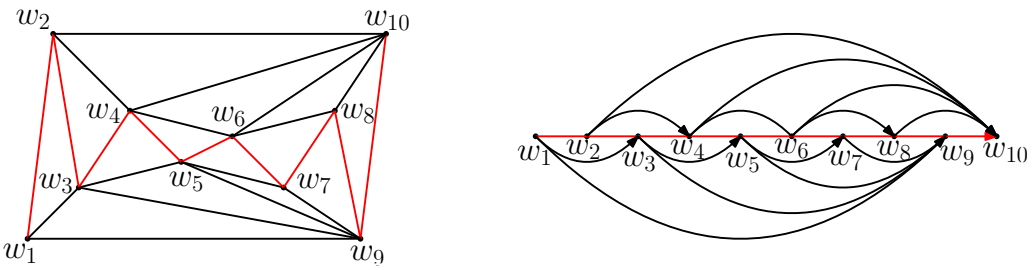

Figure 1.2.: Left: $G = (W, E)$ is a geometric graph with ten vertices. Two paths (i) $w_1\, w_2\, w_3\, w_4\, w_5\, w_6\, w_7\, w_8\, w_9\, w_{10}$ (in red) and (ii) $w_1\, w_3\, w_5\, w_4\, w_2$ are monotone with respect to the positive direction of the x-axis and the y-axis, respectively. Right: An isomorphic plane monotone directed graph where corresponding vertices are in the same order by x-coordinate.

Let $G = (W, E)$ be a plane geometric graph which is a triangulation of n points. Since a triangulation has at most $3n - 6$ edges for $n \geq 3$, it is enough to consider monotone paths in at most $2(3n - 6) = 6n - 12$ directions i.e., one direction between any two consecutive unit normal vectors of the edges. Therefore in this section and in Chapter 2 we study the upper bound on the number of monotone paths in a fixed direction, which we may assume to be the positive direction of the x-axis.

Our results. We first show that the number of monotone paths (over all directions) in a triangulation of n points in the plane is $O(1.8193^n)$, using groups of 8 vertices. We then give a sharper bound of $O(1.7864^n)$ analyzing groups of 11 vertices using a computer program[1].

Theorem. *The number of monotone paths in a geometric triangulation on n vertices in the plane is $O(1.7864^n)$.*

[1]Refer to the Appendix or the `.c` file at `arXiv:1608.04812`.

Previous works. Dumitrescu et al. [5] gave an upper and lower bound of $O(1.8393^n)$ and $\Omega(1.7003^n)$, respectively. We provide a brief review of their proof. Assume that all the vertices have distinct x-coordinates and the vertices lie on the x-axis. Label the vertices as $w_1, w_2, \ldots, w_n$ sorted by their x-coordinates and orient each edge $w_iw_j \in E$ from w_i to w_j, if $i < j$. G contains a Hamiltonian path $\xi_0 = (w_1, w_2, \ldots, w_n)$ since w_iw_{i+1} is in E for all $1 \leq i \leq n-1$ by [5, Lemma 3]. Fig. 1.2 shows this process of transforming a plane geometric graph to such an isomorphic plane monotone directed graph. Let $T(i)$ denote the number of maximal (with respect to inclusion) x-monotone paths starting at w_{n-i+1}.

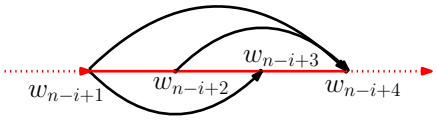

Figure 1.3.: Every vertex has at most three outgoing edges to the next three vertices.

Observe Fig. 1.3. Every vertex w_{n-i+1} has at most three outgoing edges to vertices at distance at least 1, 2, and 3 from w_{n-i+1}, obtaining the recurrence

$$T(i) \leq T(i-1) + T(i-2) + T(i-3) \quad \forall i \geq 4$$

with initial values $T(1) = T(2) = 1$ and $T(3) = 2$. The recurrence solves to $T(n) = O(\alpha^n)$ where $\alpha = 1.8392\ldots$ is the unique real root of $x^3 - x^2 - x - 1 = 0$. So the maximum number of x-monotone paths in plane monotone graph is $O(n^3\, T(n)) = O(1.8393^n)$. Continuing in this direction we improve this bound to $O(1.7864^n)$. Table 1.1 summarizes the latest results [5].

Configurations	Lower bound	Upper bound
Convex polygons	$\Omega(1.5028^n)$	$O(1.5029^n)$
Star-shaped polygons	$\Omega(1.70^n)$	$O(n^3\alpha^n) = O(1.8393^n)$
Directed simple paths	$\Omega(\alpha^n) = \Omega(1.8392^n)$	$O(n^2 3^n)$
Monotone paths	$\Omega(1.70^n)$	$O(1.7864^n)$

Table 1.1.: Upper and lower bounds for the maximum number of configurations in an n-vertex plane graph. Here $\alpha = 1.8392\ldots$ is the real root of $x^3 - x^2 - x - 1 = 0$.

A divide and conquer technique (fingerprinting technique). Here we have used a divide and conquer technique to count the maximum number of x-monotone paths. An x-monotone path can be represented uniquely by the subset of vertices in the path. A trivial upper bound of 2^n can be deduced just from this representation. For $V \subseteq W$, a set of k consecutive vertices of ξ_0, an *incidence pattern* of V is a subset of V that is in a monotone path ξ. $I(V)$ denotes the set of all incidence patterns of V. Therefore $|I(V)| \leq 2^k$.

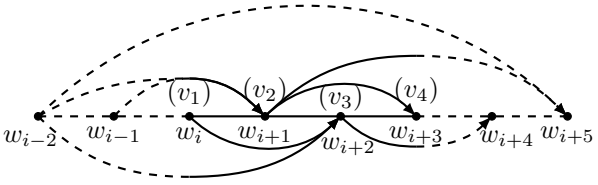

Figure 1.4.: $V = \{v_1, v_2, v_3, v_4\}$, where $v_1 = w_i$ for some i.

Observe Fig. 1.4. Let $V = \{v_1v_2v_3v_4\}$ be a group of four consecutive vertices of ξ_0, where $v_1 = w_i$ for some i. All vertices preceding and succeeding V are mapped to new vertices v_0 and v_5 respectively, see Fig. 1.5 (left). The vertices v_2v_4 are in the path $w_{i-2}\, v_2\, v_4\, w_{i+5}$ (i.e., $w_{i-2}\, w_{i+1}\ w_{i+3}\, w_{i+5}$). So $v_2v_4 \in I(V)$. Carefully observing all the monotone paths passing through V, we get $I(V) = \{\emptyset, v_1v_2, v_1v_2v_3, v_1v_2v_3v_4, v_1v_2v_4, v_1v_3, v_1v_3v_4, v_2, v_2v_3, v_2v_3v_4, v_2v_4, v_3, v_3v_4\}$. Here $|I(V)| = 13 < 16$ as the incidence patterns v_1, v_4 and v_1v_4 are not in $I(V)$.

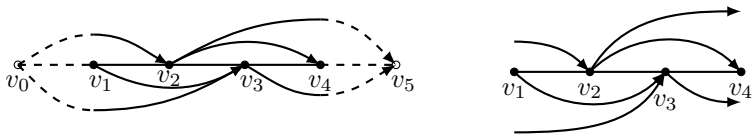

Figure 1.5.: Left: All vertices preceding and succeeding V are mapped to new vertices v_0 and v_{k+1} (here $k = 4$) respectively. Right: The fingerprint of the group V.

We now describe the fingerprinting technique that forms the base of our proof. Following are the few important terms that are used in our proof.

- $p_k = \max_{|V|=k} |I(V)|$ denotes the *maximum number of incidence patterns* for V, a

set of k consecutive vertices of ξ_0, in a plane monotone triangulation.

- μ_n denotes the *maximum number of maximal x-monotone paths* in a plane geometric graph with n vertices. If n is a multiple of k, the product rule yields $\mu_n \leq p_k^{n/k}$. For an arbitrary n and constant k, we obtain

$$\mu_n \leq p_k^{\lfloor n/k \rfloor} 2^{n-k\lfloor n/k \rfloor} \leq p_k^{\lfloor n/k \rfloor} 2^k = O\left(p_k^{n/k}\right).$$

- λ_n denotes the maximum number of monotone paths in an n-vertex triangulation. Recall that it is enough to consider paths in at most $6n-12$ directions. Also every x-monotone path in G contains at most n vertices, hence it contains at most $\binom{n}{2}$ x-monotone subpaths. Therefore, we have

$$\lambda_n \leq (6n-12)\binom{n}{2} \cdot \mu_n = O(n^3 \mu_n) = O\left(n^3\, p_k^{n/k}\right).$$

Observe Fig. 1.6. Let $V = \{1, 2\}$ be a group of two consecutive vertices of ξ_0. $I(V)$ always contains the two incidence patterns $\emptyset$ and 12. Since adding more edges to a group increases the number of monotone paths we can ignore the group with $I(V) = \{\emptyset, 12\}$ from our analysis. If two groups are reflections of each other around the x-axis then we only consider one of them to keep our analysis simple. Note that two groups can be reflections of each other around the y-axis e.g., $V2$ and $V3$, and we'll keep them both in our analysis. Therefore the following are the only three groups of two vertices that we consider in our analysis. These groups are sorted in decreasing order according to the number of the incidence patterns. The incidence patterns are

$$I(V1) = \{\emptyset, 12, 1, 2\},$$
$$I(V2) = \{\emptyset, 12, 2\},$$
$$I(V3) = \{\emptyset, 12, 1\}.$$

Therefore $p_2 = |I(V1)| = 4$ which yields the upper bounds $\mu_n = O(4^{n/2})$ and consequently

$\lambda_n = O(n^3 4^{n/2}) = O(2^n)$ which is trivial.

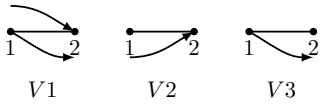

Figure 1.6.: Three groups of two vertices.

For groups of three vertices the following are the only 52 groups that we consider in our analysis, see Fig. 1.7. The first three groups $G1, G2$ and $G3$ are the only groups with seven incidence patterns which is the maximum number of patterns among groups of three vertices. The incidence patterns of $G1, G2$ and $G3$ are $I(G1) = \{\emptyset, 123, 12, 1, 23, 2, 3\}$. $I(G2) = \{\emptyset, 123, 12, 13, 23, 2, 3\}$. $I(G3) = \{\emptyset, 123, 12, 13, 1, 23, 2\}$.

Therefore $p_3 = 7$ which yields the upper bounds $\mu_n = O(7^{n/3})$ and consequently $\lambda_n = O(n^3 7^{n/3}) = O(1.913^n)$. Observe $G2$ and $G3$ among many others are reflections of each other around the y-axis.

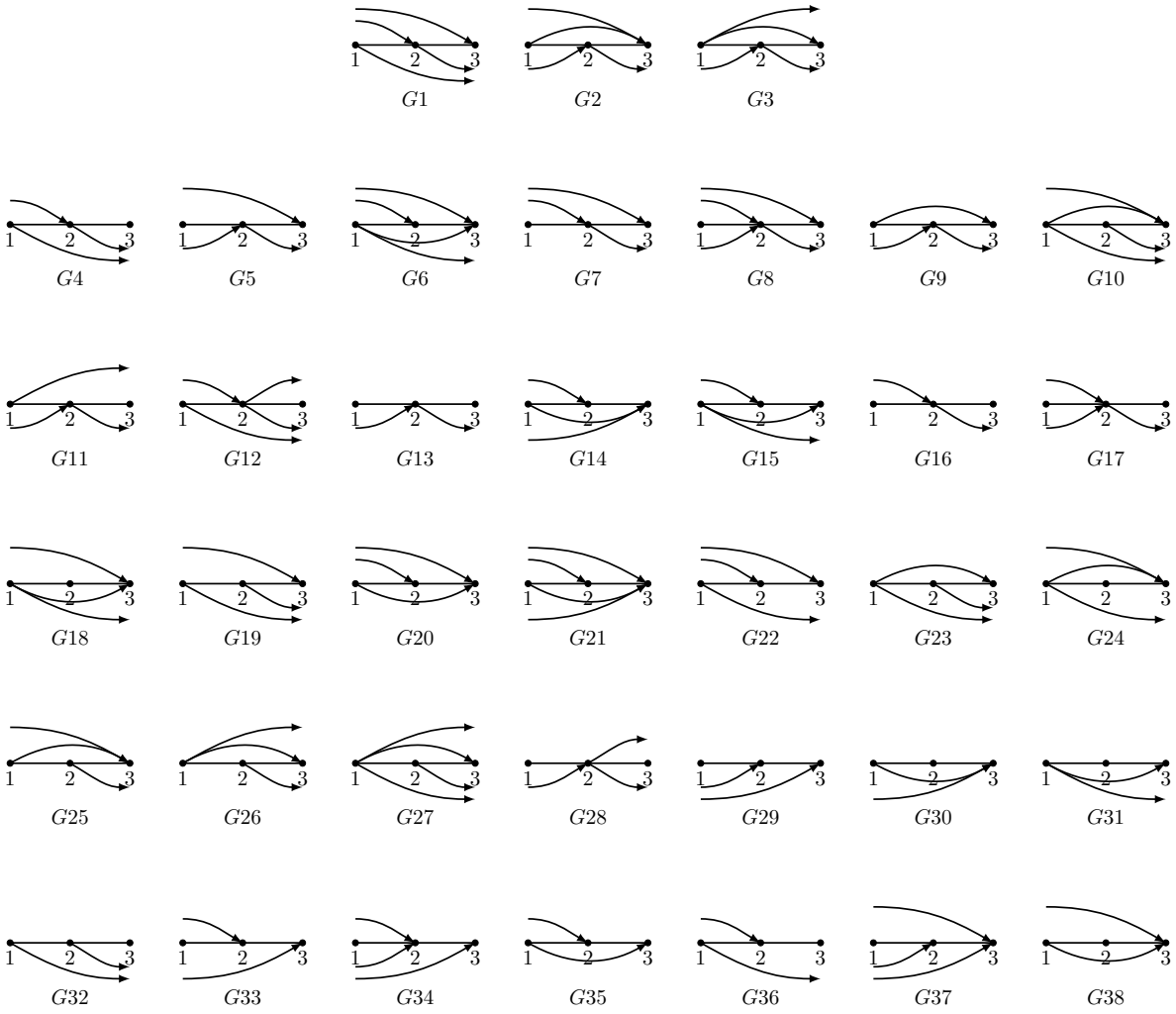

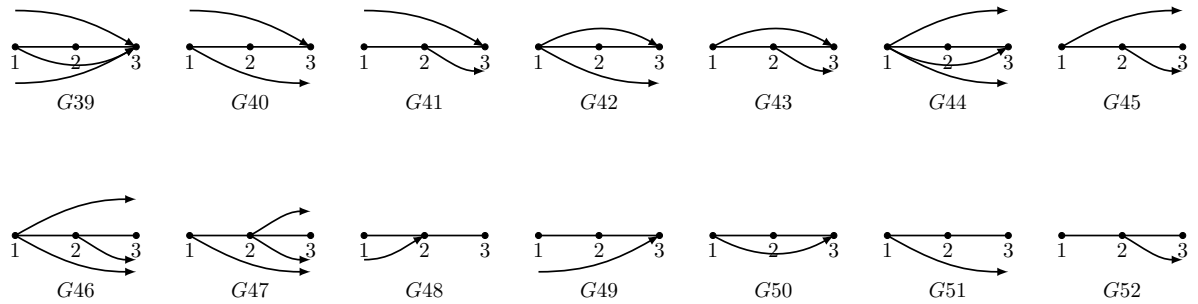

Figure 1.7.: 52 groups of three vertices.

In Section 2.3, by analysis we show that the groups A and A^R (see Fig. 1.8) are the only groups with 13 incidence patterns which is the maximum number of patterns among groups of four vertices. The incidence patterns are:

$$I(A) = I(A^R) = \{\emptyset, 12, 123, 1234, 124, 13, 134, 2, 23, 234, 24, 3, 34\}.$$

Threfore $p_4 = 13$ which yields the upper bounds $\mu_n = O(13^{n/4})$ and consequently $\lambda_n = O(n^3 13^{n/4}) = O(1.8989^n)$.

Figure 1.8.: A and A^R are the only groups of four vertices with 13 incidence patterns and they are reflections of each other around the y-axis.

In Section 2.4, further analysis shows that $p_8 = 120$, hence $\mu_n = O(120^{n/8})$ and $\lambda_n = O(n^3 120^{n/8}) = O(1.8193^n)$. In Section 2.5, Computer search shows that $p_{11} = 591$, and so $\mu_n = O(591^{n/11})$; thus providing our final result $\lambda_n = O(n^3 591^{n/11}) = O(1.7864^n)$.

Relevant paper. A. Dumitrescu, R. Mandal, and Cs. D. Tóth, Monotone Paths in Geometric Triangulations, in *Theory Comput. Syst.* 62(6): 1490–1524 (2018).

1.2. Pseudoline arrangements

In Chapter 3 we study the lower bounds on the number of pseudoline arrangements. Arrangements of pseudolines is an important topic in combinatorial geometry. Such arrangements are a generalized way of studying straight line arrangements. Grünbaum's monograph *Arrangements and Spreads* [42] is one of the first to present a collection of problems, solutions and conjectures on arrangements of pseudolines and lines. Later the relation between arrangements and oriented matroids was found which led to development of various combinatorial results. Generally pseudoline arrangements are studied in projective plane, we studied them in the Euclidean plane.

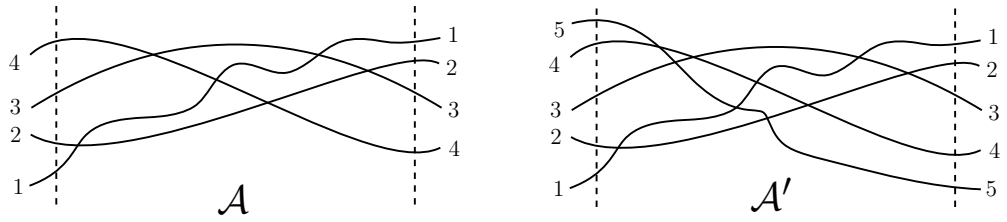

Figure 1.9.: Two arrangements $\mathcal{A}$ and $\mathcal{A}'$ with 4 and 5 pseudolines respectively.

A *pseudoline* is an x-monotone curve in the Euclidean plane. An *(Euclidean) arrangement of pseudolines* is a collection of pseudolines where each pair intersects each other exactly once, see Fig. 1.9. Such intersections are called *vertices*. The *size* of an arrangement is the number of pseudolines in it. Given an arrangement $\mathcal{A}$ of size n we label the pseudolines so that they cross a vertical line left of all vertices in increasing order from bottom to top. Note that these pseudolines cross a vertical line right of all vertices in decreasing order from bottom to top. An arrangement is *simple* if no three pseudolines have a common point of intersection. In this section the term arrangement always means simple arrangement if not specified otherwise.

There are several combinatorial representations (and encodings) of pseudoline arrangements. These representations help one count the number of arrangements. Three classic representations are *allowable sequences* (introduced by Goodman and Pollack [40, 41]), *wiring diagrams* [38], and *zonotopal tilings* [37].

A *simple allowable sequence* is a sequence Σ of $\binom{n}{2}+1$ permutations of $\{1, 2, \ldots, n\}$ satisfying two properties: (i) The first element of Σ is the identity permutation $(1, 2, \ldots, n)$

and the last element of Σ is the reverse permutation $(n, \ldots, 2, 1)$; and (ii) Two consecutive permutations in Σ differ by the reversal of an adjacent pair ij, where $i < j$ [36]. A *wiring diagram* is a Euclidean arrangement of pseudolines consisting of piece-wise linear 'wires', each horizontal except for a short segment where it crosses another wire. Each pair of wires cross exactly once; see Fig. 3.1 (center). Wiring diagrams are also known as *reflection networks*, i.e., networks that bring n wires labeled from 1 to n into their reflection by means of performing switches of adjacent wires; see [45, p. 35]. Lastly, they are also known under the name of *primitive sorting networks*; see [46, Ch. 5.3.4].

Number of allowable sequences. A_n denotes the number of simple allowable sequences on $1, 2, \ldots, n$. The following closed formula for A_n was established by Stanley [53]:

$$A_n = \frac{\binom{n}{2}!}{\prod_{k=1}^{n-1}(2n-2k-1)^k}.$$

From this formula we can derive that the asymptotic growth of A_n is $2^{\Theta(n^2 \log n)}$; see sequence `A005118` in [52] for more.

Arrangements with 3 and 4 pseudolines. The following are the two arrangements with 3 pseudolines, i.e., $A_3 = 2$.

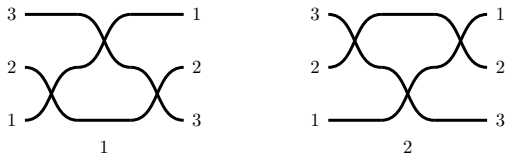

Figure 1.10.: 1 & 2 are the only two arrangements with 3 pseudolines.

The following are the sixteen arrangements with 4 pseudolines, i.e., $A_4 = 16$.

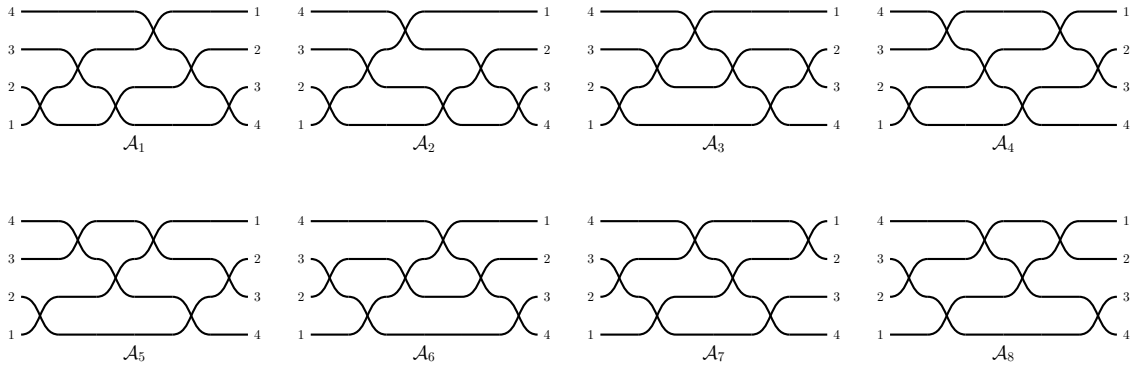

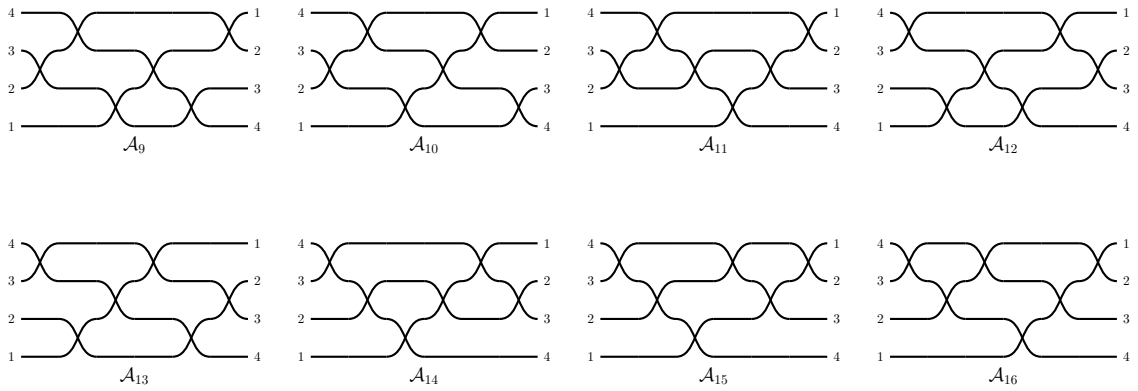

Figure 1.11.: $\mathcal{A}_1 - \mathcal{A}_{16}$ are the only sixteen arrangements with 4 pseudolines.

Isomorphism of arrangements. Two arrangements are *isomorphic*, i.e., considered the same, if they can be mapped onto each other by a homeomorphism of the plane [39]. Equivalently, two arrangements are isomorphic if there is an isomorphism between the induced cell decomposition [37, Ch. 6]. Observe Fig. 1.12 for an illustration of this concept and the correspondence with allowable sequences. $\mathcal{A}_1$ and $\mathcal{A}_2$ are isomorphic where $\mathcal{A}_3$ is nonisomorphic to $\mathcal{A}_2$ and $\mathcal{A}_1$. Note that the relative position of two vertices from distinct pairs of pseudolines is irrelevant. $\mathcal{A}_1$ and $\mathcal{A}_2$ are isomorphic since the positions of the vertices 23 (in red) and 14 (in cyan) can be switched. $\mathcal{A}_3$ is nonisomorphic to $\mathcal{A}_2$ (and $\mathcal{A}_1$) since the positions of the vertices 23 (in red) and 34 (in green) can not be switched because they have a common pseudoline.

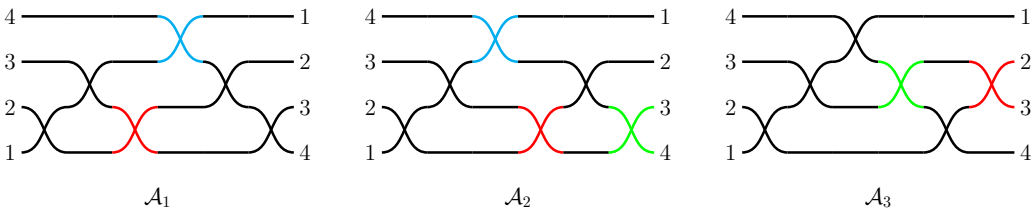

Figure 1.12.: $\mathcal{A}_1$, $\mathcal{A}_2$ and $\mathcal{A}_3$ are three arrangements with four pseudolines. $\mathcal{A}_1$ and $\mathcal{A}_2$ are isomorphic where $\mathcal{A}_3$ is nonisomorphic to $\mathcal{A}_2$ and $\mathcal{A}_1$.

Since $\mathcal{A}_1$ and $\mathcal{A}_2$ are the same (isomorphic) arrangement, they (and their allowable sequences) can be represented by a *canonical arrangement* $\mathcal{B}_1$, see Fig. 1.13. The allowable sequence for $\mathcal{B}_1$ is

$$1234 \xrightarrow{12} 2134 \xrightarrow{13} 2314 \xrightarrow{23,14} 3241 \xrightarrow{24} 3421 \xrightarrow{34} 4321.$$

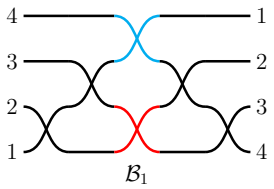

Figure 1.13.: $\mathcal{B}_1$ is the canonical arrangement representing $\mathcal{A}_1$ and $\mathcal{A}_2$.

Clearly the isomorphism is an equivalence relation which provides a partition of disjoint equivalence classes. The eight equivalence classes from the sixteen arrangements (from Fig. 1.11) are presented in the Table 1.2. Observe that not all the classes contain same number of elements. A canonical arrangement can be drawn to represent an equivalence class of isomorphic arrangements. Eight canonical arrangements with four pseudolines are shown in Fig. 1.14).

$\mathcal{B}_1$	$\mathcal{B}_2$	$\mathcal{B}_3$	$\mathcal{B}_4$	$\mathcal{B}_5$	$\mathcal{B}_6$	$\mathcal{B}_7$	$\mathcal{B}_8$
$\mathcal{A}_1, \mathcal{A}_2$	$\mathcal{A}_3$	$\mathcal{A}_4, \mathcal{A}_5, \mathcal{A}_{12}, \mathcal{A}_{13}$	$\mathcal{A}_6$	$\mathcal{A}_7, \mathcal{A}_8, \mathcal{A}_9, \mathcal{A}_{10}$	$\mathcal{A}_{11}$	$\mathcal{A}_{14}$	$\mathcal{A}_{15}, \mathcal{A}_{16}$

Table 1.2.: Eight equivalence classes from the sixteen arrangements with 4 pseudolines.

The number of *nonisomorphic* arrangements of n pseudolines is denoted by B_n (sequence `A006245` in [52]); this is the number of equivalence classes of all arrangements of n pseudolines; see [45, p. 35]. So $B_n \leq A_n$, we will show that B_n is asymptotically smaller than A_n. Unlike A_n, an exact enumeration of B_n is not found yet, but asymptotic bounds have been established. Here we study the growth rate of B_n; so let $b_n = \log_2 B_n$.

Nonisomorphic arrangements with 3 and 4 pseudolines. There are two nonisomorphic arrangements with 3 pseudolines, i.e., $B_3 = 2$. They are the same as shown in Fig. 1.10. There are eight nonisomorphic arrangements with 4 pseudolines, i.e., $B_4 = 8$ (see Fig. 1.14).

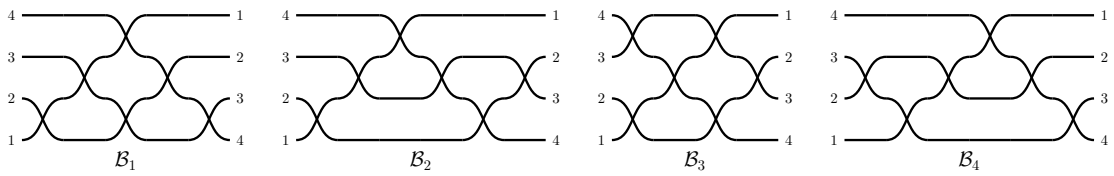

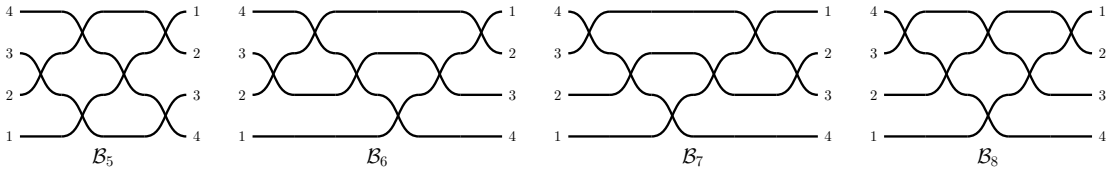

Figure 1.14.: $\mathcal{B}_1 - \mathcal{B}_8$ are the only eight nonisomorphic arrangements with 4 pseudolines.

Previous works. Knuth [45, p. 37] used a recursive construction of reflection networks. The number of nonisomorphic arrangements of n pseudolines in his construction, $T(n)$, yields $T(n) \geq 2^{n^2/6-5n/2}$, therefore $B_n \geq 2^{n^2/6-5n/2}$.

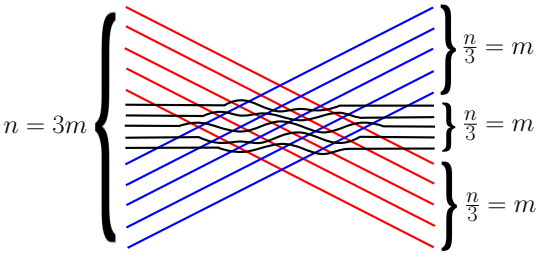

Figure 1.15.: Grid construction for a lower bound on B_n.

Observe Fig. 1.15. Matoušek provided a new recursive construction [49, Sec. 6.2]. Let n be a multiple of 3 and $m = \frac{n}{3}$ (assume that m is odd). The $2m$ lines in the two extreme bundles form a regular grid of m^2 points and the lines in the central bundle are incident to $\frac{3m^2+1}{4}$ of these grid points. At each such point, there are 2 choices; going below it or above it, thus creating at least $\frac{3m^2}{4} = \frac{3(n/3)^2}{4} = \frac{n^2}{12}$ binary choices. So $T(n)$ obeys the recurrence

$$T(n) \geq 2^{n^2/12} \cdot (T(n/3))^3,$$

which by induction yields $T(n) \geq 2^{n^2/8}$, implying $B_n \geq 2^{n^2/8}$.

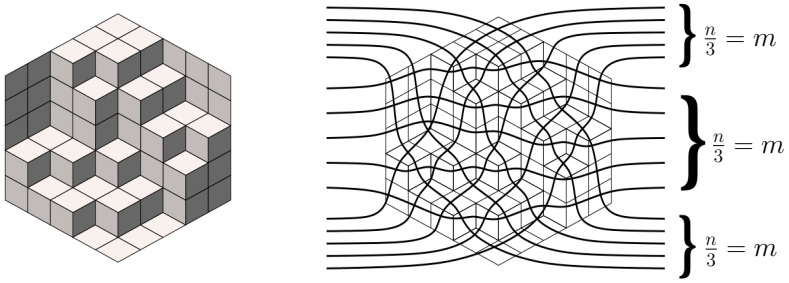

Figure 1.16.: The hexagon $H(5, 5, 5)$ with one of its rhombic tilings and a consistent partial arrangement corresponding to the tiling. This figure is reproduced from [39].

Felsner and Valtr [39] used rhombic tilings of a centrally symmetric hexagon in a recursive construction for a lower bound on B_n. This construction yields the lower bound $b_n \geq 0.1887\, n^2$ for large n; this is the previous best lower bound, see Fig. 1.16.

Our results. We extend the method of recursive grid construction used by Matoušek to establish sharper lower bounds. We present a family of constructions, gradually increasing the number of slopes, providing sharper bounds. With the increase in the number of slopes, the complexity of the corresponding proofs increases too. Our main result [33] is summarized in the following.

Theorem. *Let B_n be the number of nonisomorphic arrangements of n pseudolines. Then $B_n \geq 2^{cn^2 - O(n \log n)}$, for some constant $c > 0.2083$. In particular, $B_n \geq 2^{0.2083\, n^2}$ for large n.*

Relevant paper. A. Dumitrescu, R. Mandal, New lower bounds for the number of pseudoline arrangements, in *Journal of Computational Geometry* 11(1): 60–92 (2020).

2. Monotone Paths in Geometric Triangulations

2.1. Introduction

A directed polygonal path ξ in $\mathbb{R}^d$ is *monotone* if there exists a nonzero vector $\mathbf{u} \in \mathbb{R}^d$ that has a positive inner product with every directed edge of ξ. The study of combinatorial properties of monotone paths is motivated by the classical simplex algorithm in linear programming, which finds an optimal solution by tracing a monotone path in the 1−skeleton of a d-dimensional polytope of feasible solutions. It remains an elusive open problem whether there is a pivoting rule for the simplex method that produces a monotone path whose length is polynomial in d and n [1].

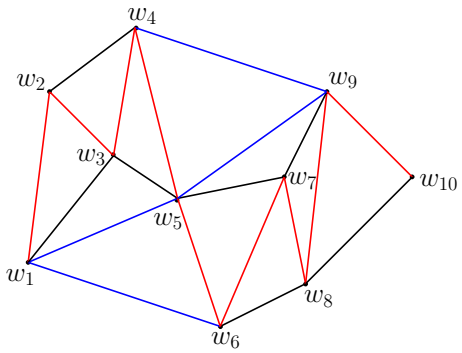

Figure 2.1.: $G = (W, E)$ is a geometric graph with ten vertices. Two paths (i) $w_1\, w_2\, w_3\, w_4\, w_5\, w_6\, w_7\, w_8\, w_9\, w_{10}$ (shown in red) and (ii) $w_6\, w_1\, w_5\, w_9\, w_4$ (shown in blue) are monotone with respect to the positive direction of the x-axis and the y-axis, respectively.

Let S be a set of n points in the plane. A *geometric graph* G is a graph drawn in the plane so that the vertex set consists of the points in S and the edges are drawn as straight line segments between the corresponding points in S. A *plane geometric graph* is one in

which edges intersect only at common endpoints. In this chapter, we are interested in the maximum number of monotone paths over all plane geometric graphs with n vertices. It is easy to see that triangulations maximize the number of such paths since adding edges can only increase the number of monotone paths.

Our results. We first show that the number of monotone paths (over all directions) in a triangulation of n points in the plane is $O(1.8193^n)$, using a fingerprinting technique in which incidence patterns of 8 vertices are analyzed. We then give a sharper bound of $O(1.7864^n)$ using the same strategy, by enumerating fingerprints of 11 vertices using a computer program[1].

Theorem 2.1. *The number of monotone paths in a geometric triangulation on n vertices in the plane is $O(1.7864^n)$.*

Related previous work. We derive a new upper bound on the maximum number of monotone paths in geometric triangulations of n points in the plane. Analogous problems have been studied for cycles, spanning cycles, spanning trees, and matchings [4] in n-vertex edge-maximal planar graphs, which are defined in purely graph theoretic terms. In contrast, the monotonicity of a path depends on the embedding of the point set in the plane, i.e., it is a *geometric* property. The number of geometric configurations contained (as a subgraph) in a triangulation of n points have been considered only recently. The maximum number of *convex polygons* is known to be between $\Omega(1.5028^n)$ and $O(1.5029^n)$ [9, 16]. For the number of *monotone paths*, Dumitrescu et al. [5] gave an upper bound of $O(1.8393^n)$; we briefly review their proof in Section 2.2. A lower bound of $\Omega(1.7003^n)$ is established in the same paper. It can be deduced from the following construction illustrated in Fig. 2.2. Let $n = 2^\ell + 2$ for an integer $\ell \in \mathbb{N}$; the plane graph G has n vertices $W = \{w_1, \ldots, w_n\}$, it contains the Hamiltonian path $\xi_0 = (w_1, \ldots, w_n)$, and it has edge (w_i, w_{i+2^k}), for $1 \le i \le n - 2^k$, iff $i - 1$ or $i - 2$ is a multiple of 2^k.

Every n-vertex triangulation contains $\Omega(n^2)$ monotone paths, since there is a monotone path between any two vertices (by a straightforward adaptation of [6, Lemma 1] from

[1]Refer to the Appendix or the `.c` file at `arXiv:1608.04812`.

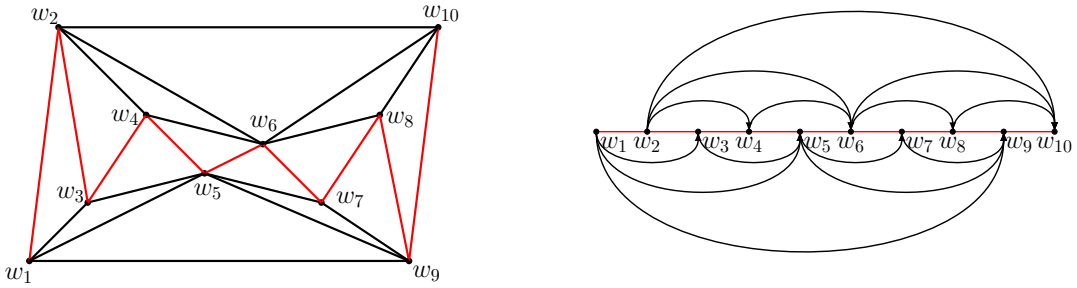

Figure 2.2.: Left: A graph on $n = 2^\ell + 2$ vertices (here $\ell = 3$) that contains a Hamiltonian path $\xi_0 = (w_1, \ldots, w_n)$ shown in red. Right: An isomorphic plane monotone graph where corresponding vertices are in the same order by x-coordinate; and edges above (resp., below) ξ_0 remain above (resp., below) ξ_0. For n sufficiently large, a graph in this family contains $\Omega(1.7003^n)$ x-monotone paths.

convex subdivisions to triangulations). The *minimum* number of monotone paths in an n-vertex triangulation lies between $\Omega(n^2)$ and $O(n^{3.17})$ [5].

The number of several common crossing-free structures (such as matchings, spanning trees, spanning cycles, triangulations) on a set of n points in the plane is known to be exponential [2, 7, 10, 19, 22, 23, 24, 25]; see also [8, 26]. Early upper bounds in this area were obtained by multiplying an upper bound on the maximum number of triangulations on n points with an upper bound on the maximum number of desired configurations in an n-vertex triangulation; valid upper bounds result since every plane geometric graph can be augmented into a triangulation.

For a polytope $P \subset \mathbb{R}^d$, let $G(P)$ denote its *1-skeleton*, which is the graph consisting of the vertices and edges of P. The efficiency of the simplex algorithm and its variants hinges on extremal bounds on the *length* of a monotone paths in the 1-skeleton of a polytope. For example, the *monotone Hirsch conjecture* [29] states that for every $\mathbf{u} \in \mathbb{R}^d \setminus \{\mathbf{0}\}$, the 1-skeleton of every d-dimensional polytope with n facets contains a $\mathbf{u}$-monotone path with at most $n - d$ edges from any vertex to a $\mathbf{u}$-maximal vertex (i.e., a vertex whose orthogonal projection onto $\mathbf{u}$ is maximal). Klee [15] verified the conjecture for 3-dimensional polytopes, but counterexamples have been found in dimensions $d \geq 4$ [27] (see also [20]). Kalai [13, 14] gave a subexponential upper bound for the length of a *shortest* monotone path between any two vertices (better bounds are known for the diameter of the 1-skeleta of polyhedra [28], but the shortest path between two vertices

need *not* be monotone). However, even in $\mathbb{R}^3$, no deterministic pivot rule is known to find a monotone path of length $n-3$ [12], and the expected length of a path found by randomized pivot rules requires averaging over all $\mathbf{u}$-monotone paths [11, 17]. See also [21] for a summary of results of the `polymath 3` project on the *polynomial Hirsch conjecture*.

2.2. Preliminaries

A polygonal path $\xi = (v_1, v_2, \ldots, v_t)$ in $\mathbb{R}^d$ is *monotone in direction* $\mathbf{u} \in \mathbb{R}^d \setminus \{\mathbf{0}\}$ ($\mathbf{u}$-*monotone*, for short) if every directed edge of ξ has a positive inner product with $\mathbf{u}$, that is, $\langle \overrightarrow{v_i v_{i+1}}, \mathbf{u} \rangle > 0$ for $i = 1, \ldots, t-1$; here $\mathbf{0}$ is the origin. A path $\xi = (v_1, v_2, \ldots, v_t)$ is *monotone* if it is monotone in some direction $\mathbf{u} \in \mathbb{R}^d \setminus \{\mathbf{0}\}$. A path ξ in the plane is *x-monotone*, if it is monotone with respect to the positive direction of the x-axis, i.e., monotone in direction $\mathbf{u} = (1, 0)$.

Let S be a set of n points in the plane. A (geometric) *triangulation* of S is a plane geometric graph with vertex set S such that the bounded faces are triangles that jointly tile of the convex hull of S. Since a triangulation has at most $3n-6$ edges for $n \geq 3$, and the $\mathbf{u}$-monotonicity of an edge (a, b) depends on the sign of $\langle \overrightarrow{ab}, \mathbf{u} \rangle$, it is enough to consider monotone paths in at most $2(3n-6) = 6n-12$ directions (one direction between any two consecutive unit normal vectors of the edges). In the remainder of this chapter, we obtain an upper bound on the number of monotone paths in a fixed direction, which we may assume to be the positive direction of the x-axis.

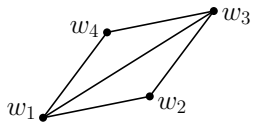

Figure 2.3.: G is a triangulation of four points. There are 7 x-monotone paths in G : w_1w_2, $w_1w_2w_3, w_1w_3, w_1w_4, w_1w_4w_3, w_2w_3, w_4w_3$. These are also y-monotone in this example.

Let $G = (S, E)$ be a plane geometric graph with n vertices. An x-monotone path ξ in G is *maximal* if ξ is not a proper subpath (consisting of consecutive vertices) of some x-monotone path in G. Every x-monotone path in G contains at most n vertices, hence it contains at most $\binom{n}{2}$ x-monotone subpaths. Conversely, every x-monotone path can be

extended to a maximal x-monotone path.

- Let λ_n denote the maximum number of monotone paths in an n-vertex triangulation (summed over all directions $\mathbf{u}$).
- Let μ_n denote the maximum number (over all directions $\mathbf{u}$) of maximal $\mathbf{u}$-monotone paths in an n-vertex triangulation.

Therefore we have

$$\lambda_n \leq (6n-12)\binom{n}{2} \cdot \mu_n = O(n^3\mu_n). \tag{2.1}$$

We prove an upper bound for a broader class of graphs, *plane monotone graphs*, in which every edge is an x-monotone Jordan arc. Consider a plane monotone graph G on n vertices with a maximum number of x-monotone paths. We may assume that the vertices have distinct x-coordinates; otherwise we can perturb the vertices without decreasing the number of x-monotone paths. Since inserting new edges can only increase the number of x-monotone paths, we may also assume that G is fully triangulated [18, Lemma 3.1], i.e., it is an edge-maximal planar graph. Conversely, every plane monotone graph is isomorphic to a plane geometric graph in which the x-coordinates of the corresponding vertices are the same [18, Theorem 2]. Consequently, the number of maximal x-monotone paths in G equals μ_n.

Denote the vertex set of G by $W = \{w_1, \ldots, w_n\}$, ordered by increasing x-coordinates; and direct each edge $w_iw_j \in E(G)$ from w_i to w_j if $i < j$; we thereby obtain a directed graph G. By [5, Lemma 3], all edges w_iw_{i+1} must be present, i.e., G contains a Hamiltonian path $\xi_0 = (w_1, w_2, \ldots, w_n)$. If $T(i)$ denotes the number of maximal (w.r.t. inclusion) x-monotone paths in G starting at vertex w_{n-i+1}, it was shown in the same paper that $T(i)$ satisfies the recurrence $T(i) \leq T(i-1) + T(i-2) + T(i-3)$ for $i \geq 4$, with initial values $T(1) = T(2) = 1$ and $T(3) = 2$ (one-vertex paths are also counted). This recurrence solves to $T(n) = O(\alpha^n)$, where $\alpha = 1.8392\ldots$ is the unique real root of the cubic equation $x^3 - x^2 - x - 1 = 0$. Consequently, any n-vertex geometric triangulation admits at most $O(n^3\,T(n)) = O(1.8393^n)$ monotone paths. Theorem 2.1 improves this bound to $O(1.7864^n)$.

Fingerprinting technique. An x-monotone path can be represented uniquely by the subset of visited vertices. This unique representation gives the trivial upper bound of 2^n for the number of x-monotone paths. For a set of k vertices $V \subseteq W$, an *incidence pattern* of V (*pattern*, for short) is a subset of V that appears in a monotone path ξ (i.e., the intersection between V and a monotone path ξ). Denote by $I(V)$ the set of all incidence patterns of V; see Fig. 2.5. For instance, $v_1v_3 \in I(V)$ implies that there exists a monotone path ξ in G that is incident to v_1 and v_3 in V, but no other vertices in V. The incidence pattern $\emptyset \in I(V)$ denotes an empty intersection between ξ and V, i.e., a monotone path that has no vertices in V.

We now describe a *divide & conquer* application of the fingerprinting technique we use in our proof. For $k \in \mathbb{N}$, let $p_k = \max_{|V|=k} |I(V)|$ denote the maximum number of incidence patterns for a set V of k consecutive vertices in a plane monotone triangulation. We trivially have $p_k \leq 2^k$, and it immediately follows from the definition that $p_k \leq p_i p_j$ for all $i, j \geq 1$ with $i + j = k$; in particular, we have $p_{2k} \leq p_k^2$. Assuming that n is a multiple of k, the product rule yields $\mu_n \leq p_k^{n/k}$. For arbitrary n and constant k, we obtain

$$\mu_n \leq p_k^{\lfloor n/k \rfloor} 2^{n-k\lfloor n/k \rfloor} \leq p_k^{\lfloor n/k \rfloor} 2^k = O\left(p_k^{n/k}\right). \tag{2.2}$$

Combining the results from Equations (2.1) and (2.2), we have

$$\lambda_n = O(n^3\, p_k^{n/k}) \tag{2.3}$$

Given $V = \{v_1\}$, it is clear that $p_1 = 2$ with $I(V) = \{\emptyset, v_1\}$. Similarly given $V = \{v_1, v_2\}$, we have $p_2 = 4$ with $I(V) = \{\emptyset, v_1, v_2, v_1v_2\}$. It is not difficult to see that $p_3 = 7$ (note that $p_3 < p_1p_2$).

The two groups of vertices U and V with two vertices have each 4 patterns; $I(U) = \{\emptyset,$ $u_1,$ $u_2,$ $u_1u_2\}$, $I(V) = \{\emptyset,$ $v_1,$ $v_2,$ $v_1v_2\}$, see Fig. 2.4 (left). Using these two groups, a new group UV with four vertices can be constructed having 13 patterns, see Fig. 2.4 (right). For example patterns u_1u_2 and v_2 in $I(U)$ and $I(V)$ respectively, constitute the pattern $u_1u_2v_2$ in $I(UV)$. Similarly patterns $\emptyset$ and v_1 in $I(U)$ and $I(V)$ respectively, constitute

the pattern v_1 in $I(UV)$. Observing UV, we can find that $I(UV) = \{\emptyset,\ u_1u_2,\ u_1u_2v_1,\ u_1u_2v_1v_2,\ u_1u_2v_2,\ u_1v_1,\ u_1v_1v_2,\ u_2,\ u_2v_1,\ u_2v_1v_2,\ u_2v_2,\ v_1,\ v_1v_2\}$. Note that the three patterns u_1, v_2, u_1v_2 are not in $I(UV)$.

Figure 2.4.: Left: Two groups U and V with two vertices. Right: UV with four vertices.

- We prove $p_4 = 13$ (and so $p_4 < p_2^2 = 16$) by analytic methods (Section 2.3). Using Equations. (2.2) and (2.3), this yields the upper bounds $\mu_n = O(13^{n/4})$ and consequently $\lambda_n = O(n^3\, 13^{n/4}) = O(1.8989^n)$.

- A careful analysis of the edges between two consecutive groups of 4 vertices shows that $p_8 = 120$, and so p_8 is significantly smaller than $p_4^2 = 13^2 = 169$ (Lemma 2.10), hence $\mu_n = O(120^{n/8})$ and $\lambda_n = O(n^3\, 120^{n/8}) = O(1.8193^n)$.

- Computer search shows that $p_{11} = 591$, and so $\mu_n = O(591^{n/11})$ and $\lambda_n = O(n^3\, 591^{n/11}) = O(1.7864^n)$ (Section 2.5). Efficient algorithms and computer search were important in verifying that no pattern was missed.

Table 2.1 summarizes the upper bounds obtained by this approach.

k	p_k	$\mu_n = O\left(p_k^{n/k}\right)$	$\lambda_n = O(n^3\mu_n)$
2	4	2^n	$O(n^3\, 2^n)$
3	7	$O(7^{n/3})$	$O(n^3\, 7^{n/3}) = O(1.913^n)$
4	13	$O(13^{n/4})$	$O(n^3\, 13^{n/4}) = O(1.8989^n)$
5	23	$O(23^{n/5})$	$O(n^3\, 23^{n/5}) = O(1.8722^n)$
6	41	$O(41^{n/6})$	$O(n^3\, 41^{n/6}) = O(1.8570^n)$
7	70	$O(70^{n/7})$	$O(n^3\, 70^{n/7}) = O(1.8348^n)$
8	120	$O(120^{n/8})$	$O(n^3\, 120^{n/8}) = O(1.8193^n)$
9	201	$O(201^{n/9})$	$O(n^3\, 201^{n/9}) = O(1.8027^n)$
10	346	$O(346^{n/10})$	$O(n^3\, 346^{n/10}) = O(1.7944^n)$
11	591	$O(591^{n/11})$	$O(n^3\, 591^{n/11}) = O(1.7864^n)$

Table 2.1.: Upper bounds obtained via the fingerprinting technique for $k \leq 11$.

The analysis of p_k, for $k \geq 12$, using the same technique is expected to yield further improvements. Handling incidence patterns on 12 or 13 vertices is still realistic (although time consuming), but working with larger groups is currently prohibitive, both by analytic methods and with computer search. Significant improvement over our results may require new ideas.

Definitions and notations for a single group. Let G be a directed plane monotone triangulation that contains a Hamiltonian path $\xi_0 = (w_1, w_2, \ldots, w_n)$. Denote by G^- (resp., G^+) the path ξ_0 together with all edges below (resp., above) ξ_0. Let $V = \{v_1, \ldots, v_k\}$ be a set of k consecutive vertices of ξ_0. For the purpose of identifying the edges relevant for the incidence patterns of V, the edges between a vertex $v_i \in V$ and any vertex preceding V (resp., succeeding V) are equivalent since they correspond to the same incidence pattern. We therefore apply a graph homomorphism φ on G^- and G^+, respectively, that maps all vertices preceding V to a new node v_0, and all vertices succeeding V to a new node v_{k+1}. The path ξ_0 is mapped to a new path $(v_0, v_1, \ldots, v_k, v_{k+1})$. Denote the edges in $\varphi(G^- \setminus \xi_0)$ and $\varphi(G^+ \setminus \xi_0)$, respectively, by $E^-(V)$ and $E^+(V)$; they are referred to as the *upper side* and the *lower side*; and let $E(V) = E^-(V) \cup E^+(V)$. The incidence pattern of the vertex set V is determined by the triple $(V, E^-(V), E^+(V))$. We call this triple the *group* induced by V, or simply the *group* V.

Figure 2.5.: Left: A group U with incidence patterns $I(U) = \{\emptyset,\ u_1u_2,\ u_1u_2u_3,\ u_1u_2u_3u_4,\ u_1u_2u_4,\ u_2,\ u_2u_3,\ u_2u_3u_4,\ u_2u_4,\ u_3,\ u_3u_4\}$. Right: A group V with $I(V) = \{\emptyset,\ v_1v_2,\ v_1v_2v_3,\ v_1v_2v_3v_4,\ v_1v_2v_4,\ v_1v_3,\ v_1v_3v_4,\ v_2,\ v_2v_3,\ v_2v_3v_4,\ v_2v_4,\ v_3,\ v_3v_4\}$.

Observe Fig. 2.6. Now we define a few important terms related to our proof. Note that v_0 and v_{k+1} are not in V.

- The edges $v_iv_j \in E(V)$, $1 \leq i < j \leq k$, are called *inner edges*. e.g.v_2v_4.
- The edges v_0v_i, $1 \leq i \leq k$, are called *incoming edges* of $v_i \in V$. e.g.v_0v_2.

- the edges v_iv_{k+1}, $1 \leq i \leq k$, are *outgoing edges* of $v_i \in V$. e.g.v_3v_5.

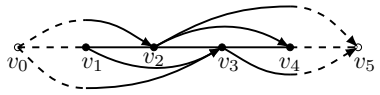

Figure 2.6.: All vertices preceding and succeeding V are mapped to new vertices v_0 and v_{k+1} (here $k = 4$) respectively.

An incoming edge v_0v_i for $1 < i \leq k$ (resp., and outgoing edge v_iv_{k+1} for $1 \leq i < k$) may be present in both $E^-(V)$ and $E^+(V)$. Denote by $\texttt{In}(v)$ and $\texttt{Out}(v)$, respectively, the number of incoming and outgoing edges of a vertex $v \in V$; and note that $\texttt{In}(v)$ and $\texttt{Out}(v)$ can be 0, 1 or 2.

For $1 \leq i \leq k$, let V_{*i} denote the set of incidence patterns in the group V ending at i. For example in Fig. 2.5 (right), $V_{*3} = \{v_1v_2v_3, v_1v_3, v_2v_3, v_3\}$. By definition we have $|V_{*i}| \leq 2^{i-1}$. Similarly V_{i*} denotes the set of incidence patterns in the group V starting at i. In Fig. 2.5 (left), $U_{2*} = \{u_2, u_2u_3, u_2u_3u_4, u_2u_4\}$. Observe that $|V_{i*}| \leq 2^{k-i}$. Note that

$$|I(V)| = 1 + \sum_{i=1}^{k} |V_{*i}| \qquad \text{and} \qquad |I(V)| = 1 + \sum_{i=1}^{k} |V_{i*}|. \tag{2.4}$$

Reflecting all components of a triple $(V, E^-(V), E^+(V))$ with respect to the x-axis generates a new group denoted by $(V, E^-(V), E^+(V))^R$, or V^R for a shorthand notation. By definition, both V and V^R have the same set of incidence patterns.

Remark. Our counting arguments pertain to maximal x-monotone paths. Suppose that a maximal x-monotone path ξ has an incidence pattern in V_{*i}, for some $1 \leq i < k$. By the maximality of ξ, ξ must leave the group after v_i, and so v_i must be incident to an outgoing edge. Similarly, the existence of a pattern in V_{i*} for $1 < i \leq k$, implies that v_i is incident to an incoming edge.

2.3. Groups of 4 vertices

In this section we analyze the incidence patterns of groups with 4 vertices. We prove that $p_4 = 13$ and find the only two groups with 4 vertices that have 13 patterns (Lemma 2.5). We also prove important properties of groups that have exactly 11 or 12 patterns, respectively (Lemmata 2.2, 2.3 and 2.4).

Lemma 2.1. *Let V be a group of 4 vertices with at least 10 incidence patterns. Then there is*

(i) *an outgoing edge from v_2 or v_3; and*

(ii) *an incoming edge into v_2 or v_3.*

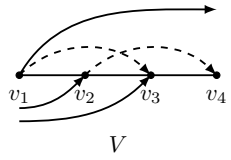

Figure 2.7.: v_1 cannot be the last vertex with an outgoing edge from a group $V = \{v_1, v_2, v_3, v_4\}$ with at least 10 incidence patterns.

Proof. (i) There is at least one outgoing edge from $\{v_1, v_2, v_3\}$, since otherwise $V_{*1} = V_{*2} = V_{*3} = \emptyset$ implying $|I(V)| = |V_{*4}| + 1 \leq 9$. Assume there is no outgoing edge from v_2 and v_3; then $V_{*1} = \{v_1\}$ and $V_{*2} = V_{*3} = \emptyset$. From (2.4), we have $|V_{*4}| = 8$ and this implies $\{v_1v_3v_4, v_2v_4, v_3v_4\} \subset V_{*4}$. The patterns $v_1v_3v_4$ and v_2v_4, respectively, imply that $v_1v_3, v_2v_4 \in E(V)$. The patterns v_2v_4 and v_3v_4, respectively, imply there are incoming edges into v_2 and v_3. Refer to Fig. 2.7. Without loss of generality, an outgoing edge from v_1 is in $E^+(V)$. By planarity, all incoming edges into v_2 or v_3 have to be in $E^-(V)$. Then v_1v_3 and v_2v_4 both have to be in $E^+(V)$, which by planarity is impossible.

(ii) By symmetry in a vertical axis, there is an incoming edge into v_2 or v_3. □

Lemma 2.2. *Let V be a group of 4 vertices with at least 11 incidence patterns. Then there is*

(i) *an incoming edge into v_2; and*

(ii) *an outgoing edge from v_3.*

Proof. (i) Assume $\texttt{In}(v_2) = 0$. Then $|V_{2*}| = 0$. By Lemma 2.1 (ii), we have $\texttt{In}(v_3) > 0$. By definition $|V_{3*}| \leq 2$. We distinguish two cases.

Case 1: $\texttt{In}(v_4) = 0$. In this case, $|V_{4*}| = 0$. Refer to Fig. 2.8 (left). By planarity, the edge v_1v_4 and an outgoing edge from v_2 cannot coexist with an incoming edge into v_3. So either v_1v_4 or v_1v_2 is not in V_{1*}, which implies $|V_{1*}| < 8$. Therefore, (2.4) yields $|I(V)| = |V_{1*}| + |V_{3*}| + 1 < 8 + 2 + 1 = 11$, which is a contradiction.

Case 2: $\texttt{In}(v_4) > 0$. In this case, $|V_{4*}| = 1$. If the incoming edges into v_3 and v_4 are on opposite sides (see Fig. 2.8 (center)), then by planarity there are outgoing edges from neither v_1 nor v_2, which implies that the patterns v_1 and v_1v_2 are not in V_{1*}, and so $|V_{1*}| \leq 8 - 2 = 6$. If the incoming edges into v_3 and v_4 are on the same side (see Fig. 2.8 (right)), then by planarity either the edges v_1v_4 and v_2v_4 or an outgoing edge from v_3 cannot exist, which implies that either v_1v_4 and $v_1v_2v_4$ are not in V_{1*} or v_1v_3 and $v_1v_2v_3$ are not in V_{1*}. In both cases, $|V_{1*}| \leq 8 - 2 = 6$.

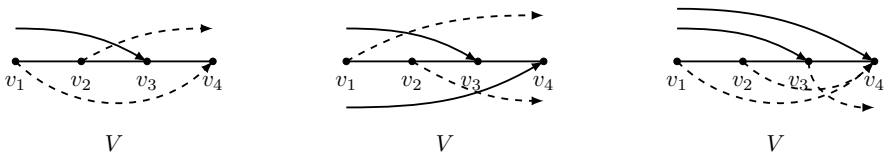

Figure 2.8.: Left: an incoming edge arrives into v_3, but not into v_4. Center and right: incoming edges arrive into both v_3 and v_4; either on the same or on opposite sides of ξ_0.

Therefore, irrespective of the relative position of the incoming edges into v_3 and v_4 (on the same side or on opposite sides), (2.4) yields $|I(V)| = |V_{1*}| + |V_{3*}| + |V_{4*}| + 1 \leq 6 + 2 + 1 + 1 = 10$, which is a contradiction.

(ii) By symmetry in a vertical axis, $\texttt{Out}(v_3) > 0$. □

Lemma 2.3. *Let V be a group of 4 vertices with exactly 11 incidence patterns. Then the following hold.*

(i) *If $\texttt{In}(v_3) = 0$, then all the incoming edges into v_2 are on the same side of ξ_0, $|V_{1*}| \geq 5$, and $|V_{2*}| \geq 3$.*

(ii) *If $\texttt{In}(v_3) > 0$, then all the incoming edges into v_3 are on the same side of ξ_0, $|V_{1*}| \geq 4$, $|V_{2*}| \geq 2$, and $|V_{3*}| = 2$.*

Proof. By Lemma 2.2, $\texttt{In}(v_2) \neq 0$ and $\texttt{Out}(v_3) \neq 0$. Therefore $\{v_2v_3, v_2v_3v_4\} \subseteq V_{2*}$, implying $|V_{2*}| \geq 2$. By definition $|V_{4*}| \leq 1$.

(i) Assume that $\texttt{In}(v_3) = 0$. Then we have $|V_{3*}| = 0$. By (2.4), we obtain $|V_{1*}|+|V_{2*}| \geq 9$. By definition $|V_{2*}| \leq 4$, implying $|V_{1*}| \geq 5$. All incoming edges into v_2 are on the same side, otherwise the patterns $\{v_1, v_1v_3, v_1v_3v_4, v_1v_4\}$ cannot exist, which would imply $|V_{1*}| < 5$. If $|V_{2*}| < 3$, then v_2 and v_2v_4 are not in V_{2*} implying that v_1v_2 and $v_1v_2v_4$ are not in V_{1*}; hence $|V_{1*}| \leq 6$ and thus $|V_{1*}| + |V_{2*}| < 9$, which is a contradiction. We conclude that $|V_{2*}| \geq 3$.

(ii) Assume that $\texttt{In}(v_3) > 0$. Then we have $\{v_3, v_3v_4\} \subseteq V_{3*}$, hence $|V_{3*}| = 2$. By (2.4), we obtain $|V_{1*}|+|V_{2*}| \geq 7$. If $|V_{1*}| < 4$, then $|V_{2*}| \geq 4$ and so $\{v_2, v_2v_3, v_2v_4, v_2v_3v_4\} \subseteq V_{2*}$. This implies $\{v_1v_2, v_1v_2v_3, v_1v_2v_4, v_1v_2v_3v_4\} \subseteq V_{1*}$, hence $|V_{1*}| \geq 4$, which is a contradiction. We conclude that $|V_{1*}| \geq 4$. All incoming edges into v_3 are on the same side, otherwise the patterns $\{v_1, v_1v_2, v_1v_2v_4, v_1v_4, v_2, v_2v_4\}$ cannot exist, and thus $|I(V)| \leq 10$, which is a contradiction. □

Lemma 2.4. *Let V be a group of 4 vertices with exactly 12 incidence patterns. Then the following hold.*

(i) *For $i = 1, 2, 3$, all outgoing edges from v_i, if any, are on the same side of ξ_0.*

(ii) *If V has outgoing edges from exactly one vertex, then this vertex is v_3 and we have $|V_{*3}| = 4$ and $|V_{*4}| = 7$. Otherwise there are outgoing edges from v_2 and v_3, and we have $|V_{*2}| = 2$, $|V_{*3}| \geq 3$ and $|V_{*4}| \geq 5$.*

(iii) *For $i = 2, 3, 4$, all incoming edges into v_i, if any, are on one side of ξ_0.*

(iv) *If V has incoming edges into exactly one vertex, then this vertex is v_2 and we have $|V_{2*}| = 4$ and $|V_{1*}| = 7$. Otherwise there are incoming edges into v_3 and v_2, and we have $|V_{3*}| = 2$, $|V_{2*}| \geq 3$ and $|V_{1*}| \geq 5$.*

Proof. (i) By Lemma 2.2 (i), there is an incoming edge into v_2. So by planarity, all outgoing edges from v_1, if any, are on one side of ξ_0.

If there are outgoing edges from v_2 on both sides, then by planarity the edges v_1v_3, v_1v_4 and any incoming edge into v_3 cannot exist, hence the five patterns $\{v_1v_3,\ v_1v_3v_4,\ v_1v_4,\ v_3,\ v_3v_4\}$ are not in $I(V)$ and thus $|I(V)| \leq 16 - 5 = 11$, which is a contradiction.

If there are outgoing edges from v_3 on both sides (see Fig. 2.9 (a)), then by planarity the edges v_1v_4, v_2v_4 and an incoming edge into v_4 cannot exist, hence the four patterns $\{v_1v_2v_4, v_1v_4, v_2v_4, v_4\}$ are not in $I(V)$. Without loss of generality, an incoming edge into v_2 is in $E^+(V)$. Then by planarity, any outgoing edge of v_1 and the edge v_1v_3 (which must be present) are in $E^-(V)$. Also by planarity, either an incoming edge into v_3 or an outgoing edge from v_2 cannot exist. So either the patterns $\{v_3, v_3v_4\}$ or the patterns $\{v_1v_2, v_2\}$ are not in $I(V)$. Hence $|I(V)| \leq 16 - (4 + 2) = 10$, which is a contradiction. Consequently, all outgoing edges of v_i are on the same side of ξ_0, for $i = 1, 2, 3$.

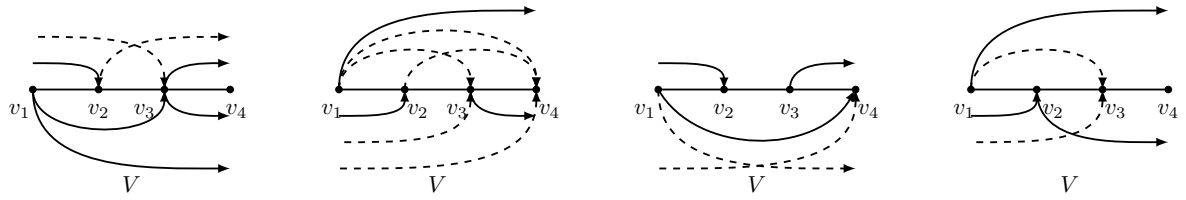

Figure 2.9.: (a) Having outgoing edges from v_3 on both sides is impossible. (b) Existence of outgoing edges only from $\{v_1v_3\}$ is impossible. (c) $|V_{*3}| \geq 3$. (d) $|V_{*4}| \geq 5$.

(ii) If V has outgoing edges from exactly one vertex, then by Lemma 2.2 (ii), this vertex is v_3. Consequently, $V_{*1} = V_{*2} = \emptyset$. Using (2.4), $|V_{*3}| + |V_{*4}| = 11$. So $|V_{*4}| \geq 7$, since by definition $|V_{*3}| \leq 4$. If $|V_{*4}| = 8$, then $\{v_1v_2v_3v_4, v_1v_3v_4, v_2v_3v_4, v_3v_4\} \subset V_{*4}$. Existence of these 4 patterns along with an outgoing edge from v_3 implies $\{v_1v_2v_3, v_1v_3, v_2v_3, v_3\} \subseteq V_{*3}$ and thus $|V_{*3}| + |V_{*4}| = 4 + 8 = 12$, which is a contradiction. Therefore $|V_{*4}| = 7$ and $|V_{*3}| = 4$.

If V has outgoing edges from more than one vertex, the possible vertex sets with outgoing edges are $\{v_1, v_3\}$, $\{v_2, v_3\}$, and $\{v_1, v_2, v_3\}$. We show that it is impossible that all outgoing edges are from $\{v_1, v_3\}$, which will imply that there are outgoing edges from both v_2 and v_3.

If there are outgoing edges from $\{v_1, v_3\}$ only, we may assume the ones from v_1 are in $E^+(V)$ and then by planarity all incoming edges into v_2 are in $E^-(V)$, see Fig. 2.9 (b). Then by planarity, either v_1v_3 or v_2v_4 or an incoming edge into v_3 cannot exist implying

that $\{v_1v_3, v_1v_3v_4\}$ or $\{v_1v_2v_4, v_2v_4\}$ or $\{v_3, v_3v_4\}$ is not in $I(V)$. By the same token, depending on the side the outgoing edges from v_3 are on, either the edge v_1v_4 or an incoming edge into v_4 cannot exist, implying that either v_1v_4 or v_4 is not in $I(V)$. Since $V_{*2} = \emptyset$, $\{v_1v_2, v_2\}$ are not in $I(V)$. So $|I(V)| \leq 16 - (2 + 1 + 2) = 11$, which is a contradiction. Therefore the existence of outgoing edges only from v_1 and v_3 is impossible.

If there are outgoing edges from (precisely) $\{v_2, v_3\}$ or $\{v_1, v_2, v_3\}$, then we have $\{v_1v_2, v_2\} \subseteq V_{*2}$ and $\{v_1v_2v_3, v_2v_3\} \subseteq V_{*3}$, since $\texttt{In}(v_2) \neq 0$ and $\texttt{Out}(v_3) \neq 0$ by Lemma 2.2. Therefore $|V_{*2}| = 2$ and $|V_{*3}| \geq 2$. If $|V_{*3}| < 3$, then $v_1v_3, v_3 \notin V_{*3}$, which implies that v_1v_3 and an incoming edge into v_3 are not in $E(V)$. So, $v_1v_3v_4$, $v_3v_4 \notin I(V)$. Observe Fig. 2.9 (c). By planarity the edge v_1v_4, an incoming edge into v_4 and an outgoing edge from v_1 cannot exist together with an incoming edge into v_2 and an outgoing edge from v_3. So at least one of the patterns $\{v_1, v_1v_4, v_4\}$ is missing implying $|I(V)| \leq 16-(2+2+1) = 11$, which is a contradiction. So $|V_{*3}| \geq 3$. If $|V_{*4}| < 5$, then (2.4) yields $|V_{*3}| = 4$, $|V_{*2}| = 2$ and $|V_{*1}| = 1$. We may assume that all outgoing edges from v_1 are in $E^+(V)$; see Fig. 2.9 (d). By planarity, the incoming edges into v_2 are in $E^-(V)$. Depending on the side the outgoing edges from v_2 are on, either v_1v_3 or an incoming edge into v_3 cannot exist, implying that either v_1v_3 or v_3 is not in V_{*3}, therefore $|V_{*3}| < 4$, creating a contradiction. We conclude that $|V_{*4}| \geq 5$.

(iii) By symmetry, (iii) immediately follows from (i).

(iv) By symmetry, (iv) immediately follows from (ii). □

Lemma 2.5. *Let V be a group of 4 vertices. Then V has at most 13 incidence patterns. If V has 13 incidence patterns, then V is either A or A^R in Fig. 2.10. Consequently, $p_4 = 13$.*

Figure 2.10.: $I(A) = I(A^R) = \{\emptyset, 12, 123, 1234, 124, 13, 134, 2, 23, 234, 24, 3, 34\}$. A and A^R are the only groups with 13 incidence patterns.

Proof. Observe that group A in Fig. 2.10 has 13 patterns. Let V be a group of 4 vertices with at least 13 patterns.

We first **claim** that V has an incoming edge into v_3 and an outgoing edge from v_2. Their existence combined with Lemma 2.2 implies that $\{v_3v_4, v_3\} \subset I(V)$ and $\{v_1v_2, v_2\} \subset I(V)$, respectively. At least one of these two edges has to be in $E(V)$, otherwise V has at most $16 - (2 + 2) = 12$ patterns. Assume that one of the two, without loss of generality, the outgoing edge from v_2 is not in $E(V)$. Then $\{v_1v_3, v_2v_4\} \subseteq E(V)$, otherwise either patterns $\{v_1v_3, v_1v_3v_4\}$ or $\{v_1v_2v_4, v_2v_4\}$ are not in $I(V)$ and there are at most $16-(2+2) = 12$ patterns. By Lemma 2.2, there is an incoming edge into v_2 and an outgoing edge from v_3. Without loss of generality, the outgoing edge from v_3 is in $E^-(V)$. So by planarity v_2v_4 is in $E^+(V)$, which implies that v_1v_3 and the incoming edge into v_3 are in $E^-(V)$. By the same token, the incoming edge into v_2 is in $E^+(V)$. So by planarity the edge v_1v_4 and an outgoing edge from v_1 cannot be in $E(V)$. Then the patterns $\{v_1v_4, v_1\}$ are not in $I(V)$, thus V has at most $16 - (2 + 2) = 12$ patterns, which is a contradiction. This completes the proof of the claim.

We may assume without loss of generality (by applying a reflection in the x-axis if necessary) that the incoming edge into v_3 is in $E^-(V)$. By planarity, the outgoing edge from v_2 is in $E^+(V)$. By the same token the edge v_1v_4 cannot be in $E(V)$, which implies that $v_1v_4 \notin I(V)$. So $I(V) \leq 16 - 1 = 15$. By Lemma 2.2, there is an incoming edge into v_2 and an outgoing edge from v_3. By planarity, if the incoming edge into v_2 is in $E^+(V)$ then the outgoing edge from v_1 cannot be in $E(V)$, therefore the pattern v_1 is not in $I(V)$. But if the incoming edge into v_2 is in $E^-(V)$ then the edge v_1v_3 cannot be in $E(V)$ therefore neither v_1v_3 nor $v_1v_3v_4$ is in $I(V)$. By a similar argument, if the outgoing edge from v_3 is in $E^-(V)$ then the incoming edge into v_4 cannot be in $E(V)$, therefore the pattern v_4 is not in $I(V)$. But if the outgoing edge from v_3 is in $E^+(V)$ then the edge v_2v_4 cannot be in $E(V)$, therefore neither v_2v_4 nor $v_1v_2v_4$ is in $I(V)$. Since $I(V) \geq 13$, the only solution is $v_1 \notin I(V)$ and $v_4 \notin I(V)$. Therefore V induces the group A and has exactly 13 patterns. If the incoming edge into v_3 is in $E^+(V)$, then V induces A^R (with exactly 13 patterns). □

2.4. Groups of 8 vertices

In this section, we analyze two consecutive groups, U and V, each with 4 vertices, and show that $p_8 = 120$ (Lemma 2.10). Let $U = \{u_1, u_2, u_3, u_4\}$ and $V = \{v_1, v_2, v_3, v_4\}$, and put $UV = U \cup V$ for short. We may assume that $|I(V)| \leq |I(U)|$ (by applying a reflection about the vertical axis if necessary), and we have $|I(U)| \leq 13$ by Lemma 2.5. This yields a trivial upper bound $|I(UV)| \leq |I(U)| \cdot |I(V)| \leq 13^2 = 169$. It is enough to consider cases in which $10 \leq |I(V)| \leq |I(U)| \leq 13$, otherwise the trivial bound is already less than 120.

In all cases where $|I(U)| \cdot |I(V)| > 120$, we improve on the trivial bound by finding edges between U and V that cannot be present in the group UV. If edge u_iv_j is not in $E(UV)$, then any of the $|U_{*i}| \cdot |V_{j*}|$ patterns that contain u_iv_j is excluded. Since every maximal x-monotone path has at most one edge between U and V, distinct edges u_iv_j exclude disjoint sets of patterns, and we can use the sum rule to count the excluded patterns. We continue with a case analysis.

Lemma 2.6. *Consider a group UV consisting of two consecutive groups of 4 vertices, where $|I(U)| \geq 10$ and $|I(V)| = 10$. Then UV allows at most 120 incidence patterns.*

Proof. If U has at most 12 patterns, then UV has at most $12 \times 10 = 120$ patterns, and the proof is complete. We may thus assume that U has 13 patterns. By Lemma 2.5, U is either A or A^R. We may assume, by reflecting UV about the horizontal axis if necessary, that U is A. Refer to Fig. 2.11 (left). Therefore $|U_{*2}| = 2$, $|U_{*3}| = 4$ and $|U_{*4}| = 6$, according to Fig. 2.10. The cross product of the patterns of U and V produce $13 \times 10 = 130$ possible patterns. We show that at least 10 of them are incompatible in each case. It follows that $|I(UV)| \leq 130 - 10 = 120$. Let v_i denote the first vertex with an incoming edge in $E(V)$, where $i \neq 1$. By Lemma 2.1 (ii), $i = 2$ or 3.

Case 1: $(u_4, v_i) \in E(UV)$. We first show that $|V_{1*}| \geq 3$. By definition $|V_{3*}| \leq 2$ and $|V_{4*}| \leq 1$. By (2.4), $|V_{1*}| + |V_{2*}| \geq 9 - (2 + 1) = 6$. If $|V_{2*}| \leq 3$, then $|V_{1*}| \geq 3$. Otherwise $|V_{2*}| = 4$ implying $V_{2*} = \{v_2v_3v_4, v_2v_3, v_2v_4, v_2\}$. This implies there are outgoing edges from v_2 and v_3 in $E(V)$. Therefore $\{v_1v_2v_3v_4, v_1v_2v_3, v_1v_2\} \subset V_{1*}$ and $|V_{1*}| \geq 3$.

Case 1.1: $(u_4, v_i) \in E^-(UV)$; see Fig. 2.11 (right). As $i = 2$ or 3, by planarity $(u_3, v_1) \notin E(UV)$. Hence at least $|U_{*3}|\ |V_{1*}| \geq 4 \times 3 = 12$ combinations are incompatible.

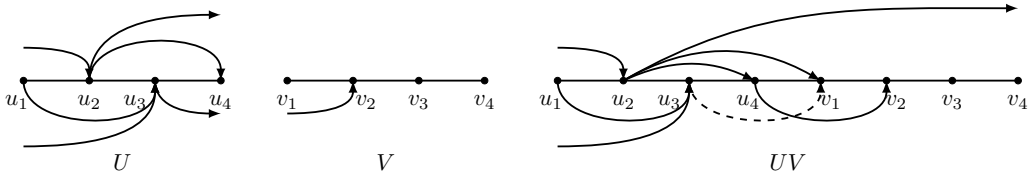

Figure 2.11.: Left: $|I(U)| = 13$ and $|I(V)| = 10$. Right: $(u_4, v_i) \in E^-(UV)$; $i = 2$ here.

Case 1.2: $(u_4, v_i) \in E^+(UV)$; see Fig. 2.12 (right). Then by planarity $(u_2, v_1) \notin E(UV)$ and $|U_{*2}||V_{1*}| \geq 2 \times 3 = 6$ combinations are incompatible.

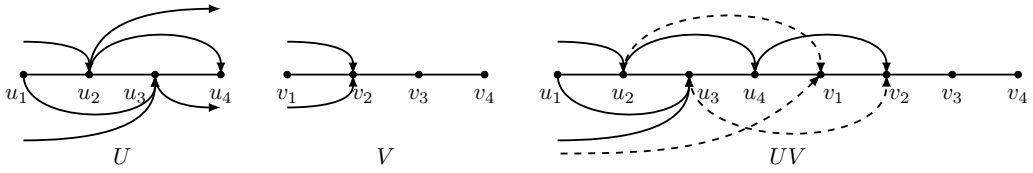

Figure 2.12.: Left: $|I(U)| = 13$ and $|I(V)| = 10$. Right: $(u_4, v_i) \in E^+(UV)$; $i = 2$ here.

An incoming edge into v_i in $E(V)$ implies $|V_{i*}| \geq 1$. If $u_3v_i \notin E(UV)$, then $|U_{*3}||V_{i*}| \geq 4 \times 1 = 4$ combinations are incompatible. Hence there are at least $6+4 = 10$ incompatible patterns. If $u_3v_i \in E(UV)$, then by planarity an incoming edge into v_1 in $E(UV)$ cannot exist and $|\{\emptyset\}||V_{1*}| \geq 1 \times 3 = 3$ combinations are incompatible. If $u_2v_i \in E(UV)$, then by planarity an outgoing edge from u_4 cannot exist. So $|U_{*4}||\{\emptyset\}| \geq 6 \times 1 = 6$ combinations are incompatible. So there are at least $6+3+6 = 15$ incompatible patterns. If $u_2v_i \notin E(UV)$, then $|U_{*2}||V_{1*}| \geq 2 \times 1 = 2$ combinations are incompatible. Hence there are at least $6 + 3 + 2 = 11$ incompatible patterns.

Case 2: $(u_4, v_i) \notin E(UV)$. By showing $|V_{i*}| \geq 2$ for all possible values of i (i.e., 2 and 3), we can conclude that at least $|U_{*4}||V_{i*}| \geq 6 \times 2 = 12$ combinations are incompatible.

If $i = 2$, then $v_2v_3v_4 \in V_{2*}$. By Lemma 2.1 (i), there is an outgoing edge from v_2 or v_3 in $E(V)$, which implies $v_2 \in V_{2*}$ or $v_2v_3 \in V_{2*}$. Hence $|V_{2*}| \geq 2$.

If $i = 3$ and there is no outgoing edge from v_3 in $E(V)$, then by Lemma 2.1 (i), there is an outgoing edge from v_2. In that case by planarity, there are only 7 possible incidence

patterns $\{\emptyset, v_1v_2v_3v_4, v_1v_2v_4,\ v_1v_3v_4, v_1v_2, v_3v_4, v_4\}$ in V, which is a contradiction. So if $i = 3$, then there is an outgoing edge from v_3 in $E(V)$, which implies $\{v_3v_4, v_3\} \subset V_{3*}$ therefore $|V_{3*}| \geq 2$. □

Lemma 2.7. *Consider a group UV consisting of two consecutive groups of 4 vertices, where $|I(U)| \geq 11$ and $|I(V)| = 11$. Then UV allows at most 120 incidence patterns.*

Proof. We distinguish three cases depending on $|I(U)|$.

Case 1: $|I(U)| = 11$. Since $|I(UV)| \leq |I(U)|\cdot|I(V)| = 11\times11 = 121$, it suffices to show that at least one of these patterns is incompatible. By Lemma 2.2, there is an outgoing edge from u_3 in $E(U)$ and an incoming edge into v_2 in $E(V)$. Therefore $u_1u_2u_3 \in U_{*3}$ and $v_2v_3v_4 \in V_{2*}$. Refer to Fig. 2.13 (left). If $(u_3v_2) \notin E(UV)$, then $u_1u_2u_3v_2v_3v_4$ is not in $I(UV)$. If $(u_3v_2) \in E(UV)$, then by planarity either an outgoing edge from u_4 w.r.t. UV, or an incoming edge into v_1 w.r.t. UV, cannot be in $E(UV)$, implying that either $u_1u_2u_3u_4$ or $v_1v_2v_3v_4$ is not in $I(UV)$.

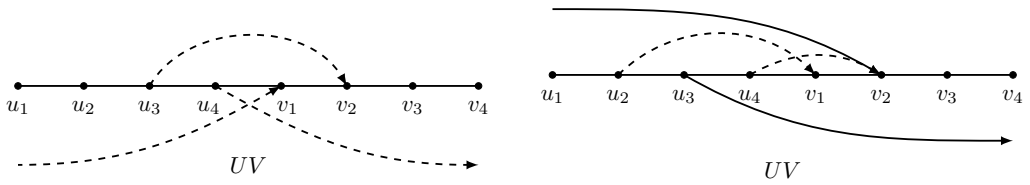

Figure 2.13.: Left: $|I(U)| = |I(V)| = 11$. Right: outgoing edge from u_3 is in $E^-(UV)$ and outgoing edge from u_2 is in $E^+(UV)$.

Case 2: $|I(U)| = 12$. By Lemma 2.4 (ii), if U has outgoing edges from exactly one vertex, then they are from u_3 and we have $|U_{*3}| = 4$, $|U_{*4}| = 7$, otherwise $|U_{*3}| \geq 3$ and $|U_{*4}| \geq 5$. By Lemma 2.4 (i), all the outgoing edges from u_3 in $E(U)$ are on one side of U. For simplicity assume those are in $E^-(U)$. Since $|I(UV)| \leq |I(U)|\cdot|I(V)| = 12\times11 = 132$, it suffices to show that at least $132 - 120 = 12$ of these patterns are incompatible.

Case 2.1: There is no incoming edge into v_3 in $E(V)$. Then by Lemma 2.3 (i), all the incoming edges into v_2 in $E(V)$ are on one side of V and we have $|V_{1*}| \geq 5$ and $|V_{2*}| \geq 3$.

Case 2.1.1: The incoming edges into v_2 w.r.t. V are in $E^+(V)$. So by planarity $u_3v_2 \notin E(UV)$ and at least $|U_{*3}||V_{2*}|$ patterns are incompatible. If U has outgoing edges

from exactly one vertex, then $|U_{*3}||V_{2*}| \geq 4 \times 3 = 12$ and we are done. Otherwise U has outgoing edges from u_2, where $|U_{*2}| = 2$ and at least $|U_{*3}||V_{2*}| \geq 3 \times 3 = 9$ patterns are incompatible. Also by Lemma 2.4 (i), all the outgoing edges from u_2 in $E(U)$ are on one side of U. If the outgoing edges from u_2 w.r.t. U are in $E^+(U)$, see Fig. 2.13 (right), then u_2v_1 and u_4v_2 can only be in $E^+(UV)$; by planarity both edges cannot be in $E(UV)$ and thus at least $\min(|U_{*2}||V_{1*}|, |U_{*4}||V_{2*}|) \geq \min(2 \times 5, 5 \times 3) = 10$ patterns are incompatible. If the outgoing edges from u_2 w.r.t. U are in $E^-(U)$, then by planarity $u_2v_2 \notin E(UV)$ and thus at least $|U_{*2}||V_{2*}| \geq 2 \times 3 = 6$ patterns are incompatible. Therefore irrespective of the relative position of the outgoing edge from u_2 in $E(U)$, at least $9 + \min(10, 6) = 15$ patterns are incompatible and we are done.

Case 2.1.2: The incoming edges into v_2 w.r.t. V are in $E^-(V)$. Therefore u_3v_1 and u_4v_2 can only be in $E^-(UV)$. By planarity both edges cannot be in $E(UV)$. Hence at least $\min(|U_{*3}||V_{1*}|, |U_{*4}||V_{2*}|) = \min(3 \times 5, 5 \times 3) = 15$ patterns are incompatible.

Case 2.2: There is an incoming edge into v_3 in $E(V)$. By Lemma 2.3 (ii), all the incoming edges into v_3 in $E(V)$ are on one side of V, $|V_{1*}| \geq 4$, $|V_{2*}| \geq 2$ and $|V_{3*}| = 2$.

Case 2.2.1: The incoming edges into v_2 in $E(V)$ are on both sides of V.

If the incoming edges into v_3 w.r.t. V are in $E^+(V)$, see Fig. 2.14 (left), then by planarity $u_3v_3 \notin E(UV)$. So at least $|U_{*3}||V_{3*}| \geq 3 \times 2 = 6$ patterns are incompatible. By planarity an outgoing edge from u_4 w.r.t. UV, an incoming edge into v_3 w.r.t. UV and u_3v_2 cannot coexist in $E(UV)$. Therefore at least $\min(|\{\emptyset\}||V_{3*}|, |U_{*4}||\{\emptyset\}|, |U_{*3}||V_{2*}|) \geq \min(1 \times 2, 5 \times 1, 3 \times 2) = 2$ patterns are incompatible. By the same argument, the edges u_3v_2, u_4v_2 and an incoming edge into v_1 w.r.t. UV cannot be in $E(UV)$ together. Hence at least $\min(|U_{*3}||V_{2*}|, |U_{*4}||V_{2*}|, |\{\emptyset\}||V_{1*}|) = \min(3 \times 2, 5 \times 2, 1 \times 4) = 4$ patterns are incompatible. Therefore at least $6 + 2 + 4 = 12$ patterns are incompatible.

If incoming edges into v_3 w.r.t. V are in $E^-(V)$, see Fig. 2.14 (right), then either an outgoing edge from u_3 w.r.t. UV or an incoming edge into v_3 w.r.t. UV cannot be in $E(UV)$. So at least $\min(|U_{*3}||\{\emptyset\}|, |\{\emptyset\}||V_{3*}|) \geq \min(3 \times 1, 1 \times 2) = 2$ patterns are incompatible. Also u_3v_1 and u_4v_3 can only be in $E^-(UV)$. By planarity both edges cannot be in $E(UV)$. Hence at least $\min(|U_{*3}||V_{1*}|, |U_{*4}||V_{3*}|) \geq \min(3 \times 4, 5 \times 2) = 10$

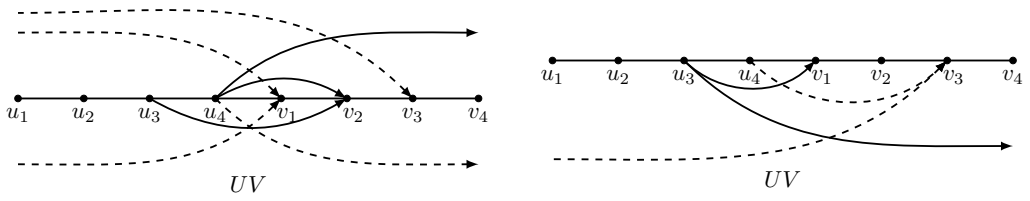

Figure 2.14.: Left: incoming edges into v_2 are in both $E^+(V)$ and $E^-(V)$ and incoming edge into v_3 is in $E^+(V)$. Right: incoming edges into v_2 are in both $E^+(V)$ and $E^-(V)$ and incoming edge into v_3 is in $E^-(V)$.

patterns are incompatible. Therefore at least $2 + 10 = 12$ patterns are incompatible.

Case 2.2.2: All the incoming edges into v_2 in $E(V)$ are on one side of V and the incoming edges into v_2 and v_3 in $E(V)$ are on same side of V.

If the incoming edges into v_2 and v_3 w.r.t. V are in $E^+(V)$, see Fig. 2.15 (left), then by planarity u_3v_2 and u_3v_3 are not in $E(UV)$. So at least $|U_{*3}||V_{2*}|+|U_{*3}||V_{3*}| \geq 3\times2+3\times2 = 12$ patterns are incompatible.

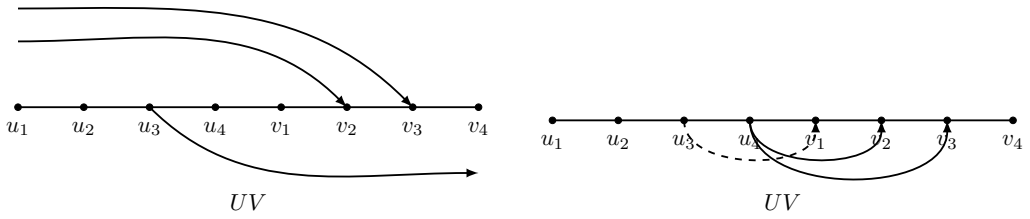

Figure 2.15.: Left: both incoming edges into v_2 and v_3 are in $E^+(V)$. Right: both incoming edges into v_2 and v_3 are in $E^-(V)$.

If the incoming edges into v_2 and v_3 w.r.t. V are in $E^-(V)$, see Fig. 2.15 (right), then u_3v_1 and both u_4v_2 and u_4v_3 can only be in $E^-(UV)$. By planarity either u_3v_1 or both u_4v_2 and u_4v_3 are not in $E(UV)$. Consequently, at least $\min(|U_{*3}||V_{1*}|, |U_{*4}||V_{2*}|+|U_{*4}||V_{3*}|) = \min(3 \times 4, 5 \times 2 + 5 \times 2) = 12$ patterns are incompatible.

Case 2.2.3: All the incoming edges into v_2 in $E(V)$ are on one side of V and all the incoming edges into v_3 in $E(V)$ are on the opposite side of V. Let the incoming edges w.r.t. V in $E^+(V)$ are into v_i and the incoming edges w.r.t. V in $E^-(V)$ are into v_j. So either $i = 2$, $j = 3$ or $i = 3$, $j = 2$, see Fig. 2.16. Therefore $|V_{i*}|$, $|V_{j*}|$ are at least $\min(|V_{2*}|, |V_{3*}|) = 2$. By planarity $u_3v_i \notin E(UV)$. So at least $|U_{*3}||V_{i*}| \geq 3 \times 2 = 6$ patterns are incompatible. Also u_3v_1 and u_4v_j can only be in $E^-(UV)$. By planarity both

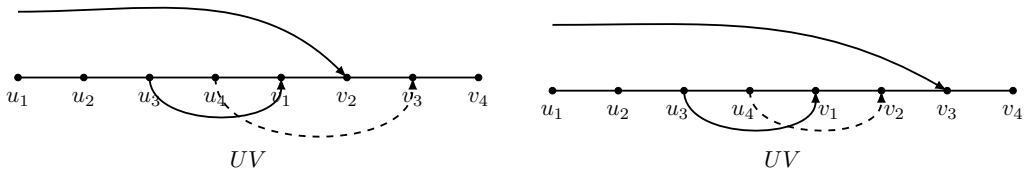

Figure 2.16.: Left: incoming edge into v_2 is $E^+(V)$ and incoming edge into v_3 is in $E^-(V)$. Right: incoming edge into v_2 is in $E^-(V)$ and incoming edge into v_3 is in $E^+(V)$.

edges cannot be in $E(UV)$. Hence at least $\min(|U_{*3}||V_{1*}|, |U_{*4}||V_{j*}|) = \min(3 \times 4, 5 \times 2) = 10$ patterns are incompatible. Therefore at least $6 + 10 = 16$ patterns are incompatible.

Case 3: $|I(U)| = 13$. By Lemma 2.5, U is either A or A^R. We may assume, by reflecting UV about the horizontal axis if necessary, that U is A. Therefore $|U_{*2}| = 2$, $|U_{*3}| = 4$ and $|U_{*4}| = 6$, see Fig. 2.10. Since $|I(UV)| \leq |I(U)| \cdot |I(V)| = 13 \times 11 = 143$, it suffices to show that at least $143 - 120 = 23$ of these patterns are incompatible.

Case 3.1: There is no incoming edge into v_3 in $E(V)$. Then by Lemma 2.3 (i), all the incoming edges into v_2 in $E(V)$ are on one side of V, $|V_{1*}| \geq 5$ and $|V_{2*}| \geq 3$.

If the incoming edges into v_2 w.r.t. V are in $E^-(V)$, see Fig. 2.17 (left), by planarity $u_2v_2 \notin E(UV)$. So at least $|U_{*2}||V_{2*}| \geq 2 \times 3 = 6$ patterns are incompatible. Also u_4v_2 and u_3v_1 can only be in $E^-(UV)$. By planarity both edges cannot be in $E(UV)$. Hence at least $\min(|U_{*4}||V_{2*}|, |U_{*3}||V_{1*}|) = \min(6 \times 3, 4 \times 5) = 18$ patterns are incompatible. Therefore at least $6 + 18 = 24$ patterns are incompatible.

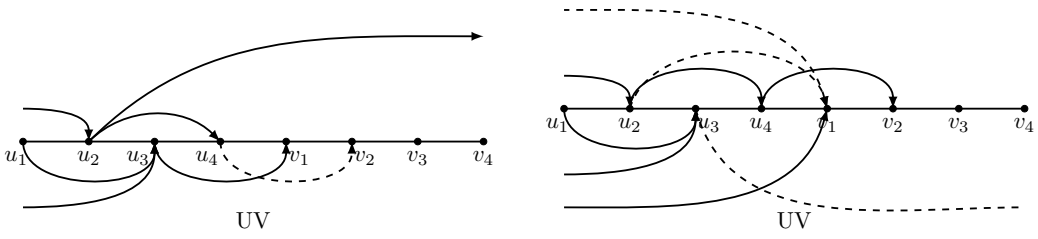

Figure 2.17.: Left: incoming edge into v_2 is in $E^-(V)$. Right: incoming edge into v_2 is in $E^+(V)$.

Similarly if the incoming edges into v_2 w.r.t. V are in $E^+(V)$, cf. Fig. 2.17 (right), by planarity $u_3v_2 \notin E(UV)$. So at least $|U_{*3}||V_{2*}| \geq 4 \times 3 = 12$ patterns are incompatible. Also u_4v_2 and u_2v_1 can only be in $E^+(UV)$. By planarity both edges cannot be in $E(UV)$. If $u_4v_2 \notin E(UV)$, then at least $|U_{*4}||V_{2*}| \geq 6 \times 3 = 18$ patterns are incompatible. Otherwise $u_2v_1 \notin E(UV)$ and either an incoming edge into v_1 w.r.t. UV or an outgoing

edge from u_3 w.r.t. UV cannot be in $E(UV)$. Hence at least

$$|U_{*2}||V_{1*}| + \min(|\{\emptyset\}||V_{1*}|, |U_{*3}||\{\emptyset\}|) \geq 2 \times 5 + \min(1 \times 5, 4 \times 1) = 14$$

patterns are incompatible. Therefore at least $12 + \min(18, 14) = 26$ patterns are incompatible.

Case 3.2: There is an incoming edge into v_3 in $E(V)$. By Lemma 2.3 (ii), all the incoming edges into v_3 are on one side of V, $|V_{1*}| \geq 4$, $|V_{2*}| \geq 2$ and $|V_{3*}| = 2$.

Case 3.2.1: The incoming edges into v_2 in $E(V)$ are on both sides of V.

If the incoming edges into v_3 w.r.t. V are in $E^+(V)$, see Fig. 2.18 (left), then by planarity $u_3v_3 \notin E(UV)$. So at least $|U_{*3}||V_{3*}| \geq 4 \times 2 = 8$ patterns are incompatible. Also u_2v_1 and u_4v_3 can only be in $E^+(UV)$. By planarity both edges cannot be in $E(UV)$. Hence at least $\min(|U_{*2}||V_{1*}|, |U_{*4}||V_{3*}|) = \min(2 \times 4, 6 \times 2) = 8$ patterns are incompatible. By the same token, an outgoing edge from u_4 w.r.t. UV and the edges u_2v_3 and u_3v_2 cannot exist together in $E(UV)$. Therefore at least

$$\min(|U_{*4}||\{\emptyset\}|, |U_{*2}||V_{3*}|, |U_{*3}||V_{2*}|) = \min(6 \times 1, 2 \times 2, 4 \times 2) = 4$$

patterns are incompatible. Similarly, by planarity, an incoming edge into v_1 w.r.t. UV and the edges u_3v_2 and u_4v_3 cannot coexist in $E(UV)$. Therefore at least

$$\min(|\{\emptyset\}||V_{1*}|, |U_{*3}||V_{2*}|, |U_{*4}||V_{3*}|) = \min(1 \times 4, 4 \times 2, 6 \times 2) = 4$$

patterns are incompatible. Hence at least $8 + 8 + 4 + 4 = 24$ patterns are incompatible.

If the incoming edges into v_3 w.r.t. V are in $E^-(V)$, see Fig. 2.18 (right), then by planarity $u_2v_3 \notin E(UV)$. So at least $|U_{*2}||V_{3*}| \geq 2 \times 2 = 4$ patterns are incompatible. Also u_3v_1 and u_4v_3 can only be in $E^-(UV)$. By planarity both the edges cannot be in $E(UV)$. Hence at least $\min(|U_{*3}||V_{1*}|, |U_{*4}||V_{3*}|) = \min(4 \times 4, 6 \times 2) = 12$ edges are incompatible. By planarity an outgoing going edge from u_3 w.r.t. UV and an incoming edge into v_3 w.r.t. UV cannot exist together in $E(UV)$. Therefore at least $\min(|U_{*3}||\{\emptyset\}|, |\{\emptyset\}||V_{3*}|) =$

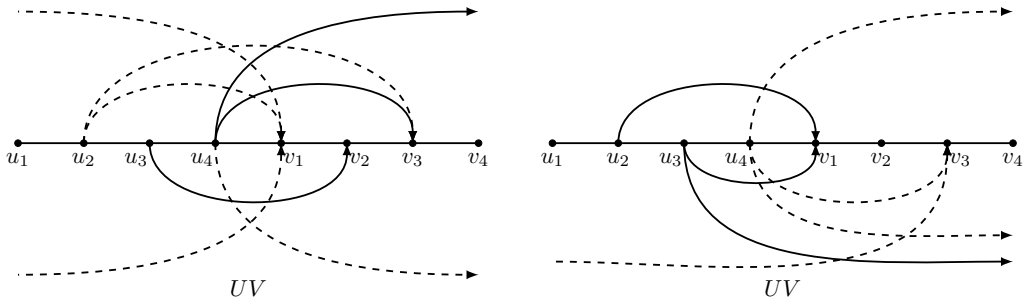

Figure 2.18.: Left: incoming edges into v_2 are on both sides and incoming edges into v_3 are in $E^+(V)$. Right: incoming edges into v_2 are on both sides and incoming edges into v_3 are in $E^-(V)$.

$\min(4 \times 1, 1 \times 2) = 2$ patterns are incompatible. By the same token, an outgoing edge from u_4 w.r.t. UV and the edges u_2v_1 and u_3v_1 cannot be together in $E(UV)$. Hence at least $\min(|U_{*2}||V_{1*}|, |U_{*3}||V_{1*}|, |U_{*4}||\{\emptyset\}|) = \min(2 \times 4, 4 \times 4, 6 \times 1) = 6$ patterns are incompatible. So at least $4 + 12 + 2 + 6 = 24$ patterns are incompatible.

Case 3.2.2: All the incoming edges into v_2 in $E(V)$ are on one side of V and all the incoming edges into v_2 and v_3 in $E(V)$ are on the same side of V.

If the incoming edges into v_2 and v_3 w.r.t. V are in $E^+(V)$, see Fig. 2.19 (left), by planarity u_3v_2 and u_3v_3 are not in $E(UV)$. So at least $|U_{*3}||V_{2*}| + |U_{*3}||V_{3*}| = 4 \times 2 + 4 \times 2 = 16$ patterns are incompatible. Also u_2v_1 and u_4v_2 can only be in $E^+(UV)$. By planarity both the edges cannot be in $E(UV)$. Hence at least $\min(|U_{*2}||V_{1*}|, |U_{*4}||V_{2*}|) = \min(2 \times 4, 6 \times 2) = 8$ patterns are incompatible. Therefore at least $16 + 8 = 24$ patterns are incompatible.

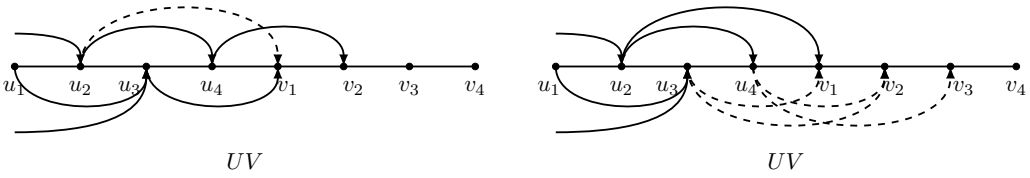

Figure 2.19.: Left: incoming edges into v_2, v_3 are in $E^+(V)$. Right: incoming edges into v_2, v_3 are in $E^-(V)$.

If the incoming edges into v_2 and v_3 w.r.t. V are in $E^-(V)$, see Fig. 2.19 (right), by planarity $u_2v_3 \notin E(UV)$. So at least $|U_{*2}||V_{3*}| \geq 2 \times 2 = 4$ patterns are incompatible. Also u_3v_1, u_3v_2 u_4v_2, u_4v_3 can only be in $E^-(UV)$. By planarity either u_3v_1 or u_4v_2 and

either u_3v_2 or u_4v_3 can be in $E(UV)$. Hence at least

$$\begin{aligned}&\min(|U_{*3}||V_{1*}|, |U_{*4}||V_{2*}|) + \min(|U_{*3}||V_{2*}|, |U_{*4}||V_{3*}|)\\ =&\min(4\times 4, 6\times 2) + \min(4\times 2, 6\times 2) = 20\end{aligned}$$

combinations are incompatible. Therefore at least $4+20 = 24$ patterns are incompatible.

Case 3.2.3: All the incoming edges into v_2 are on one side of V and all the incoming edges into v_3 are on the opposite side of V. Let the incoming edges w.r.t. V in $E^+(V)$

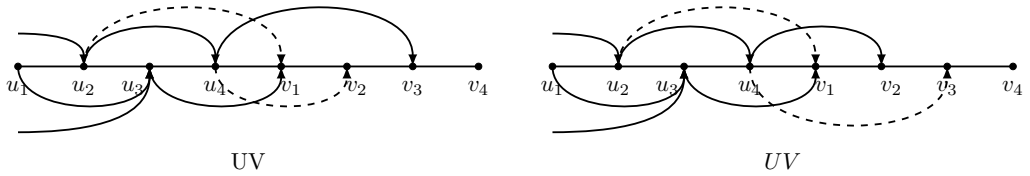

Figure 2.20.: Left: incoming edge into v_2 is in $E^-(V)$ and into v_3 is in $E^+(V)$. Right: Incoming edge into v_2 is in $E^+(V)$ and into v_3 is in $E^-(V)$.

are into v_i and the incoming edges w.r.t. V in $E^-(V)$ are into v_j. So either $i = 2$, $j = 3$ or $i = 3$, $j = 2$, see Fig. 2.20. Therefore $|V_{i*}|$, $|V_{j*}|$ are at least $\min(|V_{2*}|, |V_{3*}|) = 2$. By planarity $u_3v_i \notin E(UV)$. So at least $|U_{*3}||V_{i*}| \geq 4\times 2 = 8$ patterns are incompatible. Also u_2v_1 and u_4v_i can only be in $E^+(UV)$. By planarity both edges cannot be in $E(UV)$. Hence at least $\min(|U_{*2}||V_{1*}|, |U_{*4}||V_{i*}|) = \min(2\times 4, 6\times 2) = 8$ patterns are incompatible. Similarly both u_3v_1 and u_4v_j can only be in $E^-(UV)$. By planarity both edges cannot be in $E(UV)$. Hence at least $\min(|U_{*3}||V_{1*}|, |U_{*4}||V_{j*}|) = \min(4\times 4, 6\times 2) = 12$ patterns are incompatible. Therefore at least $8+8+12 = 28$ patterns are incompatible. □

Lemma 2.8. *Consider a group UV consisting of two consecutive groups of 4 vertices, where $|I(U)| \geq 12$ and $|I(V)| = 12$. Then UV allows at most 120 incidence patterns.*

Proof. We distinguish two cases depending on $|I(U)|$.

Case 1: $|I(U)| = 12$. Then by Lemma 2.4 (i) & (ii), for each vertex u_i, all the outgoing edges from u_i, if any, are on one side of U. Since $|I(UV)| \leq |I(U)|\cdot|I(V)| = 12\times 12 = 144$, it suffices to show that at least $144 - 120 = 24$ of these patterns are incompatible. We

distinguish three cases depending on which vertex in U have outgoing edges and which sides are containing those outgoing edges.

Case 1.1: U has outgoing edges from exactly one vertex. By Lemma 2.4 (ii), they are from u_3 and we have $|U_{*3}| = 4$ and $|U_{*4}| = 7$. For simplicity assume they are in $E^-(U)$.

Case 1.1.1: V has incoming edges into exactly one vertex. By Lemma 2.4 (iv), they are into v_2 and we have $|V_{2*}| = 4$ and $|V_{1*}| = 7$.

If the incoming edges into v_2 w.r.t. V are in $E^-(V)$, see Fig. 2.21 (left), then u_3v_1 and u_4v_2 can only be in $E^-(UV)$. By planarity both edges cannot be in $E(UV)$. So at least $\min(|U_{*3}||V_{1*}|, |U_{*4}||V_{2*}|) = \min(4 \times 7, 7 \times 4) = 28$ patterns are incompatible.

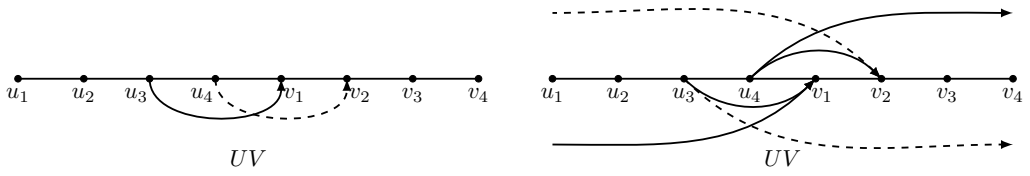

Figure 2.21.: Left: the incoming edges into v_2 w.r.t. V are in $E^-(V)$. Right: the incoming edges into v_2 w.r.t. V are in $E^+(V)$.

If the incoming edges into v_2 w.r.t. V are in $E^+(V)$, see Fig. 2.21 (right), then by planarity u_3v_2 is not in $E(UV)$. So $|U_{*3}||V_{2*}| = 4 \times 4 = 16$ patterns are incompatible. By planarity the edge u_3v_1, an outgoing edge from u_4 w.r.t. UV and an incoming edge into v_2 w.r.t. UV cannot be in $E(UV)$ together. Therefore at least

$$\min(|U_{*3}||V_{1*}|, |U_{*4}||\{\emptyset\}|, |\{\emptyset\}||V_{2*}|) = \min(4 \times 7, 7 \times 1, 1 \times 4) = 4$$

patterns are incompatible. By the same token, the edge u_4v_2, an incoming edge into v_1 w.r.t. UV and an outgoing edge from u_3 w.r.t. UV cannot coexist in $E(UV)$. Therefore at least

$$\min(|U_{*4}||V_{2*}|, |\{\emptyset\}||V_{1*}|, |U_{*3}||\{\emptyset\}|) = \min(7 \times 4, 1 \times 7, 4 \times 1) = 4$$

patterns are incompatible. So $16 + 4 + 4 = 24$ patterns are incompatible. Observe that this group, UV, has 120 patterns, which is the maximum number of patterns.

Case 1.1.2: V has incoming edges into more than one vertex. Then by Lemma 2.4 (iv), there are incoming edges into v_3 and v_2 and we have $|V_{3*}| = 2$, $|V_{2*}| \geq 3$ and $|V_{1*}| \geq 5$. We distinguish four scenarios based on which sides of V are containing the incoming edges into v_2 and v_3.

If the incoming edges into v_2 and v_3 w.r.t. V are in $E^-(V)$, see Fig. 2.22 (left), then both u_3v_1 and u_4v_2 can only be in $E^-(UV)$. By planarity both the edges cannot be in $E(UV)$. So at least $\min(|U_{*3}||V_{1*}|, |U_{*4}||V_{2*}|) = \min(4 \times 5, 7 \times 3) = 20$ patterns are incompatible. By the same token, both u_3v_2 and u_4v_3 can only be in $E^-(UV)$. By planarity both edges cannot be in $E(UV)$. So at least $\min(|U_{*3}||V_{2*}|, |U_{*4}||V_{3*}|) = \min(4 \times 3, 7 \times 2) = 12$ other patterns are incompatible. Overall, at least $20 + 12 = 32$ patterns are incompatible.

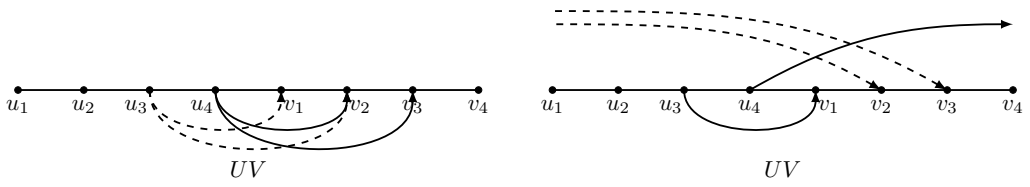

Figure 2.22.: Left: the incoming edges into v_2 and v_3 w.r.t. V are in $E^-(V)$. Right: the incoming edges into v_2 and v_3 w.r.t. V are in $E^+(V)$.

If the incoming edges into v_2 and v_3 w.r.t. V are in $E^+(V)$, see Fig. 2.22 (right), then by planarity both u_3v_2 and u_3v_3 are not in $E(UV)$. So at least $|U_{*3}||V_{2*}| + |U_{*3}||V_{3*}| = 4 \times 3 + 4 \times 2 = 20$ patterns are incompatible. By planarity incoming edges into v_2 and v_3 w.r.t. UV cannot coexist with outgoing edges from u_4 w.r.t. U and the edge u_3v_1. So at least

$$\min(|\{\emptyset\}||V_{2*}| + |\{\emptyset\}||V_{3*}|, |U_{*4}||\{\emptyset\}|, |U_{*3}||V_{1*}|) = \min(1 \times 3 + 1 \times 2, 7 \times 1, 4 \times 5) = 5$$

patterns are incompatible. So at least $20 + 5 = 25$ patterns are incompatible.

If the incoming edges into v_2 w.r.t. V are in $E^-(V)$ and the incoming edges into v_3 w.r.t. V are in $E^+(V)$, see Fig. 2.23 (left), then by planarity u_3v_3 is not in $E(UV)$. So at least $|U_{*3}||V_{3*}| = 4 \times 2 = 8$ patterns are incompatible. Also both u_3v_1 and u_4v_2 can only be in $E^-(UV)$. By planarity both edges cannot be in $E(UV)$. So at least $\min(|U_{*3}||V_{1*}|, |U_{*4}||V_{2*}|) = \min(4 \times 5, 7 \times 3) = 20$ patterns are incompatible. So at least

$8 + 20 = 28$ patterns are incompatible.

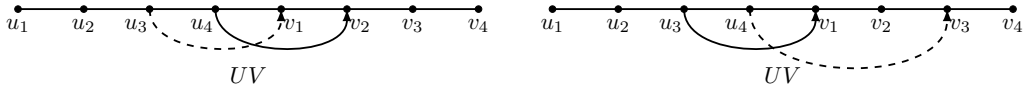

Figure 2.23.: Left: the incoming edges into v_2 w.r.t. V are in $E^-(V)$. Right: the incoming edges into v_2 w.r.t. V are in $E^+(V)$.

If the incoming edges into v_2 w.r.t. V are in $E^+(V)$ and the incoming edges into v_3 w.r.t. V are in $E^-(V)$, see Fig. 2.23 (right), then by planarity u_3v_2 is not in $E(UV)$. So at least $|U_{*3}||V_{2*}| = 4 \times 3 = 12$ patterns are incompatible. Also, both u_3v_1 and u_4v_3 can only be in $E^-(UV)$. By planarity both edges cannot be in $E(UV)$. So at least $\min(|U_{*3}||V_{1*}|, |U_{*4}||V_{3*}|) = \min(4 \times 5, 7 \times 2) = 14$ patterns are incompatible. So at least $12 + 14 = 26$ patterns are incompatible.

Case 1.2: U has outgoing edges from u_2 and u_3 and both are on the same side. By Lemma 2.4 (ii), $|U_{*2}| = 2$, $|U_{*3}| \geq 3$ and $|U_{*4}| \geq 5$. For simplicity assume that the outgoing edges are in $E^-(U)$.

Case 1.2.1: V has incoming edges into exactly one vertex. By Lemma 2.4 (iv), these are into v_2 and we have $|V_{2*}| = 4$ and $|V_{1*}| = 7$.

If the incoming edges into v_2 are in $E^-(V)$, see Fig. 2.24 (left), then both u_3v_1 and u_4v_2 can only be in $E^-(UV)$. By planarity both edges cannot be in $E(UV)$. So at least $\min(|U_{*3}||V_{1*}|, |U_{*4}||V_{2*}|) = \min(3 \times 7, 5 \times 4) = 20$ patterns are incompatible. By planarity an outgoing edge from u_4 w.r.t. UV, an incoming edges into v_1 w.r.t. UV and the edge u_2v_2 cannot coexist in $E(UV)$. So at least

$$\min(|U_{*4}||\{\emptyset\}|, |\{\emptyset\}||V_{1*}|, |U_{*2}||V_{2*}|) = \min(5 \times 1, 1 \times 7, 2 \times 4) = 5$$

patterns are incompatible. So in total at least $20 + 5 = 25$ incidence patterns are incompatible.

If the incoming edges into v_2 are in $E^+(V)$, see Fig. 2.24 (right), then by planarity u_2v_2 and u_3v_2 are not in $E(UV)$. So at least $|U_{*2}||V_{2*}| + |U_{*3}||V_{2*}| = 2 \times 4 + 3 \times 4 = 20$ patterns

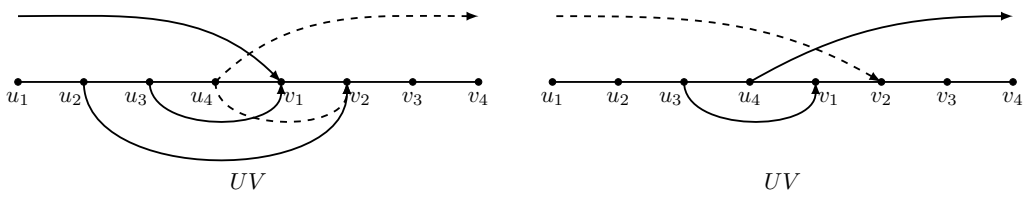

Figure 2.24.: Left: the incoming edges into v_2 w.r.t. V are in $E^-(V)$. Right: the incoming edges into v_2 w.r.t. V are in $E^+(V)$.

are incompatible. By planarity an outgoing edge from u_4 w.r.t. UV, an incoming edges into v_2 w.r.t. UV and the edge u_3v_1 cannot exist together in $E(UV)$. So at least

$$\min(|U_{*4}||\{\emptyset\}|, |\{\emptyset\}||V_{2*}|, |U_{*3}||V_{1*}|) = \min(5 \times 1, 1 \times 4, 3 \times 7) = 4$$

patterns are incompatible. So in total at least $20 + 4 = 24$ incidence patterns are incompatible.

Case 1.2.2: V has incoming edges into more than one vertex. Then by Lemma 2.4 (iv), there are incoming edges into v_3 and v_2 and we have $|V_{3*}| = 2$, $|V_{2*}| \geq 3$ and $|V_{1*}| \geq 5$. We distinguish four scenarios based on which sides of V are containing the incoming edges into v_2 and v_3.

If the incoming edges into v_2 and v_3 w.r.t. V are in $E^-(V)$, see Fig. 2.25 (left), then both u_3v_1 and u_4v_2 can only be in $E^-(UV)$. By planarity both the edges cannot be in $E(UV)$. So at least $\min(|U_{*3}||V_{1*}|, |U_{*4}||V_{2*}|) = \min(3 \times 5, 5 \times 3) = 15$ patterns are incompatible. By the same token, both u_2v_1 and u_4v_3 can only be in $E^-(UV)$. By planarity both the edges cannot be in $E(UV)$. So at least $\min(|U_{*2}||V_{1*}|, |U_{*4}||V_{3*}|) = \min(2 \times 5, 5 \times 2) = 10$ patterns are incompatible. So at least $15 + 10 = 25$ patterns are incompatible.

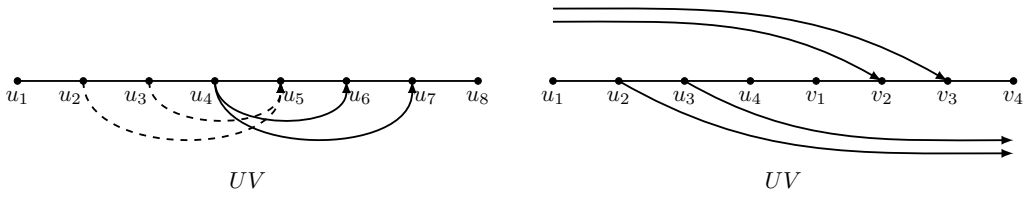

Figure 2.25.: Left: the incoming edges into v_2 and v_3 w.r.t. V are in $E^-(V)$. Right: the incoming edges into v_2 and v_3 w.r.t. V are in $E^+(V)$.

If the incoming edges into v_2 and v_3 w.r.t. V are in $E^+(V)$, see Fig. 2.25 (right), then

by planarity u_2v_2, u_2v_3, u_3v_2 and u_3v_3 are not in $E(UV)$. So at least

$$|U_{*2}||V_{2*}| + |U_{*2}||V_{3*}| + |U_{*3}||V_{2*}| + |U_{*3}||V_{3*}| = 2 \times 3 + 2 \times 2 + 3 \times 3 + 3 \times 2 = 25$$

patterns are incompatible.

If the incoming edges into v_2 w.r.t. V are in $E^-(V)$ and the incoming edges into v_3 w.r.t. V are in $E^+(V)$, see Fig. 2.26 (left), then by planarity u_2v_3 and u_3v_3 are not in $E(UV)$. So at least $|U_{*2}||V_{3*}| + |U_{*3}||V_{3*}| = 2 \times 2 + 3 \times 2 = 10$ patterns are incompatible. Both u_3v_1 and u_4v_2 can only be in $E^-(UV)$. By planarity both edges cannot be in $E(UV)$. So at least $\min(|U_{*3}||V_{1*}|, |U_{*4}||V_{2*}|) = \min(3 \times 5, 5 \times 3) = 15$ patterns are incompatible. So at least $10 + 15 = 25$ patterns are incompatible.

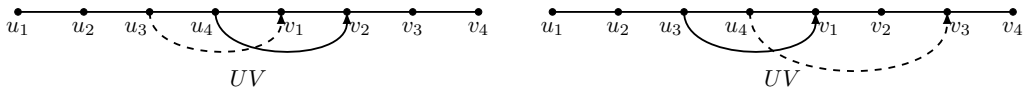

Figure 2.26.: Left: the incoming edges into v_2 w.r.t. V are in $E^-(V)$. Right: the incoming edges into v_2 w.r.t. V are in $E^+(V)$.

If the incoming edges into v_2 w.r.t. V are in $E^+(V)$ and the incoming edges into v_3 w.r.t. V are in $E^-(V)$, see Fig. 2.26 (right), then by planarity u_2v_2 and u_3v_2 are not in $E(UV)$. So at least $|U_{*2}||V_{2*}| + |U_{*3}||V_{2*}| = 2 \times 3 + 3 \times 3 = 15$ patterns are incompatible. Both u_3v_1 and u_4v_3 can only be in $E^-(UV)$. By planarity both the edges cannot be in $E(UV)$. So at least $\min(|U_{*3}||V_{1*}|, |U_{*4}||V_{3*}|) = \min(3 \times 5, 5 \times 2) = 10$ patterns are incompatible. So at least $15 + 10 = 25$ patterns are incompatible.

Case 1.3: U has outgoing edges from u_2 and u_3 and both are on opposite sides. By Lemma 2.4 (ii), $|U_{*2}| = 2$, $|U_{*3}| \geq 3$ and $|U_{*4}| \geq 5$. For simplicity assume that the outgoing edges from u_3 w.r.t. U are in $E^-(U)$.

Case 1.3.1: V has incoming edges into exactly one vertex. By Lemma 2.4 (iv), they are into v_2 and we have $|V_{2*}| = 4$ and $|V_{1*}| = 7$.

If the incoming edges into v_2 w.r.t. V are in $E^-(V)$, see Fig. 2.27 (left), then by planarity u_2v_2 is not in $E(UV)$. So at least $|U_{*2}||V_{2*}| = 2 \times 4 = 8$ patterns are incompatible. Also

both u_3v_1 and u_4v_2 can only be in $E^-(UV)$. By planarity both edges cannot be in $E(UV)$. So at least $\min(|U_{*3}||V_{1*}|, |U_{*4}||V_{2*}|) = \min(3 \times 7, 5 \times 4) = 20$ patterns are incompatible. So at least $8 + 20 = 28$ patterns are incompatible.

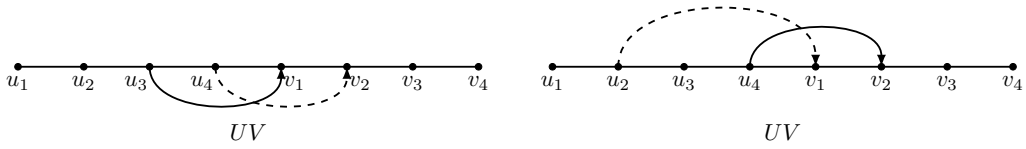

Figure 2.27.: Left: the incoming edges into v_2 w.r.t. V are in $E^-(V)$. Right: the incoming edges into v_2 w.r.t. V are in $E^+(V)$.

If the incoming edges into v_2 w.r.t. V are in $E^+(V)$, see Fig. 2.27 (right), then by planarity u_3v_2 is not in $E(UV)$. So at least $|U_{*3}||V_{2*}| = 3 \times 4 = 12$ patterns are incompatible. Also both u_2v_1 and u_4v_2 can only be in $E^+(UV)$. By planarity both edges cannot be in $E(UV)$. So at least $\min(|U_{*2}||V_{1*}|, |U_{*4}||V_{2*}|) = \min(2 \times 7, 5 \times 4) = 14$ patterns are incompatible. So at least $12 + 14 = 26$ patterns are incompatible.

Case 1.3.2: V has incoming edges into more than one vertex. Then by Lemma 2.4 (iv), there are incoming edges into v_3 and v_2 and we have $|V_{3*}| = 2$, $|V_{2*}| \geq 3$ and $|V_{1*}| \geq 5$. We distinguish four scenarios based on which sides of V are containing the incoming edges into v_2 and v_3.

If the incoming edges into v_2 and v_3 w.r.t. V are in $E^-(V)$, see Fig. 2.28 (left), then by planarity u_2v_2 and u_2v_3 are not in $E(UV)$. So at least $|U_{*2}||V_{2*}| + |U_{*2}||V_{3*}| = 2 \times 3 + 2 \times 2 = 10$ patterns are incompatible. Also both u_3v_1 and u_4v_2 can only be in $E^-(UV)$. By planarity both edges cannot be in $E(UV)$. So at least $\min(|U_{*3}||V_{1*}|, |U_{*4}||V_{2*}|) = \min(3 \times 5, 5 \times 3) = 15$ patterns are incompatible. So at least $10 + 15 = 25$ patterns are incompatible.

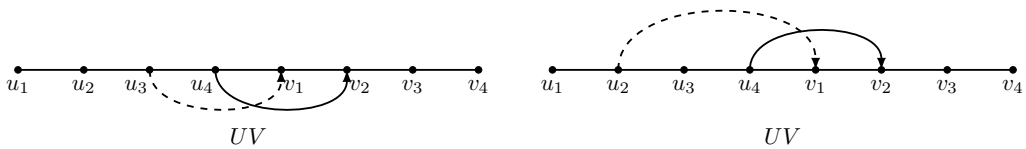

Figure 2.28.: Left: the incoming edges into v_2 and v_3 w.r.t. V are in $E^-(V)$. Right: the incoming edges into v_2 and v_3 w.r.t. V are in $E^+(V)$.

If the incoming edges into v_2 and v_3 w.r.t. V are in $E^+(V)$, see Fig. 2.28 (right), then

by planarity u_3v_2 and u_3v_3 are not in $E(UV)$. So at least $|U_{*3}||V_{2*}| + |U_{*3}||V_{3*}| = 3 \times 3 + 3 \times 2 = 15$ patterns are incompatible. Also both u_2v_1 and u_4v_2 can only be in $E^+(UV)$. By planarity both edges cannot be in $E(UV)$. So at least $\min(|U_{*2}||V_{1*}|, |U_{*4}||V_{2*}|) = \min(2 \times 5, 5 \times 3) = 10$ patterns are incompatible. So at least $15 + 10 = 25$ patterns are incompatible.

If the incoming edges into v_2 w.r.t. V is in $E^-(V)$ and the incoming edges into v_3 w.r.t. V are in $E^+(V)$, see Fig. 2.29 (left), then both u_2v_1 and u_4v_3 can only be in $E^+(UV)$. By planarity both edges cannot be in $E(UV)$. So at least $\min(|U_{*2}||V_{1*}|, |U_{*4}||V_{3*}|) = \min(2 \times 5, 5 \times 2) = 10$ patterns are incompatible. By similar token both u_3v_1 and u_4v_2 can only be in $E^-(UV)$. By planarity both edges cannot be in $E(UV)$. So at least $\min(|U_{*3}||V_{1*}|, |U_{*4}||V_{2*}|) = \min(3 \times 5, 5 \times 3) = 15$ patterns are incompatible. So at least $10 + 15 = 25$ patterns are incompatible.

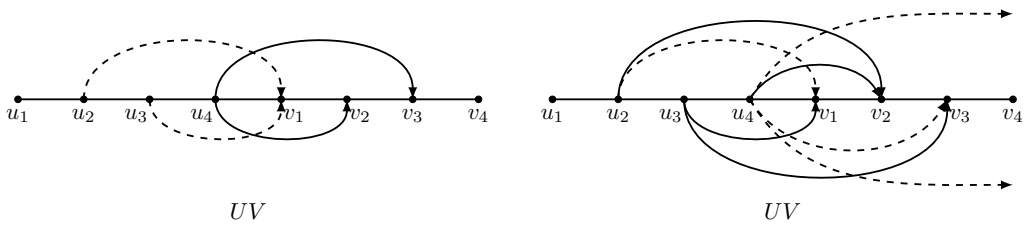

Figure 2.29.: Left: the incoming edges into v_2 w.r.t. V are in $E^-(V)$. Right: the incoming edges into v_2 w.r.t. V are in $E^+(V)$.

If the incoming edges into v_2 w.r.t. V is in $E^+(V)$ and the incoming edges into v_3 w.r.t. V are in $E^-(V)$, see Fig. 2.29 (right), then both u_2v_1 and u_4v_2 can only be in $E^+(UV)$. By planarity both edges cannot be in $E(UV)$. So at least

$$\min(|U_{*2}||V_{1*}|, |U_{*4}||V_{2*}|) = \min(2 \times 5, 5 \times 3) = 10$$

patterns are incompatible. Also both u_3v_1 and u_4v_3 can only be in $E^-(UV)$. By planarity both edges cannot be in $E(UV)$. So at least

$$\min(|U_{*3}||V_{1*}|, |U_{*4}||V_{3*}|) = \min(3 \times 5, 5 \times 2) = 10$$

patterns are incompatible. By planarity an outgoing edge from u_4 w.r.t. UV, the edge

u_2v_2 and the edge u_3v_3 cannot exist together in $E(UV)$. So at least

$$\min(|U_{*4}||\{\emptyset\}|, |U_{*2}||V_{2*}|, |U_{*3}||V_{3*}|) = \min(5 \times 1, 2 \times 3, 3 \times 2) = 5$$

patterns are incompatible. So in total at least $10 + 10 + 5 = 25$ incidence patterns are incompatible.

Case 2: $|I(U)| = 13$. By Lemma 2.5, U is either A or A^R. If U is A^R, then after reflecting UV about the horizontal axis, U is A. We analyze the cases based on this assumption. Since $|I(UV)| \leq |I(U)| \cdot |I(V)| = 13 \times 12 = 156$, it suffices to show that at least $156 - 120 = 36$ of these patterns are incompatible.

Case 2.1: V has incoming edges into exactly one vertex. Then by Lemma 2.4 (iv), they are into v_2 and we have $|V_{2*}| = 4$ and $|V_{1*}| = 7$.

If the incoming edges into v_2 w.r.t. V are in $E^-(V)$, see Fig. 2.30 (left), then by planarity u_2v_2 is not in $E(UV)$. So at least $|U_{*2}||V_{2*}| = 2 \times 4 = 8$ patterns are incompatible. Both u_3v_1 and u_4v_2 can only be in $E^-(UV)$. By planarity both edges cannot be in $E(UV)$. So at least $\min(|U_{*3}||V_{1*}|, |U_{*4}||V_{2*}|) = \min(4 \times 7, 6 \times 4) = 24$ patterns are incompatible. By planarity an outgoing edge from u_4 w.r.t. UV, the edge u_2v_1 and the edge u_3v_2 cannot exist together in $E(UV)$. So at least

$$\min(|U_{*4}||\{\emptyset\}|, |U_{*2}||V_{1*}|, |U_{*3}||V_{2*}|) = \min(6 \times 1, 2 \times 7, 4 \times 4) = 6$$

patterns are incompatible. So in total at least $8 + 24 + 6 = 38$ incidence patterns are incompatible.

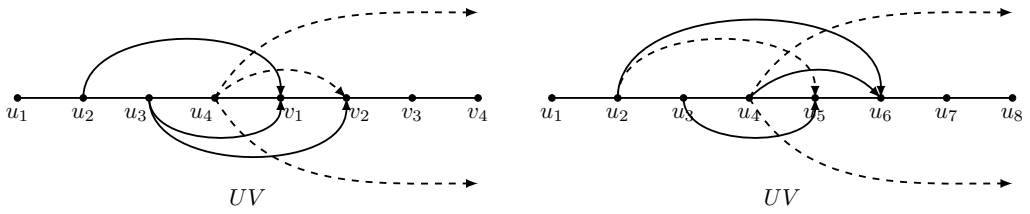

Figure 2.30.: Left: the incoming edges into v_2 w.r.t. V are in $E^-(V)$. Right: the incoming edges into v_2 w.r.t. V are in $E^+(V)$.

If the incoming edges into v_2 w.r.t. V are in $E^+(V)$, see Fig. 2.30 (right), then by

planarity u_3v_2 is not allowed. So at least $|U_{*3}||V_{2*}| = 4\times4 = 16$ patterns are incompatible. Both u_2v_1 and u_4v_2 can only be in $E^+(UV)$. By planarity both edges cannot be in $E(UV)$. So at least $\min(|U_{*2}||V_{1*}|, |U_{*4}||V_{2*}|) = \min(2 \times 7, 6 \times 4) = 14$ patterns are incompatible. By planarity an outgoing edge from u_4 w.r.t. UV, the edge u_2v_2 and the edge u_3v_1 cannot exist together in $E(UV)$. So at least

$$\min(|U_{*4}||\{\emptyset\}|, |U_{*2}||V_{2*}|, |U_{*3}||V_{1*}|) = \min(6 \times 1, 2 \times 4, 4 \times 7) = 6$$

patterns are incompatible. So at least $16 + 14 + 6 = 36$ patterns are incompatible.

Case 2.2: V has incoming edges into more than one vertex. By Lemma 2.4 (iv), there are incoming edges into v_3 and v_2 and we have $|V_{3*}| = 2$, $|V_{2*}| \geq 3$ and $|V_{1*}| \geq 5$. We distinguish four scenarios based on which sides of V are containing the incoming edges into v_2 and v_3.

If the incoming edges into v_2 and v_3 w.r.t. V are in $E^-(V)$, see Fig. 2.31 (left), then by planarity u_2v_2 is not in $E(UV)$. So at least $|U_{*2}||V_{2*}| = 2 \times 3 = 6$ patterns are incompatible. Both u_3v_1 and u_4v_2 can only be in $E^-(UV)$. By planarity both edges cannot be in $E(UV)$. So at least $\min(|U_{*3}||V_{1*}|, |U_{*4}||V_{2*}|) = \min(4 \times 5, 6 \times 3) = 18$ patterns are incompatible. Similarly both u_3v_2 and u_4v_3 can only be in $E^-(UV)$. By planarity both edges cannot be in $E(UV)$. So at least $\min(|U_{*3}||V_{2*}|, |U_{*4}||V_{3*}|) = \min(4\times 3, 6 \times 2) = 12$ patterns are incompatible. So at least $6 + 18 + 12 = 36$ patterns are incompatible.

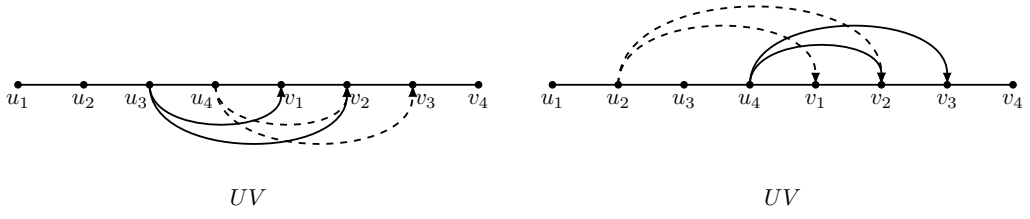

Figure 2.31.: Left: the incoming edges into v_2 and v_3 w.r.t. V are in $E^-(V)$. Right: the incoming edges into v_2 and v_3 w.r.t. V are in $E^+(V)$.

If the incoming edges into v_2 and v_3 w.r.t. V are in $E^+(V)$, see Fig. 2.31 (right), then

by planarity both u_3v_2 and u_3v_3 are not in $E(UV)$. So at least

$$|U_{*3}||V_{2*}| + |U_{*3}||V_{3*}| = 4 \times 3 + 4 \times 2 = 20$$

patterns are incompatible. Also both u_2v_1 and u_4v_2 can only be in $E^+(UV)$. By planarity both edges cannot be in $E(UV)$. So at least

$$\min(|U_{*2}||V_{1*}|, |U_{*4}||V_{2*}|) = \min(2 \times 5, 6 \times 3) = 10$$

patterns are incompatible. Similarly both u_2v_2 and u_4v_3 can only be in $E^+(UV)$. By planarity both edges cannot be in $E(UV)$. So at least

$$\min(|U_{*2}||V_{2*}|, |U_{*4}||V_{3*}|) = \min(2 \times 3, 6 \times 2) = 6$$

patterns are incompatible. So at least $20 + 10 + 6 = 36$ patterns are incompatible.

If the incoming edges into v_2 w.r.t. V is in $E^-(V)$ and the incoming edges into v_3 w.r.t. V are in $E^+(V)$, see Fig. 2.32 (left), then by planarity u_3v_3 is not in $E(UV)$. So at least $|U_{*3}||V_{3*}| = 4 \times 2 = 8$ patterns are incompatible. Both u_2v_1 and u_4v_3 can only be in $E^+(UV)$. By planarity both edges cannot be in $E(UV)$. So at least $\min(|U_{*2}||V_{1*}|, |U_{*4}||V_{3*}|) = \min(2 \times 5, 6 \times 2) = 10$ patterns are incompatible. Similarly both u_3v_1 and u_4v_2 can only be in $E^-(UV)$. By planarity both edges cannot be in $E(UV)$. So at least $\min(|U_{*3}||V_{1*}|, |U_{*4}||V_{2*}|) = \min(4 \times 5, 6 \times 3) = 18$ patterns are incompatible. So at least $8 + 10 + 18 = 36$ patterns are incompatible.

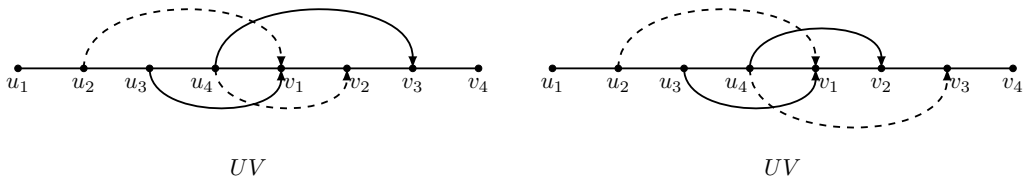

Figure 2.32.: Left: the incoming edges into v_2 w.r.t. V are in $E^-(V)$. Right: the incoming edges into v_2 w.r.t. V are in $E^+(V)$.

If the incoming edges into v_2 w.r.t. V is in $E^+(V)$ and the incoming edges into v_3 w.r.t. V are in $E^-(V)$, see Fig. 2.32 (right), then by planarity both u_2v_3 and u_3v_2 are not

in $E(UV)$. So at least $|U_{*2}||V_{3*}|+|U_{*3}||V_{2*}| = 2\times2+4\times3 = 16$ patterns are incompatible. Both u_2v_1 and u_4v_2 can only be in $E^+(UV)$. By planarity both edges cannot be in $E(UV)$. So at least $\min(|U_{*2}||V_{1*}|, |U_{*4}||V_{2*}|) = \min(2\times5, 6\times3) = 10$ patterns are incompatible. Similarly both u_3v_1 and u_4v_3 can only be in $E^-(UV)$. By planarity both edges cannot be in $E(UV)$. So at least $\min(|U_{*3}||V_{1*}|, |U_{*4}||V_{3*}|) = \min(4\times5, 6\times2) = 12$ patterns are incompatible. So at least $16+10+12 = 38$ patterns are incompatible. □

Lemma 2.9. *Consider a group UV consisting of two consecutive groups of 4 vertices, where $|I(U)| = |I(V)| = 13$. Then UV allows at most 120 incidence patterns.*

Proof. By Lemma 2.5, U is either A or A^R. We may assume, after reflecting UV about a horizontal axis, that U is A. Therefore $|U_{*2}| = 2$, $|U_{*3}| = 4$ and $|U_{*4}| = 6$, see Fig. 2.10. Similarly, Lemma 2.5 implies that V is either A or A^R. We distinguish two cases depending on whether V is A or A^R. The cross product of $I(U)$ and $I(V)$ yields $13\times13 = 169$ possible patterns. It suffices to show that at least $169-120 = 49$ of these patterns are incompatible.

Case 1: V is A, see Fig. 2.33 (left). By planarity u_2v_3 and u_3v_2 are not in $E(UV)$. So at least $|U_{*2}||V_{3*}|+|U_{*3}||V_{2*}| = 2\times2+4\times4 = 20$ patterns are incompatible. Further, u_2v_1 and u_4v_2 can only be in $E^+(UV)$. By planarity both edges cannot be in $E(UV)$. Hence at least $\min(|U_{*2}||V_{1*}|, |U_{*4}||V_{2*}|) = \min(2\times6, 6\times4) = 12$ patterns are incompatible. Similarly u_3v_1 and u_4v_3 can only be in $E^-(UV)$. By planarity both edges cannot be in $E(UV)$. Therefore at least $\min(|U_{*3}||V_{1*}|, |U_{*4}||V_{3*}|) = \min(4\times6, 6\times2) = 12$ patterns are incompatible. By planarity an outgoing edge from u_4 w.r.t. UV and the edges u_2v_2 and u_3v_1 cannot exist together in $E(UV)$. So at least

$$\min(|U_{*4}||\emptyset|, |U_{*2}||V_{2*}|, |U_{*3}||V_{3*}|) = \min(6\times1, 2\times4, 4\times2) = 6$$

patterns are incompatible. Overall, at least $20+12+12+6 = 50$ patterns are incompatible.

Case 2: V is A^R, see Fig. 2.33 (right). By planarity u_2v_2 and u_3v_3 are not in $E(UV)$. So at least $|U_{*2}||V_{2*}|+|U_{*3}||V_{3*}| = 2\times4+4\times2 = 16$ patterns are incompatible. Also u_2v_1

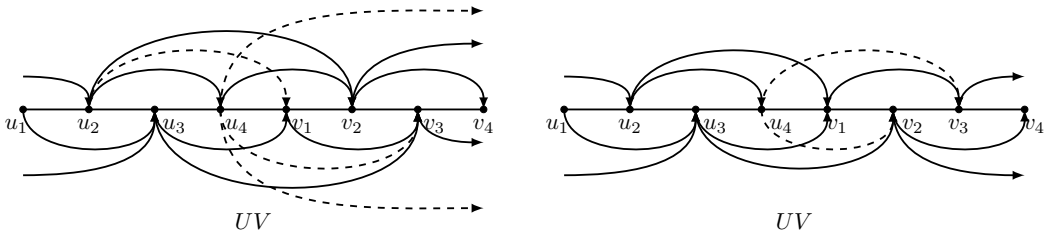

Figure 2.33.: Left: V is A. Right: V is A^R.

and u_4v_3 can only be in $E^+(UV)$. By planarity both edges cannot be in $E(UV)$. Hence at least $\min(|U_{*2}||V_{1*}|, |U_{*4}||V_{3*}|) = \min(2 \times 6, 6 \times 2) = 12$ patterns are incompatible. Similarly u_3v_1 and u_4v_2 can only be in $E^-(UV)$. By planarity both edges cannot be in $E(UV)$. Hence at least $\min(|U_{*3}||V_{1*}|, |U_{*4}||V_{2*}|) = \min(4 \times 6, 6 \times 4) = 24$ patterns are incompatible. Overall, at least $16 + 12 + 24 = 52$ patterns are incompatible. □

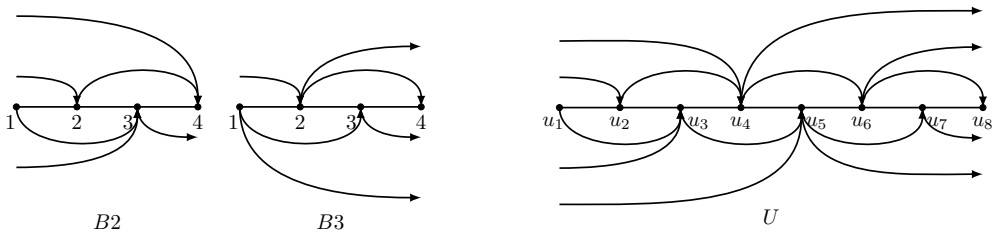

Figure 2.34.: U has 120 patterns. The 24 missing patterns are 123678, 12367, 12368, 1236, 123, 13678, 1367, 1368, 136, 13, 23678, 2367, 2368, 236, 23, 3678, 367, 368, 36, 3, 678, 67, 68, 6.

Lemma 2.10. *Every group on 8 vertices has at most 120 incidence patterns, and this bound is the best possible. Consequently,* $p_8 = 120$.

Proof. A group of 8, denoted by UV, where U and V are the groups induced by the first and last four vertices of UV, respectively. If $|I(U)| \leq 9$ or $|I(V)| \leq 9$, then $|I(UV)| \leq |I(U)| \cdot |I(V)| \leq 9 \times 13 = 117$ by Lemma 2.5. Otherwise, Lemmas 2.6–2.9 show that $|I(UV)| \leq 120$.

Consider the group $(U, E^-(U), E^+(U))$ of 8 vertices depicted in Fig. 2.34 (right). The first and second half of U are the groups $B2$ and $B3$ in Fig. 2.34 (left), each with 12 patterns. Observe that exactly 24 patterns are incompatible, thus U has exactly $|I(B2)| \cdot |I(B3)| - 24 = 12 \times 12 - 24 = 120$ patterns. Aside from reflections, the extremal group of 8 vertices in Fig. 2.34 (right) is unique. □

2.5. Groups of 9, 10, and 11 vertices via computer search

The application of the same fingerprinting technique to groups of 9, 10, and 11 vertices via a computer program[2] shows the following.

A group of 9 vertices allows at most 201 incidence patterns; the extremal configuration appears in Fig. 2.35. This yields the upper bound of $O(n^3\,201^{n/9}) = O(1.8027^n)$ for the number of monotone paths in an n-vertex triangulation. Aside from reflections, the extremal group of 9 vertices in Fig. 2.35 (left) is unique.

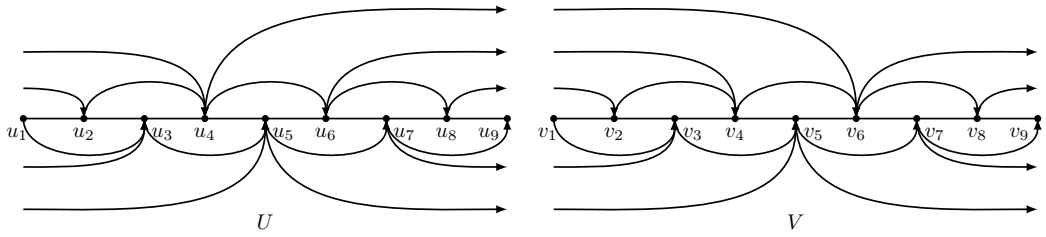

Figure 2.35.: Groups U and V (hence also U^R and V^R) are the only groups of 9 vertices with 201 incidence patterns. Observe that V is the reflection of U in the y-axis.

A group of 10 vertices allows at most 346 incidence patterns; the extremal configuration appears in Fig. 2.36. This yields the upper bound of $O(n^3\,346^{n/10}) = O(1.7944^n)$ for the number of monotone paths in an n-vertex triangulation, as given in Theorem 2.1. Aside from reflections, the extremal group of 10 vertices in Fig. 2.36 is unique.

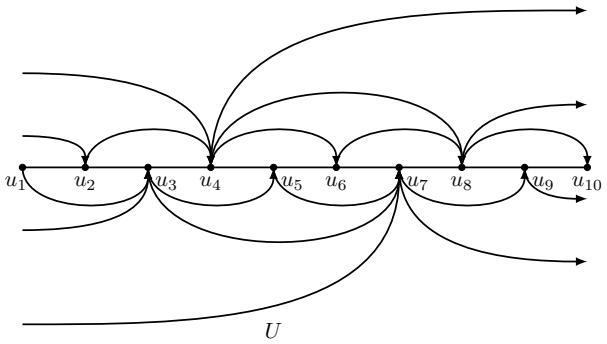

Figure 2.36.: Group U (hence also U^R) is the only group of 10 vertices with 346 incidence patterns. Observe that the reflection of U in the y-axis is U^R.

A group of 11 vertices allows at most 591 incidence patterns; the extremal configuration appears in Fig. 2.37. This yields the upper bound of $O(n^3\,591^{n/11}) = O(1.7864^n)$ for the

[2]Refer to the Appendix or the `.c` file at `arXiv:1608.04812`.

number of monotone paths in an n-vertex triangulation. Aside from reflections, the extremal group of 11 vertices in Fig. 2.37 (left) is unique.

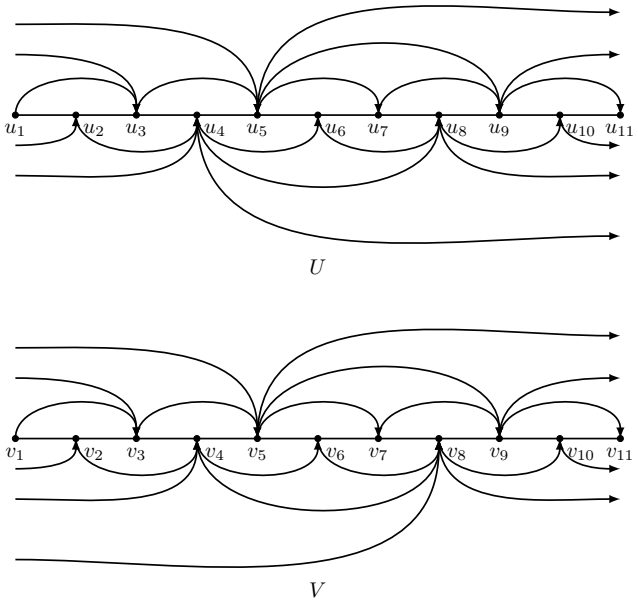

Figure 2.37.: Groups U and V (hence also U^R and V^R) are the only groups of 11 vertices with 591 incidence patterns. Observe that V is the reflection of U in the y-axis.

To generate all groups of k vertices, the program first generates all possible *sides* of k vertices, essentially by brute force. A side of k vertices $V = \{v_1, \dots v_k\}$ is represented by a directed planar graph with $k+2$ vertices, where the edges v_0v_i and v_iv_{k+1}, for $1 \leq i \leq k$, denote an incoming edge into v_i and an outgoing edge from v_i, respectively. The edge v_0v_{k+1} represents the $\emptyset$ pattern. Note that $\xi_0 \cup v_0v_{k+1}$ forms a plane cycle on $k+2$ vertices in the underlying undirected graph. Therefore, $E^+(V)$ and $E^-(V)$ can each have at most $(k+2)-3 = k-1$ edges. After all possible sides are generated, the program combines all pairs of sides with no common inner edge to generate a group $(V, E^-(V), E^+(V))$. For each generated group, the program calculates the corresponding number of patterns and in the end returns the group with the maximum number of patterns.

Remark. It is interesting to observe how the structure of the unique extremal groups of 9, 10 and 11 vertices (depicted in Figs. 2.35, 2.36 and 2.37) match that of the current best lower bound construction illustrated in Fig. 2.2 (right).

2.6. Conclusion

A path is *simple* if it has no repeated vertices; obviously every monotone path is simple. A directed polygonal path $\xi = (v_1, v_2, \ldots, v_t)$ in $\mathbb{R}^d$ is *weakly monotone* if there exists a nonzero vector $\mathbf{u} \in \mathbb{R}^d$ that has a nonnegative inner product with every directed edge of ξ, that is, $\langle \overrightarrow{v_i v_{i+1}}, \mathbf{u} \rangle \geq 0$ for $i = 1, \ldots, t-1$. In many applications such as local search, a weakly monotone path may be as good as a monotone one, since both guarantee that the objective function is nondecreasing.

It therefore appears as a natural problem to find a tight asymptotic bound on the maximum number of weakly monotone simple paths over all plane geometric graphs with n vertices. As for monotone paths, it is easy to see that triangulations maximize the number of such paths. Recall that μ_n denotes the maximum number (over all directions $\mathbf{u}$) of maximal $\mathbf{u}$-monotone paths in an n-vertex triangulation. Let β_n denote the maximum number (over all directions $\mathbf{u}$) of maximal *weakly* $\mathbf{u}$-monotone simple paths in an n-vertex triangulation.

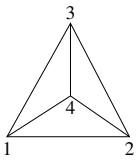

Figure 2.38.: A triangulation of 4 points: the vertices and the center of an equilateral triangle. Note that any two nonadjacent edges are orthogonal.

We clearly have $\beta_n \geq \mu_n$, and so $\beta_n = \Omega(1.7003^n)$. However, β_n could in principle grow faster than μ_n. Let $n = 4$ and consider the three vertices and the center of an equilateral triangle, and the unique triangulation of these four points; shown in Fig 2.38. Observe that: (i) the 5 paths 132, 1342, 142, 1432, and 12 are weakly $\mathbf{u}$-monotone and maximal, where $\mathbf{u} = (1, 0)$ and yield $\beta_4 = 5$; (ii) the 4 paths 143, 142, 12, and 13 are $\mathbf{u}$-monotone and maximal, where $\mathbf{u} = (\cos \pi/6, \sin \pi/6)$ and yield $\mu_4 = 4$; and so $\beta_4 > \mu_4$.

We conclude with the following open problems.

1. What upper and lower bounds can be derived for β_n? Is $\beta_n = \omega(\mu_n)$?
2. What can be said about counting and enumeration of weakly monotone paths in a given plane geometric graph?

2.7. Extremal configurations

The groups of 4 **vertices with** 12 **and** 11 **patterns.** There are exactly 4 groups with exactly 12 incidence patterns (modulo reflections about the x-axis); see Fig. 2.39.

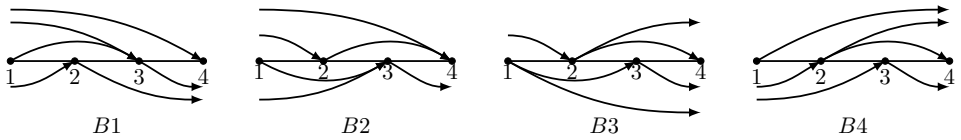

Figure 2.39.: $B1$–$B4$ are the only four groups with 12 incidence patterns.

$I(B1) = \{\emptyset, 1234, 123, 12, 134, 13, 234, 23, 2, 34, 3, 4\}$.

$I(B2) = \{\emptyset, 1234, 123, 124, 134, 13, 234, 23, 24, 34, 3, 4\}$.

$I(B3) = \{\emptyset, 1234, 123, 124, 12, 134, 13, 1, 23, 234, 24, 2\}$.

$I(B4) = \{\emptyset, 1234, 123, 124, 12, 1, 23, 234, 24, 2, 34, 3\}$.

There are exactly 20 groups with exactly 11 incidence patterns (modulo reflections about the x-axis); see Fig. 2.40.

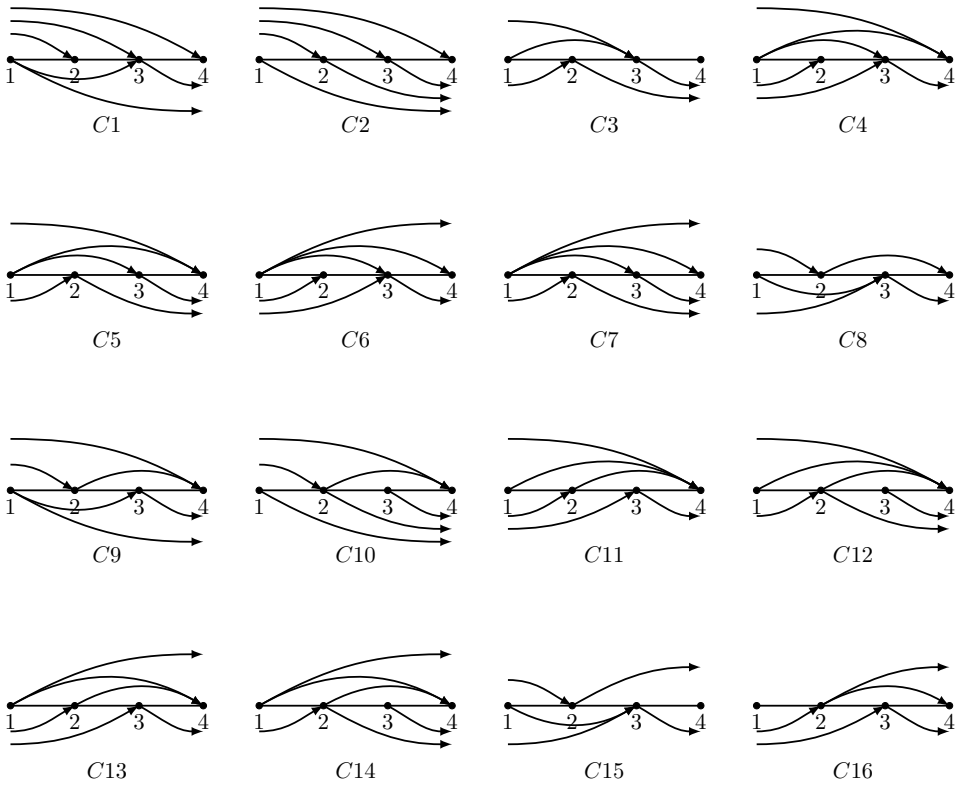

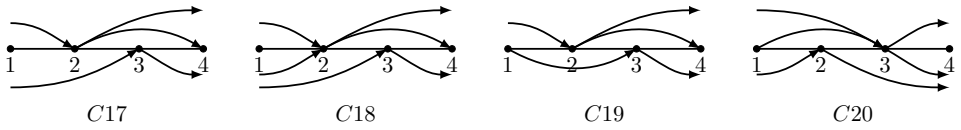

Figure 2.40.: $C1$–$C20$ are the only 20 groups with 11 incidence patterns.

$I(C1) = \{\emptyset, 1234, 123, 134, 13, 1, 234, 23, 34, 3, 4\}$.

$I(C2) = \{\emptyset, 1234, 123, 12, 1, 234, 23, 2, 34, 3, 4\}$.

$I(C3) = \{\emptyset, 1234, 123, 12, 134, 13, 234, 23, 2, 34, 3\}$.

$I(C4) = \{\emptyset, 1234, 123, 134, 13, 14, 234, 23, 34, 3, 4\}$.

$I(C5) = \{\emptyset, 1234, 123, 12, 134, 13, 14, 234, 23, 2, 4\}$.

$I(C6) = \{\emptyset, 1234, 123, 134, 13, 14, 1, 234, 23, 34, 3\}$.

$I(C7) = \{\emptyset, 1234, 123, 12, 134, 13, 14, 1, 234, 23, 2\}$.

$I(C8) = \{\emptyset, 1234, 123, 124, 134, 13, 234, 23, 24, 34, 3\}$.

$I(C9) = \{\emptyset, 1234, 123, 124, 134, 13, 1, 234, 23, 24, 4\}$.

$I(C10) = \{\emptyset, 1234, 123, 124, 12, 1, 234, 23, 24, 2, 4\}$.

$I(C11) = \{\emptyset, 1234, 123, 124, 14, 234, 23, 24, 34, 3, 4\}$.

$I(C12) = \{\emptyset, 1234, 123, 124, 12, 14, 234, 23, 24, 2, 4\}$.

$I(C13) = \{\emptyset, 1234, 123, 124, 14, 1, 234, 23, 24, 34, 3\}$.

$I(C14) = \{\emptyset, 1234, 123, 124, 12, 14, 1, 234, 23, 24, 2\}$.

$I(C15) = \{\emptyset, 1234, 123, 12, 134, 13, 234, 23, 2, 34, 3\}$.

$I(C16) = \{\emptyset, 1234, 123, 124, 12, 234, 23, 24, 2, 34, 3\}$.

$I(C17) = \{\emptyset, 1234, 123, 124, 12, 234, 23, 24, 2, 34, 3\}$.

$I(C18) = \{\emptyset, 1234, 123, 124, 12, 234, 23, 24, 2, 34, 3\}$.

$I(C19) = \{\emptyset, 1234, 123, 124, 12, 134, 13, 234, 23, 24, 2\}$.

$I(C20) = \{\emptyset, 1234, 123, 12, 134, 13, 234, 23, 2, 34, 3\}$.

Bibliography

[1] I. Adler, C. Papadimitriou, and A. Rubinstein, On simplex pivoting rules and complexity theory, *Proc. 17th IPCO*, LNCS 8494, Springer, 2014, pp. 13–24.

[2] M. Ajtai, V. Chvátal, M. Newborn, and E. Szemerédi, Crossing-free subgraphs, *Ann. Discrete Math.* **12** (1982), 9–12.

[3] M. de Berg, O. Cheong, M. van Kreveld, and M. Overmars, *Computational Geometry*, 3rd edition, Springer, 2008.

[4] K. Buchin, C. Knauer, K. Kriegel, A. Schulz, and R. Seidel. On the number of cycles in planar graphs, in *Proc. 13th COCOON*, LNCS 4598, Springer, 2007, pp. 97–107.

[5] A. Dumitrescu, M. Löffler, A. Schulz, and Cs. D. Tóth, Counting carambolas, *Graphs Combin.* **32(3)** (2016), 923–942.

[6] A. Dumitrescu, G. Rote, and Cs. D. Tóth, Monotone paths in planar convex subdivisions and polytopes, in *Discrete Geometry and Optimization*, vol. 69 of *Fields Inst. Commun.*, 2013, Springer, pp. 79–104.

[7] A. Dumitrescu, A. Schulz, A. Sheffer, and Cs. D. Tóth, Bounds on the maximum multiplicity of some common geometric graphs, *SIAM J. Discrete Math.* **27(2)** (2013), 802–826.

[8] A. Dumitrescu and Cs. D. Tóth, Computational Geometry Column 54, *SIGACT News Bulletin* **43(4)** (2012), 90–97.

[9] A. Dumitrescu and Cs. D. Tóth, Convex polygons in geometric triangulations, *Combin. Probab. Comput.* **26(5)** (2017), 641–659.

[10] A. García, M. Noy and A. Tejel, Lower bounds on the number of crossing-free subgraphs of K_N, *Comput. Geom.* **16(4)** (2000), 211–221.

[11] B. Gärtner and V. Kaibel, Two new bounds for the random-edge simplex-algorithm, *SIAM J. Discrete Math.* **21(1)** (2007), 178–190.

[12] V. Kaibel, R. Mechtel, M. Sharir, and G. M. Ziegler, The simplex algorithm in dimension three, *SIAM J. Comput.* **34(2)** (2005), 475–497.

[13] G. Kalai, Upper bounds for the diameter and height of graphs of convex polyhedra, *Discrete Comput. Geom.* **8(4)** (1992), 363–372.

[14] G. Kalai, Polytope skeletons and paths, in *Handbook of Discrete and Computational Geometry* (J. Goodman, J. O'Rourke, and C. D. Tóth, editors), Chapter 19, pp. 505–532, 3rd edition, CRC Press, Boca Raton, FL, 2017.

[15] V. Klee, Paths on polyhedra I, *J. SIAM* **13(4)** (1965), 946–956.

[16] M. van Kreveld, M. Löffler, and J. Pach, How many potatoes are in a mesh?, in *Proc. 23rd ISAAC*, LNCS 7676, Springer, 2012, pp. 166–176.

[17] J. Matoušek and T. Szabó, RANDOM EDGE can be exponential on abstract cubes, *Adv. Math.* **204(1)** (2006), 262–277.

[18] J. Pach and G. Tóth, Monotone drawings of planar graphs, *J. Graph Theory* **46** (2004), 39–47. Corrected version: `arXiv:1101.0967`, 2011.

[19] A. Razen, J. Snoeyink, and E. Welzl, Number of crossing-free geometric graphs vs. triangulations, *Electron. Notes Discrete Math.* **31** (2008), 195–200.

[20] F. Santos, A counterexample to the Hirsch conjecture, *Ann. of Math.* **176(1)**(2012), 383–412.

[21] F. Santos, Recent progress on the combinatorial diameter of polytopes and simplicial complexes, *TOP* **21(3)** (2013), 426–460.

[22] M. Sharir and A. Sheffer, Counting triangulations of planar point sets, *Electron. J. Combin.* **18** (2011), P70.

[23] M. Sharir and A. Sheffer, Counting plane graphs: cross-graph charging schemes, *Combin. Probab. Comput.* **22(6)** (2013), 935–954.

[24] M. Sharir, A. Sheffer, and E. Welzl, Counting plane graphs: perfect matchings, spanning cycles, and Kasteleyn's technique, *J. Combin. Theory, Ser. A* **120(4)** (2013), 777–794.

[25] M. Sharir and E. Welzl, On the number of crossing-free matchings, cycles, and partitions, *SIAM J. Comput.* **36(3)** (2006), 695–720.

[26] A. Sheffer, Numbers of plane graphs, `https://adamsheffer.wordpress.com/numbers-of-plane-graphs/` (version of April, 2016).

[27] M. J. Todd, The monotonic bounded Hirsch conjecture is false for dimension at least 4, *Math. Oper. Res.* **5(4)** (1980), 599–601.

[28] M. J. Todd, An improved Kalai-Kleitman bound for the diameter of a polyhedron, *SIAM J. Discrete Math.* **28** (2014), 1944–1947.

[29] G. M. Ziegler, *Lectures on Polytopes*, vol. 152 of GTM, Springer, 1994, pp. 83–93.

3. Pseudoline Arrangements

3.1. Introduction

Arrangements of pseudolines. A *pseudoline* in the Euclidean plane is an x-monotone curve extending from negative infinity to positive infinity. An *(Euclidean) arrangement of pseudolines* is a family of pseudolines where each pair of pseudolines has a unique point of intersection (called '*vertex*'). An arrangement is *simple* if no three pseudolines have a common point of intersection, see Fig. 3.1 (left). Throughout this chapter the term arrangement always means simple arrangement if not specified otherwise.

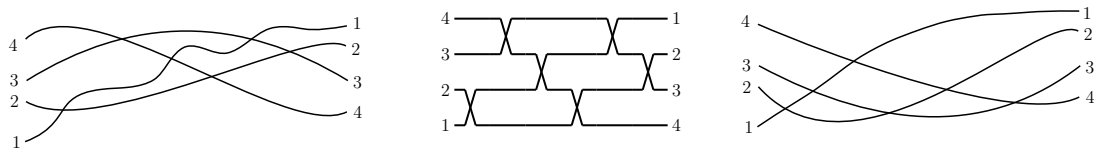

Figure 3.1.: Left: A simple arrangement $\mathcal{A}$. Center: Wiring diagram of $\mathcal{A}$. Right: An arrangement $\mathcal{A}'$ that is not isomorphic to the arrangement $\mathcal{A}$ on the left.

Topological sweep of an arrangement. A pseudoline is swept over the plane visiting all the vertices and pseudoline segments. This sweeping movement is called a *topological sweep* (*sweep*, for short). Formally, a sweep of an arrangement $\mathcal{A}$, is a sequence $c_0, c_1, \ldots, c_r$ of curves (where $r = \binom{n}{2}$) with same end points and following properties, see Fig. 3.2 (right).

1. Each curve c_i has exactly one point of intersection with each pseudoline of $\mathcal{A}$ and does not contain any vertices of $\mathcal{A}$.

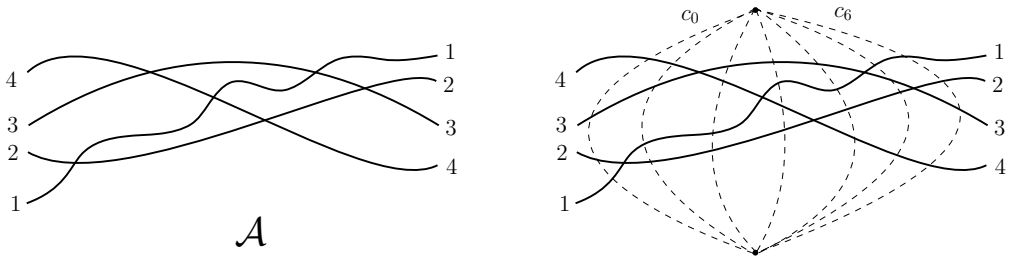

Figure 3.2.: Left: A simple arrangement $\mathcal{A}$. Right: A topological sweep for $\mathcal{A}$.

2. Any two curves c_i and c_j are interiorly disjoint. The interior of the region made by two consecutive curves contain exactly one vertex of $\mathcal{A}$. Hence, the interior of the closed curve $c_0 \cup c_r$ contains all vertices of $\mathcal{A}$.

There is a sweep sequence for every arrangement [37, Lemma 6.1]. If $c_0, c_1, \ldots, c_r$ is a sweep then the reverse $c_r, c_{r-1}, \ldots, c_1$ is also a topological sweep. Here we only consider left to right sweeps.

Representations related to arrangements. There are several combinatorial representations and encodings of pseudoline arrangements. These representations help one count the number of such arrangements.

A *wiring diagram* is a Euclidean arrangement of pseudolines consisting of piece-wise linear 'wires', each horizontal except for a short segment where it crosses another wire. Each pair of wires cross exactly once; see Fig. 3.3 (left).

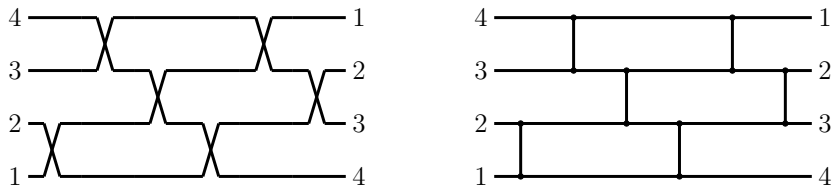

Figure 3.3.: Left: Wiring diagram of $\mathcal{A}$. Right: Reflection network of $\mathcal{A}$.

A *reflection network* is a sequence of adjacent transpositions $[i : i+1]$, which changes an array $(x_1, x_2, \ldots, x_n)$ into its reflection $(x_n, x_{n-1}, \ldots, x_1)$; see Fig. 3.3 (right).

A 2-dimensional *zonotope* is the Minkowski sum of a set of n line segments in $\mathbb{R}^2$, therefore a centrally symmetric $2n$-gon. A *simple zonotopal tiling* $\mathcal{T}$ is a tiling of a

centrally symmetric $2n$-gon with rhombi; see Fig. 3.4. Simple zonotopal tillings are normalized drawings of the duals of arrangements.

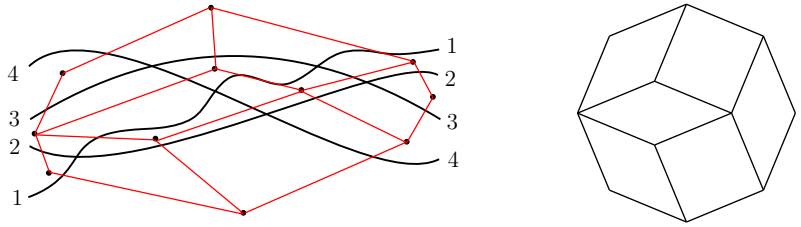

Figure 3.4.: Left: The dual of arrangement $\mathcal{A}$. Right: The zonotopal tiling of $\mathcal{A}$.

A *simple allowable sequence* is a sequence $\Sigma = \pi_0, \ldots, \pi_r$ (where $r = \binom{n}{2}$) of permutations satisfying the following two properties [36]:

1. π_0 is the permutation $(1, 2, \ldots, n)$ and π_r is the permutation $(n,\ n-1,\ \ldots,\ 1)$.
2. Each π_i is obtained by the reversal of an adjacent pair xy from π_{i-1}, where $x < y$.

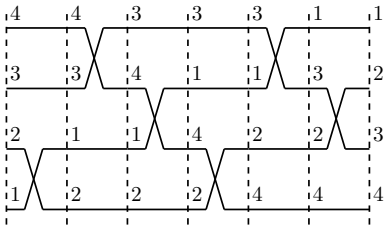

Figure 3.5.: An allowable sequence obtained from the arrangement $\mathcal{A}$.

Observe a sweep of $\mathcal{A}$ (Fig. 3.5) generates the following allowable sequence where each dashed vertical line represents a permutation;

$$1234 \xrightarrow{12} 2134 \xrightarrow{34} 2143 \xrightarrow{14} 2413 \xrightarrow{24} 4213 \xrightarrow{13} 4231 \xrightarrow{23} 4321.$$

The pair of indices written above the arrow between permutations π_{i-1} and π_i denote the adjacent pair whose reversal generates π_i from π_{i-1}.

The number of (simple) allowable sequences is denoted by A_n (sequence `A005118` in [52]). Stanley [53] established the following closed formula for A_n.

$$A_n = \frac{\binom{n}{2}!}{\prod_{k=1}^{n-1}(2n-2k-1)^k}.$$

Values of A_n for small n are shown Table 3.1.

n	A_n	$\frac{\log A_n}{n^2}$
1	1	0
2	1	0
3	2	0.1111
4	16	0.25
5	768	0.3833
6	292,864	0.5044
7	1,100,742,656	0.6129
8	48,608,795,688,960	0.7104
9	29,258,366,996,258,488,320	0.7983
10	273,035,280,663,535,522,487,992,320	0.8781

Table 3.1.: Values of A_n and $\frac{\log A_n}{n^2}$ for $n = 1$ to 10.

Isomorphism of arrangements. Two arrangements are *isomorphic*, i.e., considered the same, if they can be mapped onto each other by a homeomorphism of the plane [39]; see Figures 3.1 and 3.6. Equivalently, two arrangements are isomorphic if there is an isomorphism between the induced cell decomposition [37, Ch. 6]. The number of *nonisomorphic* arrangements of n pseudolines is denoted by B_n (sequence `A006245` in [52]); this is the number of equivalence classes of all arrangements of n pseudolines; see [45, p. 35]. It is worth pointing out that for A_n, the left to right order of the vertices in the arrangement plays a role while for B_n only the order of vertices along each particular pseudoline is important, i.e., the relative position of two vertices from distinct pairs of pseudolines does not matter. Many allowable sequences may correspond to the same arrangement. See Fig. 3.6 for an illustration of this concept. $\mathcal{A}_1$, $\mathcal{A}_2$ and $\mathcal{A}_3$ are three arrangements with four pseudolines. $\mathcal{A}_1$ and $\mathcal{A}_2$ are isomorphic since the positions of the vertices 23 (in red) and 14 (in blue) can be switched. $\mathcal{A}_3$ is nonisomorphic to $\mathcal{A}_2$ (and $\mathcal{A}_1$) since the positions of the vertices 23 (in red) and 34 (in green) can not be switched because they have a common pseudoline. The corresponding allowable sequences are:

$$\mathcal{A}_1 : 1234 \xrightarrow{12} 2134 \xrightarrow{13} 2314 \xrightarrow{23} 3214 \xrightarrow{14} 3241 \xrightarrow{24} 3421 \xrightarrow{34} 4321.$$

$$\mathcal{A}_2 : 1234 \xrightarrow{12} 2134 \xrightarrow{13} 2314 \xrightarrow{14} 2341 \xrightarrow{23} 3241 \xrightarrow{24} 3421 \xrightarrow{34} 4321.$$

$$\mathcal{A}_3 : 1234 \xrightarrow{12} 2134 \xrightarrow{13} 2314 \xrightarrow{14} 2341 \xrightarrow{34} 2431 \xrightarrow{24} 4231 \xrightarrow{23} 4321.$$

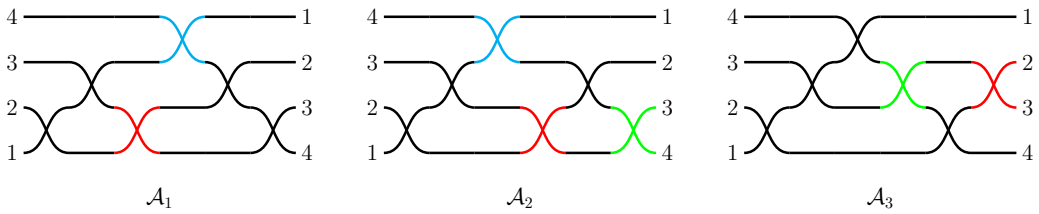

Figure 3.6.: $\mathcal{A}_1$, $\mathcal{A}_2$ and $\mathcal{A}_3$ are three arrangements with four pseudolines. $\mathcal{A}_1$ and $\mathcal{A}_2$ are isomorphic where $\mathcal{A}_3$ is nonisomorphic to $\mathcal{A}_2$ (and $\mathcal{A}_1$).

Since $\mathcal{A}_1$ and $\mathcal{A}_2$ are the same (isomorphic) arrangement, they (and their allowable sequences) can be represented by a *canonical arrangement* $\mathcal{B}_1$, see Fig. 3.7. The allowable sequence for $\mathcal{B}_1$ is $1234 \xrightarrow{12} 2134 \xrightarrow{13} 2314 \xrightarrow{23,14} 3241 \xrightarrow{24} 3421 \xrightarrow{34} 4321$.

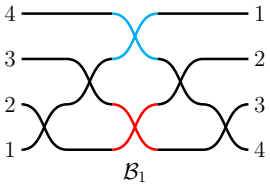

Figure 3.7.: $\mathcal{B}_1$ is the canonical arrangement representing $\mathcal{A}_1$ and $\mathcal{A}_2$.

There is a bijection between simple zonotopal tilings to classes of simple allowable sequences; an elaborate proof has been provided in [37, Lemma 6.13]. So B_n is also the number of simple zonotopal tilings of a centrally symmetric $2n$-gon.

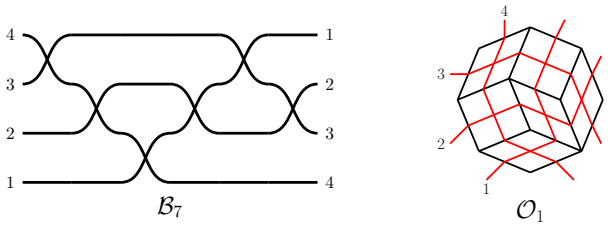

Figure 3.8.: A canonical arrangement $\mathcal{B}_7$, the corresponding rhombic tiling of an octagon $\mathcal{O}_1$ and the allowable sequence $\mathcal{B}_7 : 1234 \xrightarrow{34} 1243 \xrightarrow{24} 1423 \xrightarrow{14} 4123 \xrightarrow{12} 4213 \xrightarrow{13} 4231 \xrightarrow{23} 4321$.

Here we study the growth rate of B_n; so let[1] $b_n = \log B_n$. Knuth [45] conjectured that $b_n \leq \binom{n}{2} + o(n^2)$; see also [38, p. 147] and [36, p. 259]. This conjecture is still open.

Upper bounds on the number of pseudoline arrangements. In his seminal paper on the topic, Knuth [45] took a *vertical approach* for encoding arrangements. Let $\mathcal{A}$ be an arrangement of n pseudolines $\{\ell_1, \ldots, \ell_n\}$, see Fig. 3.9. By adding pseudoline ℓ_{n+1}

[1]Throughout this chapter, $\log x$ and $\ln x$ are the logarithms of x in base 2 and e, respectively.

to $\mathcal{A}$, we get $\mathcal{A}'$, an arrangement of $(n+1)$ pseudolines. The course of ℓ_{n+1} describes a *vertical cutpath* from top to bottom. The number of cutpaths of $\mathcal{A}$ is exactly the number of arrangements $\mathcal{A}'$ such that $\mathcal{A}' \setminus \{\ell_{n+1}\}$ is isomorphic to $\mathcal{A}$. Let γ_n denote the maximum number of cutpaths in an arrangement of n pseudolines. Therefore, one has $B_{n+1} \leq \gamma_n \cdot B_n$; and $B_3 = 2$. Knuth proved that $\gamma_n \leq 3^n$, concluding that $B_n \leq 3^{\binom{n+1}{2}}$ and thus $b_n \leq 0.5\,(n^2+n)\log 3 \leq 0.7924\,(n^2+n)$; this computation can be streamlined so that it yields $b_n \leq 0.7924\,n^2$, see [39]. Knuth also conjectured that $\gamma_n \leq n \cdot 2^n$, but this was refuted by Ondřej Bílka in 2010 [39]; see also [38, p. 147].

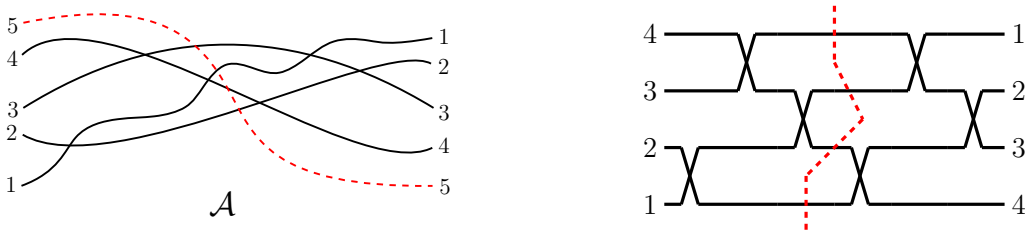

Figure 3.9.: Left: The 5th pseudoline is represented as a cutpath in $\mathcal{A}$. Right: The cutpath in the wiring diagram of $\mathcal{A}$.

Felsner [36] used a *horizontal encoding* of an arrangement in order to estimate B_n. An arrangement can be represented by a sequence of horizontal cuts. The ith cut is the list of pseudolines crossing the ith pseudoline in the order of the crossings. Let $\mathcal{T}_n$ be the set of n-tuples $(\tau_1, \tau_2, \ldots, \tau_n)$ with $\tau_i = (t_1^i, t_2^i, \ldots, t_1^{n-1})$ a binary vector and for all i $\sum_{j=1}^{n-1} t_j^i = n - i$. Then a mapping Φ can be defined from arrangements of size n to $\mathcal{T}_n$. Let $\mathcal{A}$ be an arrangement of size n. Then τ_i describes the crossings between pseudoline i and the other pseudolines as follows. If the jth crossing on pseudoline i is with a pseudoline that has index greater than i then $t_j^i = 1$ otherwise $t_j^i = 0$. Pseudoline i has exactly one crossing with each of the other $n-1$ pseudolines and $n-i$ pseudolines of them have index greater than i. This shows $(\tau_1, \tau_2, \ldots, \tau_n) = \Phi(\mathcal{A})$ is in $\mathcal{T}_n$. For example the arrangement in Fig. 3.1 (left) corresponds to the following element of $\mathcal{T}_4$. $T = ((1,1,1),(0,1,1),(1,0,0),(0,0,0))$. Not all elements of $\mathcal{T}_n$ correspond to an arrangement. The element $T = ((1,1,1),(1,0,1),(0,1,0),(0,0,0))$ of $\mathcal{T}_4$ does not have any pre-image in Φ.

Felsner [36, Thm. 1] showed that the mapping Φ is injective. Therefore,

$$B_n \leq |\mathcal{T}_n| = \binom{n-1}{0}\binom{n-1}{1}\binom{n-1}{2}\cdots\binom{n-1}{n-1}$$

Let $f(n) = \binom{n-1}{0}\cdots\binom{n-1}{n-1}$, so $f(n) = \dfrac{(n-1)^{n-1}}{(n-1)!}f(n-1)$. Using Stirling's approximation we get $\log f(n) = (n-1)\log e + \log f(n-1)$. This concludes $b_n = \log B_n \leq \sum_{k=1}^{n-1} k \log e = 0.7213(n^2 - n)$.

Felsner [36, Thm. 2] further refined this bound by using replace matrices. A *replace matrix* is a binary $n \times n$ matrix M with the properties $\sum_{j=1}^{n} m_{ij} = n - i$ for all i and $m_{ij} \geq m_{ji}$ for all $i < j$. Using this technique the upper bound $b_n \leq 0.6974\, n^2$ is established. The current best estimates on γ_n are $2.076^n \leq \gamma_n \leq 4n \cdot 2.487^n$, see [39]. The latter inequality yields $b_n \leq 0.6571\, n^2$, which is the current best upper bound.

Lower bounds on the number of pseudoline arrangements. Knuth [45, p. 37] gave a recursive construction in the setting of reflection networks. The number of nonisomorphic arrangements of n pseudolines in his construction, $T(n)$, obeys the recurrence

$$T(n) \geq 2^{n^2/8 - n/4} \cdot T(n/2).$$

By induction this yields $T(n) \geq 2^{n^2/6 - 5n/2}$, therefore $B_n \geq 2^{n^2/6 - 5n/2}$.

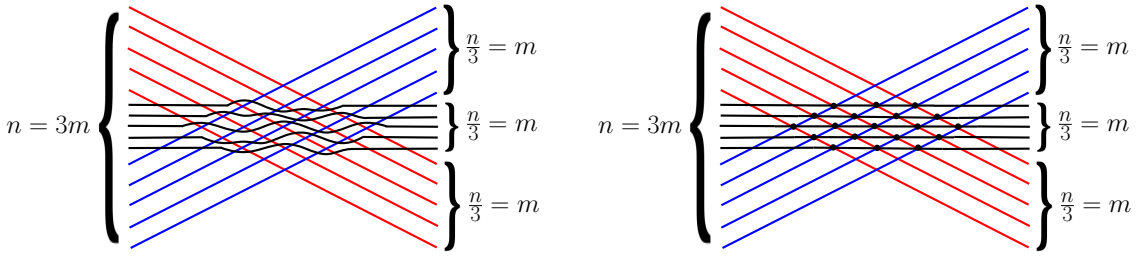

Figure 3.10.: Grid construction for a lower bound on B_n.

Matoušek sketched another recursive construction [49, Sec. 6.2], see Fig. 3.10 (left). Let n be a multiple of 3 and $m = \frac{n}{3}$ (assume that m is odd). The $2m$ lines in the two extreme bundles form a regular grid of m^2 points. The lines in the central bundle are incident to $\frac{3m^2+1}{4}$ of these grid points, shown in Fig. 3.10 (right). At each such point, there are

2 choices; going below it or above it, thus creating at least $\frac{3m^2}{4} = \frac{3(n/3)^2}{4} = \frac{n^2}{12}$ binary choices. Thus $T(n)$ obeys the recurrence

$$T(n) \geq 2^{n^2/12} \cdot (T(n/3))^3,$$

which by induction yields $T(n) \geq 2^{n^2/8}$, implying $B_n \geq 2^{n^2/8}$.

Felsner and Valtr [39] used rhombic tilings of a centrally symmetric hexagon in an elegant recursive construction for a lower bound on B_n. Consider a set of $i + j + k$ pseudolines partitioned into the following three parts: $\{1, \ldots, i\}$, $\{i + 1, \ldots, i + j\}$, $\{i + j + 1, \ldots, i + j + k\}$, see Fig. 3.11. A partial arrangement is called *consistent* if any two pseudolines from two different parts always cross but any two pseudolines from the same part never cross.

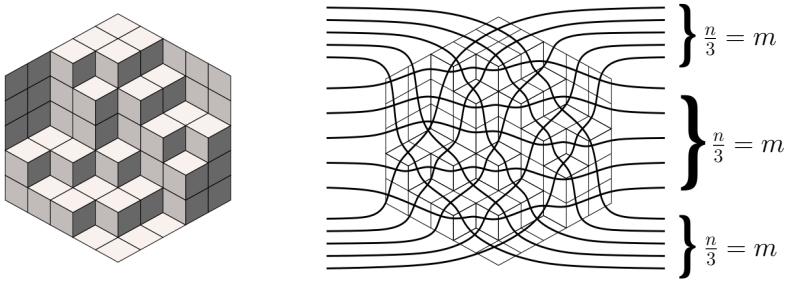

Figure 3.11.: The hexagon $H(5, 5, 5)$ with one of its rhombic tilings and a consistent partial arrangement corresponding to the tiling. This figure is reproduced from [39].

The zonotopal duals of consistent partial arrangements are rhombic tilings of the centrally symmetric hexagon $H(i, j, k)$ with side lengths i, j, k. The enumeration of rhombic tilings of $H(i, j, k)$ was solved by MacMahon [48] (see also [35]), who proved that the number of tilings is

$$P(i, j, k) = \prod_{a=0}^{i-1} \prod_{b=0}^{j-1} \prod_{c=0}^{k-1} \frac{a + b + c + 2}{a + b + c + 1}. \tag{3.1}$$

An approximation using integral calculus [39] shows that

$$\ln P(n, n, n) \approx \left(\frac{9}{2} \ln 3 - 6 \ln 2\right) n^2. \tag{3.2}$$

Assuming n to be a multiple of 3 in the recursion step, the construction yields the

recurrence

$$T(n) \geq P\left(\frac{n}{3}, \frac{n}{3}, \frac{n}{3}\right) \cdot \left(T\left(\frac{n}{3}\right)\right)^3. \tag{3.3}$$

By induction, formula (3.2) together with the recurrence (3.3) yield the lower bound $b_n \geq 0.1887\, n^2$ for large n; this is the previous best lower bound.

Table 3.2 shows the exact values of B_n, and it's growth rate (up to four digits after the decimal point) with respect to n, for small values of n. The values of B_n for $n = 1$ to 9 are from [45, p. 35] and the values of B_{10}, B_{11}, and B_{12} are from [36], [54], and [52], respectively; the values of B_{13}, B_{14}, and B_{15} have been added recently, see [44, 52].

n	B_n	$\frac{\log B_n}{n^2}$
1	1	0
2	1	0
3	2	0.1111
4	8	0.1875
5	62	0.2381
6	908	0.2729
7	24,698	0.2977
8	1,232,944	0.3161
9	112,018,190	0.3301
10	18,410,581,880	0.3409
11	5,449,192,389,984	0.3496
12	2,894,710,651,370,536	0.3566
13	2,752,596,959,306,389,652	0.3624
14	4,675,651,520,558,571,537,540	0.3672
15	14,163,808,995,580,022,218,786,390	0.3713

Table 3.2.: Values of B_n for small $n = 1$ to 15.

Our results. Here we extend the method used by Matoušek in his grid construction; observe that it uses lines of 3 slopes. In Sections 3.2 (the 2nd part) and 3.5, we use lines of 6 and 12 different slopes in hexagonal type constructions; yielding lower bounds $b_n \geq 0.1981\, n^2$ and $b_n \geq 0.2083\, n^2$ for large n, respectively. In Sections 3.3 and 3.4, we use lines of 8 and 12 different slopes in rectangular type constructions; yielding the lower bounds $b_n \geq 0.1999\, n^2$ and $b_n \geq 0.2053\, n^2$ for large n, respectively. For each of the two styles, rectangular and hexagonal,the constructions are presented in increasing order of complexity. Our main result (appeared in [33]) is summarized in the following.

Theorem 3.1. *Let B_n be the number of nonisomorphic arrangements of n pseudolines. Then $B_n \geq 2^{cn^2 - O(n \log n)}$, for some constant $c > 0.2083$. In particular, $B_n \geq 2^{0.2083\, n^2}$ for large n.*

Outline of the proof. We construct a line arrangement using lines of k different slopes (for a small k). The final construction will be obtained by a small clockwise rotation, so that there are no vertical lines. Let $m = \lfloor n/k \rfloor$ or $m = \lfloor n/k \rfloor - 1$ (whichever is odd). Each bundle consists of m equidistant parallel lines in the corresponding strip; remaining lines are discarded, or not used in the counting. An *i-wise crossing* is an intersection point of exactly i lines. Let $\lambda_i(m)$ denote the number of i-wise crossings in the arrangement where each bundle consists of m lines. Our goal is to estimate $\lambda_i(m)$ for each i. Then we can locally replace the lines around each i-wise crossing with any of the B_i nonisomorphic pseudoline arrangements; and further apply recursively this construction to each of the k bundles of parallel lines exiting this junction. This yields a simple pseudoline arrangement for each possible replacement choice. Consequently, the number of nonisomorphic pseudoline arrangements in this construction, denoted by $T(n)$, satisfies the recurrence:

$$T(n) \geq F(n) \left[T\left(\frac{n}{k}\right) \right]^k, \tag{3.4}$$

where $F(n)$ is a multiplicative factor counting the number of choices in this junction:

$$F(n) \geq \prod_{i=3}^{k} B_i^{\lambda_i(n)}. \tag{3.5}$$

Estimation of the number of i-crossings. To estimate $\lambda_i(m)$, the number of i-crossings in an arrangement where each bundle consists of m lines, we use the following steps. First, two (or three) bundles of lines are chosen to create a rectangular (or hexagonal) grid based on a rectangle (or hexagon) of unit length. To estimate the number of such grid points, we calculate the area of the regions covered by exactly i strips and the area of a grid cell. Ratio of these two are areas provides us an estimate of the number of i-crossings.

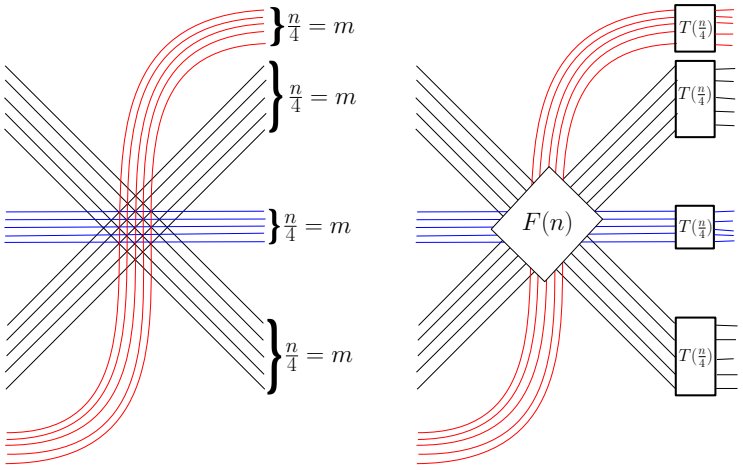

Figure 3.12.: A recursive construction with $k = 4$ showing the concept presented in Eqn. (3.4).

There are m parallel lines in each bundle. So the distance between two consecutive lines in the bundles of horizontal (also vertical) lines is $\frac{1}{m-1}$. So the area of a grid cell is $(\frac{1}{m-1})^2 \approx (\frac{1}{m})^2$. It should be noted that using this technique, the i-crossings on the boundaries of the regions are not counted which is of $O(m)$ (therefore $O(n)$). After the induction, this amounts to only $O(n \log n)$.

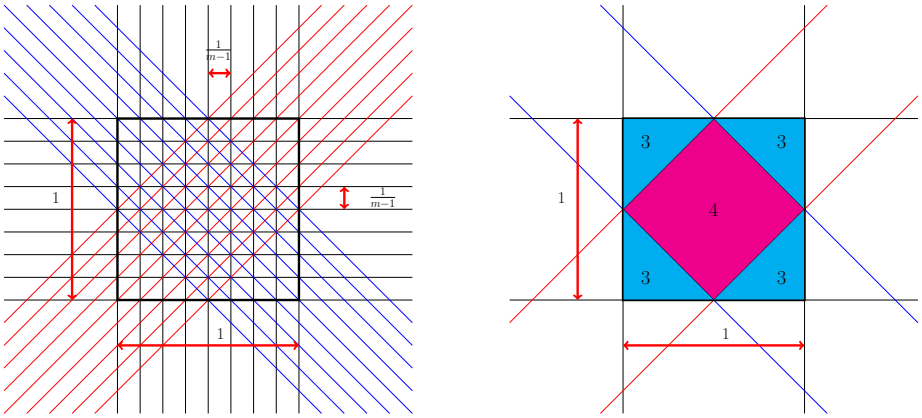

Figure 3.13.: Left: Construction with 4 slopes; here $m = 9$. Right: The regions covered by exactly three and four of the four strips are shown in cyan and magenta colors respectively.

Related work. In a comprehensive recent paper, Kynčl [47] obtained estimates on the number of isomorphism classes of simple topological graphs that realize various graphs. The author remarks that it is probably hard to obtain tight estimates on this quantity, "given that even for pseudoline arrangements, the best known lower and upper bounds on their number differ significantly". The techniques we used here can be employed to obtain improved lower bounds for topological graph drawings too.

Notations and formulas used. For a figure F, let $\mathrm{per}(F)$ denote its perimeter, i.e., the length of its boundary. For two similar polygonal figures F, F', let $\rho(F, F')$ denote their similarity ratio, i.e., the ratio between the lengths of corresponding sides of F and F' (which is equal to $\mathrm{per}(F)/\mathrm{per}(F')$). For a planar region R, let $\mathrm{area}(R)$ denote its area. By slightly abusing notation, let $\mathrm{area}(i, j, k)$ denote the area of the triangle made by three lines ℓ_i, ℓ_j and ℓ_k.

- The area of an equilateral triangle of side s is $\frac{s^2\sqrt{3}}{4}$.
- The area of a regular hexagon of side s is $\frac{s^2 3\sqrt{3}}{2}$.
- Assume that the equations of the three lines are $\alpha_s x + \beta_s y + \gamma_s = 0$, for $s = 1, 2, 3$, respectively. Then the respective triangle area can be computed as follows (for instance, see [50] or [51, pp. 27–28]:

$$\mathrm{area}(i,j,k) = \frac{A^2}{2|C_1C_2C_3|}, \text{ where } \quad A = \begin{vmatrix} \alpha_1 & \beta_1 & \gamma_1 \\ \alpha_2 & \beta_2 & \gamma_2 \\ \alpha_3 & \beta_3 & \gamma_3 \end{vmatrix}, \quad \begin{aligned} C_1 &= (\alpha_2\beta_3 - \beta_2\alpha_3), \\ C_2 &= -(\alpha_1\beta_3 - \beta_1\alpha_3), \\ C_3 &= (\alpha_1\beta_2 - \beta_1\alpha_2). \end{aligned}$$

- Let $P(i, j, g, h)$ denote the parallelogram made by the pairs of parallel lines $\ell_i \parallel \ell_j$ and $\ell_g \parallel \ell_h$. A *strip* is the set of points in between two parallel lines.

3.2. Preliminary constructions

A rectangular construction with 4 slopes. We start with a simple rectangular construction with 4 bundles of parallel lines whose slopes are $0, \infty, \pm 1$; see Fig. 3.14 (left). Let $U = [0, 1]^2$ be the unit square we work with. The axes of all four strips are incident to the center of U.

For $i = 3, 4$, let a_i denote the area of the region covered by exactly i of the 4 strips. It is easy to see that $a_3 = a_4 = 1/2$, and obviously $a_3 + a_4 = \mathrm{area}(U) = 1$. Observe that

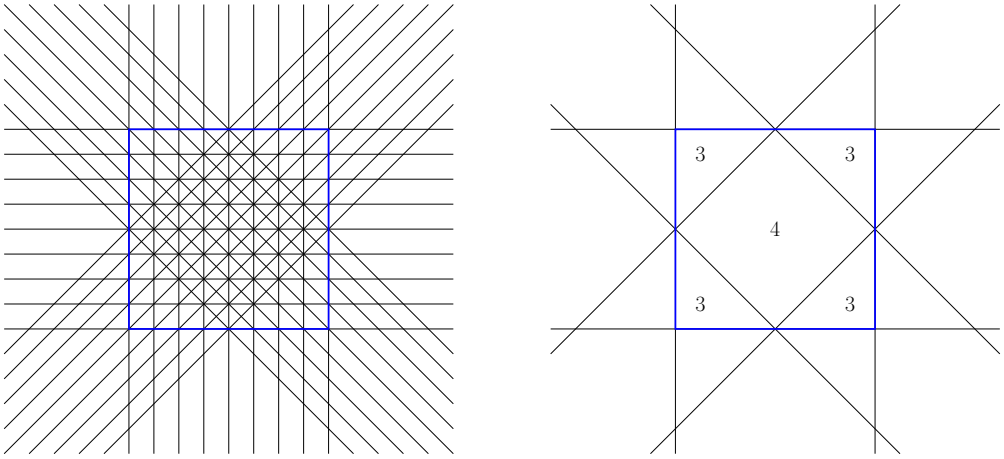

Figure 3.14.: Construction with 4 slopes; here $m = 9$. The unit square $U = [0, 1]^2$.

$\lambda_i(m)$ is proportional to a_i, for $i = 3, 4$; taking the boundary effect into account, we have

$$\lambda_3(m) = a_3\, m^2 - O(m) = \frac{m^2}{2} - O(m), \text{ and } \quad \lambda_4(m) = a_4\, m^2 - O(m) = \frac{m^2}{2} - O(m).$$

Since $m = n/4$, λ_i can be also viewed as a function of n. Therefore

$$\lambda_3(n) = n^2/32 - O(n), \text{ and } \quad \lambda_4(n) = n^2/32 - O(n),$$

and so the multiplicative factor in Eq. (3.4) is bounded from below as follows:

$$F(n) \geq \prod_{i=3}^{4} B_i^{\lambda_i(n)} \geq 2^{n^2/32 - O(n)} \cdot 8^{n^2/32 - O(n)} = 2^{n^2/8 - O(n)}. \tag{3.6}$$

Applying (3.4) for $k = 4$ yields

$$T(n) \geq F(n) \cdot (T(n/4))^4 \geq 2^{n^2/8 - O(n)} \cdot (T(n/4))^4.$$

By induction on n, the resulting lower bound is $T(n) \geq 2^{n^2/6 - O(n \log n)}$; this matches the constant $1/6$ in Knuth's lower bound described in Section 3.1.

Hexagonal construction with 6 slopes. We next describe and analyze a hexagonal construction with lines of 6 slopes, namely 6 bundles of parallel lines whose slopes are 0, ∞, $\pm 1/\sqrt{3}$, $\pm\sqrt{3}$. Let H be a regular hexagon whose side has unit length. The axes of the

6 strips containing the bundles of lines are incident to the center of H; see Fig. 3.15 (left). This construction yields the lower bound $b_n \geq 0.1981\, n^2$ for large n.

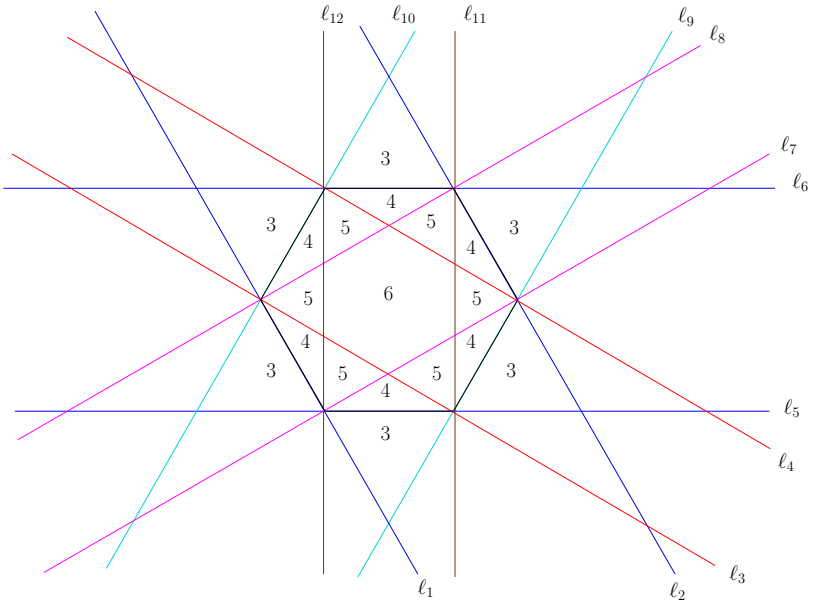

i	α_i	β_i	γ_i
1	$\sqrt{3}$	1	0
2	$\sqrt{3}$	1	$-2\sqrt{3}$
3	1	$\sqrt{3}$	-1
4	1	$\sqrt{3}$	-3
5	0	1	0
6	0	1	$-\sqrt{3}$
7	-1	$\sqrt{3}$	0
8	-1	$\sqrt{3}$	-2
9	$-\sqrt{3}$	1	$\sqrt{3}$
10	$-\sqrt{3}$	1	$-\sqrt{3}$
11	-1	0	1
12	-1	0	0

Figure 3.15.: Left: The six strips and covering multiplicities of the respective regions. These numbers only show incidences at the 3-wise crossings made by primary lines. Right: Coefficients of the lines ℓ_i for $i = 1, \ldots, 12$.

Let $\mathcal{L} = \bigcup_{i=1}^{6} \mathcal{L}_i$ be the partition of the lines into six bundles of parallel lines. The m lines in $\mathcal{L}_i$ are contained in the strip bounded by the two lines ℓ_{2i-1} and ℓ_{2i}, for $i = 1, \ldots, 6$. We refer to lines in $\mathcal{L}_1 \cup \mathcal{L}_3 \cup \mathcal{L}_5$ as the *primary* lines, and to lines in $\mathcal{L}_2 \cup \mathcal{L}_4 \cup \mathcal{L}_6$ as *secondary* lines. Three strips are bounded by the pairs of lines supporting opposite sides of H, while the other three strips are bounded by the pairs of lines supporting opposite short diagonals of H.

Assume a coordinate system where the lower left corner of H is at the origin, and the lower side of H lies along the x-axis. The equation of line ℓ_i is $\alpha_i x + \beta_i y + \gamma_i = 0$, with $\alpha_i, \beta_i, \gamma_i$, for $i = 1, \ldots, 12$, given in Fig. 3.15 (right).

Note that the distance between consecutive lines in any of the bundles of

- primary lines is $\frac{\sqrt{3}}{m}\left(1 - O\left(\frac{1}{m}\right)\right)$;
- secondary lines is $\frac{1}{m}\left(1 - O\left(\frac{1}{m}\right)\right)$.

Let $\sigma_0 = \sigma_0(m)$ and $\delta_0 = \delta_0(m)$ denote the basic parallelogram and triangle, respectively, determined by consecutive lines in $\mathcal{L}_1 \cup \mathcal{L}_3 \cup \mathcal{L}_5$ (in all three possible orientations).

The side length of σ_0 and δ_0 is $\frac{2}{m}\left(1 - O\left(\frac{1}{m}\right)\right)$. Let H' be the smaller regular hexagon bounded by the short diagonals of H; the similarity ratio $\rho(H', H)$ is equal to $\frac{1}{\sqrt{3}}$. H is the intersection of all three primary strips and H' is the intersection of all three secondary strips. Recall that (i) the area of an equilateral triangle of side s is $\frac{s^2\sqrt{3}}{4}$; and (ii) the area of a regular hexagon of side s is $\frac{s^2 3\sqrt{3}}{2}$; as such, we have

$$\begin{aligned}
\text{area}(H) &= \frac{3\sqrt{3}}{2}, \\
\text{area}(H') &= \frac{\text{area}(H)}{3} = \frac{\sqrt{3}}{2}, \\
\text{area}(\delta_0) &= \frac{4}{m^2}\frac{\sqrt{3}}{4}\left(1 - O\left(\frac{1}{m}\right)\right) = \frac{\sqrt{3}}{m^2}\left(1 - O\left(\frac{1}{m}\right)\right), \\
\text{area}(\sigma_0) &= 2 \cdot \text{area}(\delta_0) = \frac{2\sqrt{3}}{m^2}\left(1 - O\left(\frac{1}{m}\right)\right).
\end{aligned}$$

For $i = 3, 4, 5, 6$, let a_i denote the area of the (not necessarily connected) region covered by exactly i of the 6 strips. The following observations are in order: (i) the six isosceles triangles based on the sides of H inside H have unit base and height $\frac{1}{2\sqrt{3}}$; (ii) the six smaller equilateral triangles incident to the vertices of H have side-length $\frac{1}{\sqrt{3}}$. These observations yield

$$\begin{aligned}
a_3 &= \text{area}(H) = \frac{3\sqrt{3}}{2}, \\
a_4 &= 6 \cdot \text{area}(3, 5, 7) = 6 \cdot \frac{1}{4\sqrt{3}} = \frac{\sqrt{3}}{2}, \\
a_5 &= 6 \cdot \text{area}(3, 7, 11) = 6 \cdot \frac{1}{3}\frac{\sqrt{3}}{4} = \frac{\sqrt{3}}{2}, \\
a_6 &= \text{area}(H') = \frac{\sqrt{3}}{2}.
\end{aligned}$$

Observe that $a_4 + a_5 + a_6 = \text{area}(H)$. Recall that $\lambda_i(m)$ denote the number of i-wise crossings where each bundle consists of m lines. Note that $\lambda_i(m)$ is proportional to a_i, for $i = 4, 5, 6$. Indeed, $\lambda_i(m)$ is equal to the number of i-wise crossings of lines in $\mathcal{L}_1 \cup \mathcal{L}_3 \cup \mathcal{L}_5$ that lie in a region covered by i strips, which is roughly equal to the ratio $\frac{a_i}{\text{area}(\sigma_0)}$, for $i = 4, 5, 6$. More precisely, taking also the boundary effect of the relevant regions into

account, we obtain

$$\lambda_4(m) = \frac{a_4}{\text{area}(\sigma_0)} - O(m) = \frac{\sqrt{3}}{2}\frac{m^2}{2\sqrt{3}} - O(m) = \frac{m^2}{4} - O(m),$$
$$\lambda_5(m) = \frac{a_5}{\text{area}(\sigma_0)} - O(m) = \frac{m^2}{4} - O(m),$$
$$\lambda_6(m) = \frac{a_6}{\text{area}(\sigma_0)} - O(m) = \frac{m^2}{4} - O(m).$$

For estimating $\lambda_3(m)$, the situation is little bit different; see Fig. 3.16. In addition to considering 3-wise crossings of the primary lines (drawn as the crossings of 3 black lines), we also observe 3-wise crossings of the secondary lines (drawn as the crossings of 3 red lines at the centers of the small equilateral triangles contained in H'). It follows that

$$\lambda_3(m) = \frac{a_3}{\text{area}(\sigma_0)} + \frac{\text{area}(H')}{\text{area}(\delta_0)} - O(m) = \frac{3m^2}{4} + \frac{m^2}{2} - O(m) = \frac{5m^2}{4} - O(m).$$

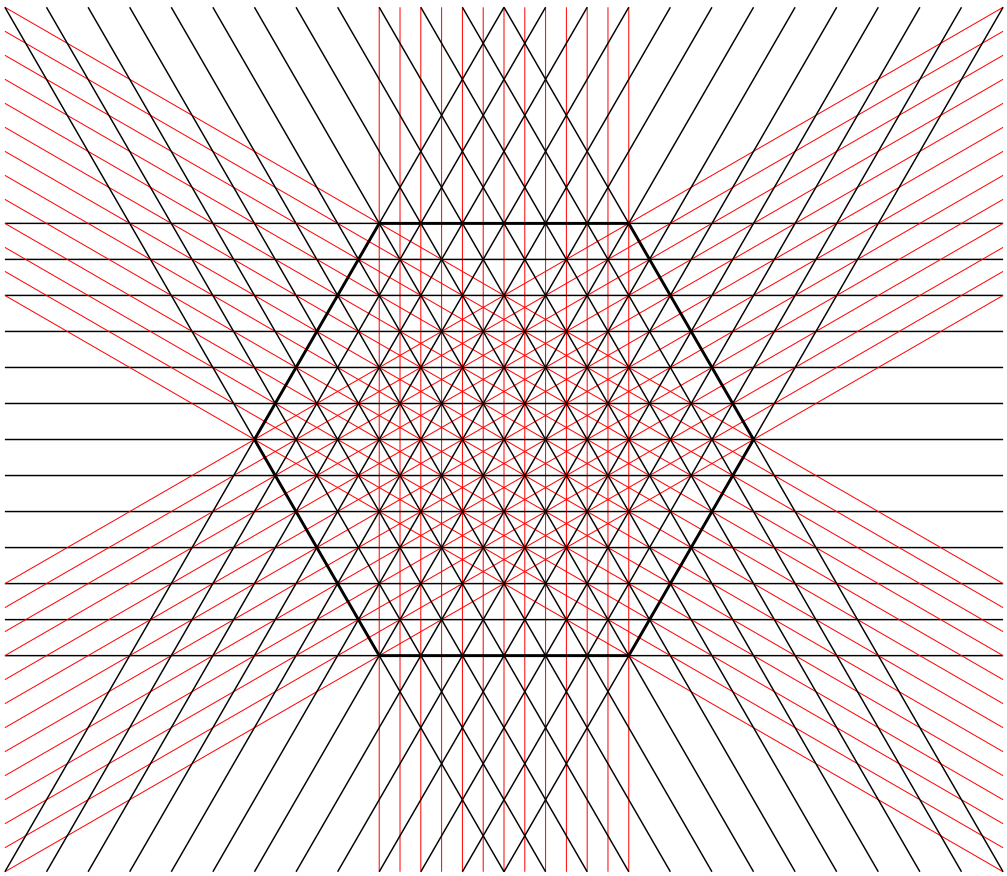

Figure 3.16.: Triple incidences of primary lines and triple incidences of secondary lines are drawn in black and red, respectively.

The values of $\lambda_i(m)$, for $i = 3, 4, 5, 6$, are summarized in Table 3.3; for convenience the linear terms are omitted. Since $m = n/6$, λ_i can be also viewed as a function of n.

i	3	4	5	6
$\lambda_i(m)$	$\frac{5m^2}{4}$	$\frac{m^2}{4}$	$\frac{m^2}{4}$	$\frac{m^2}{4}$
$\lambda_i(n)$	$\frac{5n^2}{4\cdot 36}$	$\frac{n^2}{4\cdot 36}$	$\frac{n^2}{4\cdot 36}$	$\frac{n^2}{4\cdot 36}$

Table 3.3.: The asymptotic values of $\lambda_i(m)$ and $\lambda_i(n)$ for $i = 3, 4, 5, 6$.

The multiplicative factor in Eq. (3.4) is bounded from below as follows:

$$F(n) \geq \prod_{i=3}^{6} B_i^{\lambda_i(n)} \geq 2^{5n^2/144} \cdot 8^{n^2/144} \cdot 62^{n^2/144} \cdot 908^{n^2/144} \cdot 2^{-O(n)}.$$

We prove by induction on n that $T(n) \geq 2^{cn^2 - O(n \log n)}$ for a suitable constant $c > 0$. It suffices to choose c (using the values of B_i for $i = 3, 4, 5, 6$ in Table 3.2) so that

$$\frac{8 + \log 62 + \log 908}{144} \geq \frac{5c}{6}.$$

The above inequality holds if we set $c = \dfrac{\log(256 \cdot 62 \cdot 908)}{120} > 0.1981$, and the lower bound follows.

3.3. Rectangular construction with 8 slopes

We describe and analyze a rectangular construction with lines of 8 slopes. Consider 8 bundles of parallel lines whose slopes are $0, \infty, \pm 1/2, \pm 1, \pm 2$. The axes of all strips are incident to the center of U. This construction yields the lower bound $b_n \geq 0.1999\, n^2$ for large n.

Let $\mathcal{L} = \mathcal{L}_1 \cup \ldots \cup \mathcal{L}_8$ be the partition of the lines into eight bundles of parallel lines. The m lines in $\mathcal{L}_i$ are contained in the strip Γ_i bounded by the two lines ℓ_{2i-1} and ℓ_{2i}, for $i = 1, \ldots, 8$. The equation of line ℓ_i is $\alpha_i x + \beta_i y + \gamma_i = 0$, with $\alpha_i, \beta_i, \gamma_i$, for $i = 1, \ldots, 16$ given in Fig. 3.17 (right). Observe that $U = \Gamma_4 \cap \Gamma_8$.

We refer to lines in $\mathcal{L}_4 \cup \mathcal{L}_8$ (i.e., axis-aligned lines) as the *primary* lines, and to rest

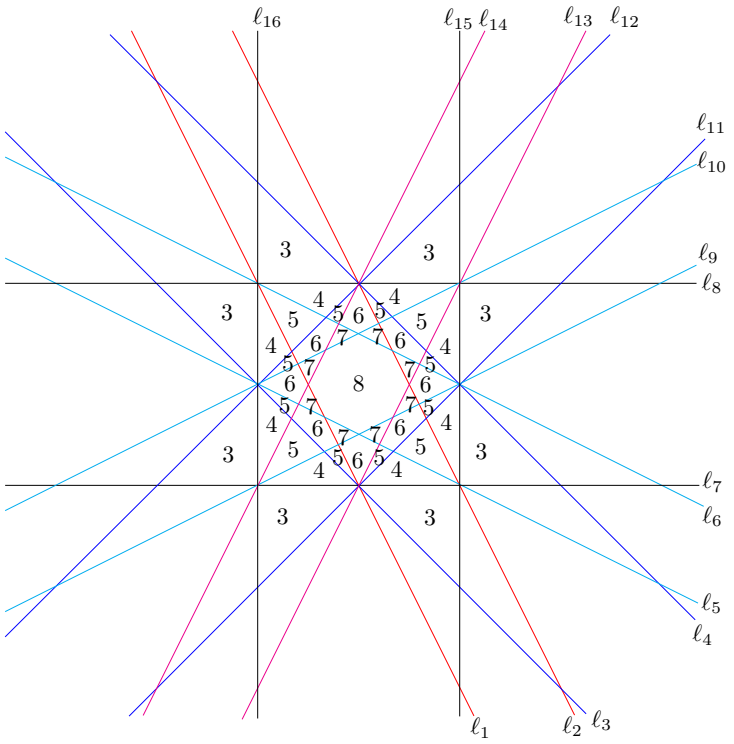

i	α_i	β_i	γ_i
1	2	1	-1
2	2	1	-2
3	1	1	-0.5
4	1	1	-1.5
5	1	2	-1
6	1	2	-2
7	0	1	0
8	0	1	-1
9	1	-2	0
10	1	-2	1
11	1	-1	-0.5
12	1	-1	0.5
13	2	-1	-1
14	2	-1	0
15	1	0	-1
16	1	0	0

Figure 3.17.: Left: The eight strips and the corresponding covering multiplicities. These numbers only reflect incidences at the grid vertices made by axis-aligned lines. Right: Coefficients of the lines ℓ_i for $i = 1, 2, \ldots, 16$.

of the lines as *secondary* lines. We refer to the intersection points of the primary lines as *grid vertices*. The slopes of the primary lines are in $\{0, \infty\}$. The slopes of the secondary lines are in $\{\pm 1/2, \pm 1, \pm 2\}$. Note that the distance between consecutive lines

- in $\mathcal{L}_4$ or $\mathcal{L}_8$ is $\frac{1}{m}\left(1 - O\left(\frac{1}{m}\right)\right)$;
- in $\mathcal{L}_2$ or $\mathcal{L}_6$ is $\frac{1}{m\sqrt{2}}\left(1 - O\left(\frac{1}{m}\right)\right)$;
- in $\mathcal{L}_1$, $\mathcal{L}_3$, $\mathcal{L}_5$, or $\mathcal{L}_7$ is $\frac{1}{m\sqrt{5}}\left(1 - O\left(\frac{1}{m}\right)\right)$.

Let $\sigma_0 = \sigma_0(m)$ denote the basic parallelogram (here, square) determined by consecutive axis-aligned lines (i.e., lines in $\mathcal{L}_4 \cup \mathcal{L}_8$); the side length of σ_0 is $\frac{1}{m}\left(1 - O\left(\frac{1}{m}\right)\right)$. We refer to these basic parallelograms as *grid cells*. Let U' be the smaller square made by $\ell_5, \ell_6, \ell_{13}, \ell_{14}$, i.e., $U' = \Gamma_3 \cap \Gamma_7$; the similarity ratio $\rho(U', U)$ is equal to $\frac{1}{\sqrt{5}}$. We have

$$\begin{aligned} \operatorname{area}(U) &= 1, \\ \operatorname{area}(U') &= \frac{\operatorname{area}(U)}{5} = \frac{1}{5}, \end{aligned}$$

$$\text{area}(\sigma_0) = \frac{1}{m^2}\left(1 - O\left(\frac{1}{m}\right)\right).$$

For $i = 3, 4, \ldots, 8$, let a_i denote the area of the (not necessarily connected) region covered by exactly i of the 8 strips. Recall that $\text{area}(i, j, k)$ denotes the area of the triangle made by ℓ_i, ℓ_j and ℓ_k. We have

$$\begin{aligned}
a_3 &= 8 \cdot \text{area}(3, 7, 15) = 1,\\
a_4 &= 8 \cdot \text{area}(5, 7, 11) = \frac{1}{3},\\
a_5 &= 4\left(2 \cdot \text{area}(5, 11, 13) + \text{area}(2, 5, 11)\right) = \frac{7}{30},\\
a_6 &= 4\left(\text{area}(6, 11, 13) - 2 \cdot \text{area}(2, 11, 9) - \text{area}(2, 9, 13)\right) = \frac{1}{5},\\
a_7 &= 8 \cdot \text{area}(5, 9, 13) = \frac{1}{15},\\
a_8 &= \text{area}(U') - 4 \cdot \text{area}(5, 9, 13) = \frac{1}{5} - \frac{1}{30} = \frac{1}{6}.
\end{aligned}$$

Observe that $a_4 + a_5 + a_6 + a_7 + a_8 = \text{area}(U) = 1$. Recall that $\lambda_i(m)$ denote the number of i-wise crossings where each bundle consists of m lines. Note that $\lambda_i(m)$ is proportional to a_i, for $i = 4, 5, 6, 7, 8$. Indeed, $\lambda_i(m)$ is equal to the number of grid points that lie in a region covered by i strips, which is roughly equal to the ratio $\frac{a_i}{\text{area}(\sigma_0)}$, for $i = 4, 5, 6, 7, 8$. More precisely, taking also the boundary effect of the relevant regions into account, we obtain

$$\begin{aligned}
\lambda_4(m) &= \frac{a_4}{\text{area}(\sigma_0)} - O(m) = \frac{m^2}{3} - O(m),\\
\lambda_5(m) &= \frac{a_5}{\text{area}(\sigma_0)} - O(m) = \frac{7m^2}{30} - O(m),\\
\lambda_6(m) &= \frac{a_6}{\text{area}(\sigma_0)} - O(m) = \frac{m^2}{5} - O(m),\\
\lambda_7(m) &= \frac{a_7}{\text{area}(\sigma_0)} - O(m) = \frac{m^2}{15} - O(m),\\
\lambda_8(m) &= \frac{a_8}{\text{area}(\sigma_0)} - O(m) = \frac{m^2}{6} - O(m).
\end{aligned}$$

For estimating $\lambda_3(m)$, in addition to considering 3-wise crossings in the exterior of U,

we also observe 3-wise crossings on the boundaries or in the interior of the small grid cells contained in some regions of U. Specifically, we distinguish exactly four types of 3-wise crossings, as illustrated and specified in Fig. 3.18. For $j = 1, 2, 3, 4$, let w_j denote the weighted area containing all crossings of type j, where the weight is the number of 3-wise crossings per grid cell. To complete the estimate of $\lambda_3(m)$, we calculate w_j for all j, from the bundles intersecting at crossings of type j; listed in Fig. 3.18 (right).

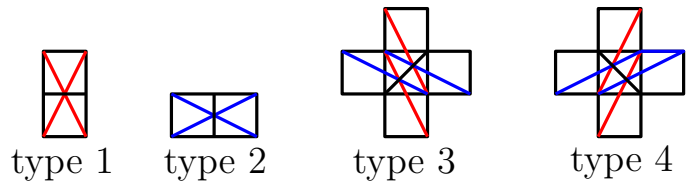

j	Bundles intersecting at vertices of type j
1	$\mathcal{L}_4, \mathcal{L}_1, \mathcal{L}_7$
2	$\mathcal{L}_8, \mathcal{L}_3, \mathcal{L}_5$
3	$\mathcal{L}_6, \mathcal{L}_1, \mathcal{L}_3$
4	$\mathcal{L}_2, \mathcal{L}_5, \mathcal{L}_7$

Figure 3.18.: Left: Other types of 3-wise crossings. Right: Intersecting bundles for these crossings.

Observe that $\Gamma_i \cap \Gamma_j$ is a parallelogram defined by the two pairs of parallel lines ℓ_{2i-1}, ℓ_{2i} and ℓ_{2j-1}, ℓ_{2j}, respectively, thus $\operatorname{area}(\Gamma_i \cap \Gamma_j) = \operatorname{area}(P(2i-1, 2i, 2j-1, 2j))$. For types 1 and 2, there is one crossing per grid cell and for types 3 and 4, there are two crossings per grid cell. Therefore we have,

$$\begin{aligned}
w_1 &= \operatorname{area}(\Gamma_4 \cap \Gamma_1 \cap \Gamma_7) = \operatorname{area}(\Gamma_1 \cap \Gamma_7) = \operatorname{area}(P(1, 2, 13, 14)) = 1/4, \\
w_2 &= \operatorname{area}(\Gamma_8 \cap \Gamma_3 \cap \Gamma_5) = \operatorname{area}(\Gamma_3 \cap \Gamma_5) = \operatorname{area}(P(5, 6, 9, 10)) = 1/4, \\
w_3 &= 2 \cdot \operatorname{area}(\Gamma_1 \cap \Gamma_3 \cap \Gamma_6) = 2 \cdot (\operatorname{area}(P(1, 2, 5, 6)) - 2 \cdot \operatorname{area}(2, 5, 11)) \\
&= 2 \cdot (1/3 - 1/12) = 1/2, \\
w_4 &= 2 \cdot \operatorname{area}(\Gamma_2 \cap \Gamma_5 \cap \Gamma_7) = 1/2.
\end{aligned}$$

It follows that

$$\lambda_3(m) = \frac{a_3 + \sum_{j=1}^{4} w_j}{\operatorname{area}(\sigma_0)} - O(m) = \left(1 + \frac{1}{4} + \frac{1}{4} + \frac{1}{2} + \frac{1}{2}\right) m^2 - O(m) = \frac{5m^2}{2} - O(m).$$

The values of $\lambda_i(m)$, for $i = 3, 4, \ldots, 8$, are summarized in Table 3.4; for convenience the linear terms are omitted. Since $m = n/8$, λ_i can be also viewed as a function of n.

i	3	4	5	6	7	8
$\lambda_i(m)$	$\frac{5m^2}{2}$	$\frac{m^2}{3}$	$\frac{7m^2}{30}$	$\frac{m^2}{5}$	$\frac{m^2}{15}$	$\frac{m^2}{6}$
$\lambda_i(n)$	$\frac{5n^2}{2\cdot 64}$	$\frac{n^2}{3\cdot 64}$	$\frac{7n^2}{30\cdot 64}$	$\frac{n^2}{5\cdot 64}$	$\frac{n^2}{15\cdot 64}$	$\frac{n^2}{6\cdot 64}$

Table 3.4.: The asymptotic values of $\lambda_i(m)$ and $\lambda_i(n)$ for $i = 3, 4, \ldots, 8$.

The multiplicative factor in Eq. (3.4) is bounded from below as follows:

$$F(n) \geq \prod_{i=3}^{8} B_i^{\lambda_i(n)} \geq 2^{\frac{5n^2}{2\cdot 64}} \cdot 8^{\frac{n^2}{3\cdot 64}} \cdot 62^{\frac{7n^2}{30\cdot 64}} \cdot 908^{\frac{n^2}{5\cdot 64}} \cdot 24698^{\frac{n^2}{15\cdot 64}} \cdot 1232944^{\frac{n^2}{6\cdot 64}} \cdot 2^{-O(n)}.$$

We prove by induction on n that $T(n) \geq 2^{cn^2 - O(n \log n)}$ for a suitable constant $c > 0$. It suffices to choose c (using the values of B_i for $i = 3, \ldots, 8$ in Table 3.2) so that

$$\frac{1}{64}\left(\frac{5}{2} + \frac{1}{3}\log 8 + \frac{7}{30}\log 62 + \frac{1}{5}\log 908 + \frac{1}{15}\log 24698 + \frac{1}{6}\log 1232944\right) \geq \frac{7c}{8}.$$

The above inequality holds if we set

$$c = \frac{1}{56}\left(\frac{5}{2} + 1 + \frac{7}{30}\log 62 + \frac{1}{5}\log 908 + \frac{1}{15}\log 24698 + \frac{1}{6}\log 1232944\right) > 0.1999, \quad (3.7)$$

and this yields the lower bound $B_n \geq 2^{cn^2 - O(n \log n)}$, for some constant $c > 0.1999$. In particular, we have $B_n \geq 2^{0.1999\, n^2}$ for large n.

3.4. Rectangular construction with 12 slopes

We next describe and analyze a rectangular construction with lines of 12 slopes. Consider 12 bundles of parallel lines whose slopes are $0, \infty, \pm 1/3, \pm 1/2, \pm 1, \pm 2, \pm 3$. The axes of all strips are incident to the center of $U = [0, 1]^2$. Refer to Fig. 3.19. This construction yields the lower bound $b_n \geq 0.2053\, n^2$ for large n.

Let $\mathcal{L} = \mathcal{L}_1 \cup \ldots \cup \mathcal{L}_{12}$ be the partition of the lines into twelve bundles of parallel lines. The m lines in $\mathcal{L}_i$ are contained in the strip Γ_i bounded by the two lines ℓ_{2i-1} and ℓ_{2i}, for $i = 1, \ldots, 12$. The equation of line ℓ_i is $\alpha_i x + \beta_i y + \gamma_i = 0$, with $\alpha_i, \beta_i, \gamma_i$, for $i = 1, \ldots, 24$

given in Table 3.5. Observe that $U = \Gamma_6 \cap \Gamma_{12}$.

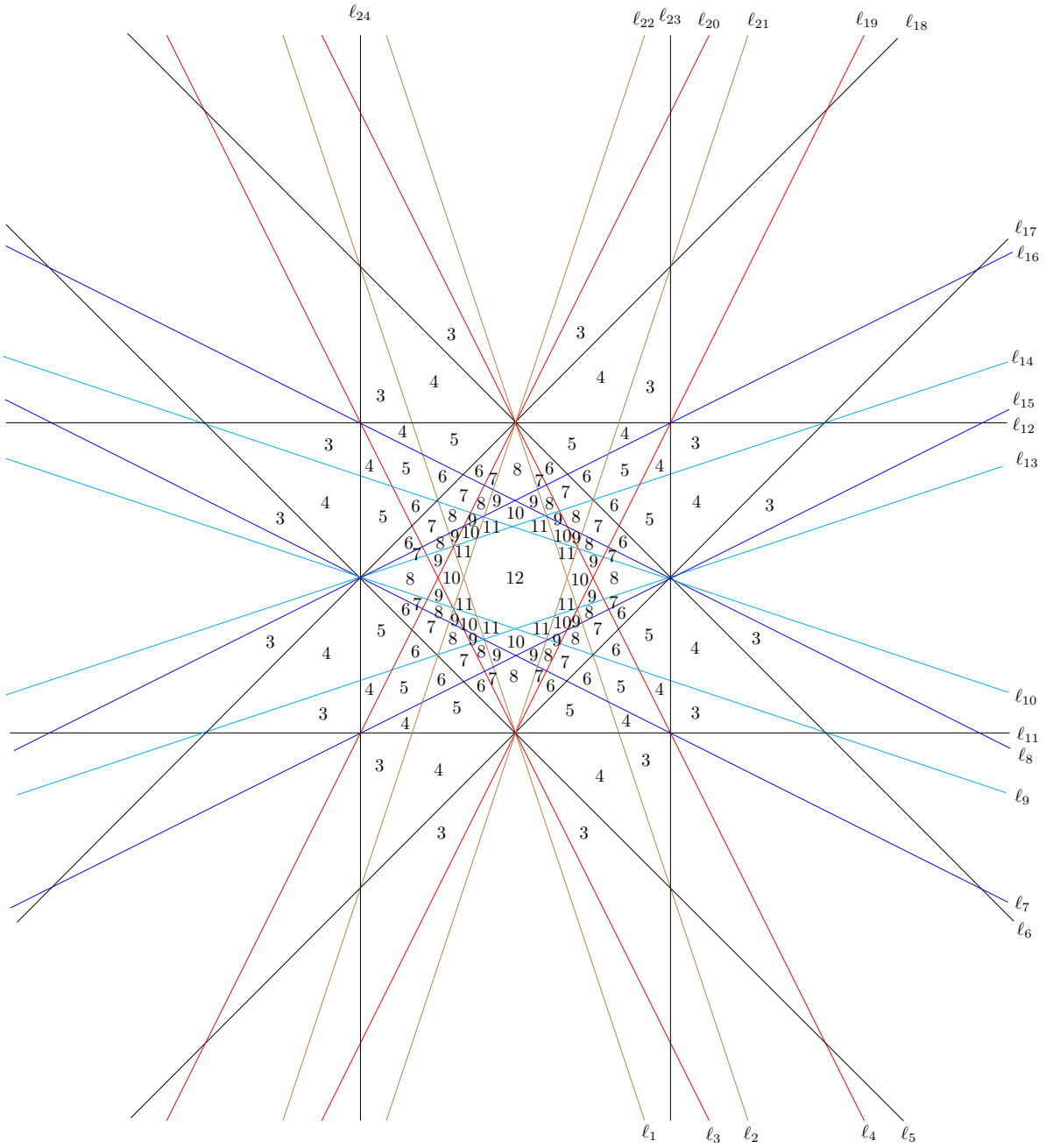

Figure 3.19.: Construction with 12 slopes. The twelve strips and the corresponding covering multiplicities. These numbers only reflect incidences at the grid vertices made by axis-aligned lines.

We refer to lines in $\mathcal{L}_6 \cup \mathcal{L}_{12}$ (i.e., axis-aligned lines) as the *primary* lines, and to rest of the lines as the *secondary* lines. We refer to the intersection points of the primary lines as *grid vertices*. The slopes of the primary lines are in $\{0, \infty\}$, and the slopes of the secondary lines are in $\{\pm 1/3, \pm 1/2, \pm 1, \pm 2, \pm 3\}$. Note that the distance between consecutive lines

- in $\mathcal{L}_6$ or $\mathcal{L}_{12}$ is $\frac{1}{m}\left(1 - O\left(\frac{1}{m}\right)\right)$;
- in $\mathcal{L}_3$ or $\mathcal{L}_9$ is $\frac{1}{m\sqrt{2}}\left(1 - O\left(\frac{1}{m}\right)\right)$;
- in $\mathcal{L}_2$, $\mathcal{L}_4$, $\mathcal{L}_8$, or $\mathcal{L}_{10}$ is $\frac{1}{m\sqrt{5}}\left(1 - O\left(\frac{1}{m}\right)\right)$;
- in $\mathcal{L}_1$, $\mathcal{L}_5$, $\mathcal{L}_7$, or $\mathcal{L}_{11}$ is $\frac{1}{m\sqrt{10}}\left(1 - O\left(\frac{1}{m}\right)\right)$.

i	α_i	β_i	γ_i
1	3	1	-1.5
2	3	1	-2.5
3	2	1	-1
4	2	1	-2
5	1	1	-0.5
6	1	1	-1.5
7	1	2	-1
8	1	2	-2

i	α_i	β_i	γ_i
9	1	3	-1.5
10	1	3	-2.5
11	0	1	0
12	0	1	-1
13	-1	3	-0.5
14	-1	3	-1.5
15	-1	2	0
16	-1	2	-1

i	α_i	β_i	γ_i
17	-1	1	0.5
18	-1	1	-0.5
19	-2	1	1
20	-2	1	0
21	-3	1	1.5
22	-3	1	0.5
23	-1	0	1
24	-1	0	0

Table 3.5.: Coefficients of the 24 lines.

Let $\sigma_0 = \sigma_0(m)$ denote the basic parallelogram (here, square) determined by consecutive axis-aligned lines (i.e., lines in $\mathcal{L}_6 \cup \mathcal{L}_{12}$); the side length of σ_0 is $\frac{1}{m}\left(1 - O\left(\frac{1}{m}\right)\right)$. We refer to these basic parallelograms as *grid cells*. Let $U_1 = \Gamma_1 \cap \Gamma_7$, be the square made by $\ell_1, \ell_2, \ell_{13}, \ell_{14}$, and let $U_2 = \Gamma_2 \cap \Gamma_8$, be the smaller square made by $\ell_3, \ell_4, \ell_{15}, \ell_{16}$. Note that $\rho(U_1, U) = \frac{1}{\sqrt{10}}$ and $\rho(U_2, U) = \frac{1}{\sqrt{5}}$. We also have

$$\begin{aligned}
\operatorname{area}(U) &= 1, \\
\operatorname{area}(U_1) &= \frac{\operatorname{area}(U)}{10} = \frac{1}{10}, \\
\operatorname{area}(U_2) &= \frac{\operatorname{area}(U)}{5} = \frac{1}{5}, \\
\operatorname{area}(\sigma_0) &= \frac{1}{m^2}\left(1 - O\left(\frac{1}{m}\right)\right).
\end{aligned}$$

Estimating the number of crossings at grid vertices. For $i = 3, \ldots, 12$, let a_i denote the area of the (not necessarily connected) region covered by exactly i of the 12 strips. Recall that $\operatorname{area}(i, j, k)$ denotes the area of the triangle bounded by ℓ_i, ℓ_j and ℓ_k. Efficient algorithms and computer search were important in verifying the areas of various regions

that are unions of cells in a line arrangement, and in verifying the coordinates and number of certain points of multiple line incidence, etc. We have

$$a_3 = 8 \cdot (\text{area}(2,11,13) + \text{area}(3,5,23)) = 8 \cdot \left(\frac{1}{8} + \frac{1}{24}\right) = \frac{4}{3},$$

$$a_4 = 8 \cdot (\text{area}(2,5,11) + \text{area}(2,7,11)) = 8 \cdot \left(\frac{1}{12} + \frac{1}{120}\right) = \frac{11}{15},$$

$$a_5 = 4 \cdot (\text{area}(11,17,23) - 2 \cdot \text{area}(2,7,11) - 2 \cdot \text{area}(2,7,17))$$
$$= 4\left(\frac{1}{8} - \frac{2}{120} - \frac{2}{120}\right) = \frac{11}{30},$$

$$a_6 = 4 \cdot (2 \cdot \text{area}(7,17,19) + 2 \cdot \text{area}(2,7,17)) = 4 \cdot \left(\frac{2}{120} + \frac{2}{120}\right) = \frac{2}{15},$$

$$a_7 = 4 \cdot (2 \cdot \text{area}(7,19,21) + 2 \cdot (\text{area}(9,17,19) - \text{area}(7,17,19)))$$
$$= 4 \cdot \left(\frac{1}{140} + 2 \cdot \left(\frac{1}{56} - \frac{1}{120}\right)\right) = \frac{11}{105},$$

$$a_8 = 8 \cdot (\text{area}(9,19,21) - \text{area}(7,19,21)) + 4 \cdot (\text{area}(2,9,15) - \text{area}(9,15,19))$$
$$+ 8 \cdot \text{area}(7,21,25) = \frac{13}{105},$$

$$a_9 = 8 \cdot (\text{area}(7,15,21) + \text{area}(9,15,19)) = 8 \cdot \left(\frac{1}{280} + \frac{1}{840}\right) = \frac{4}{105},$$

$$a_{10} = 4 \cdot ((\text{area}(7,13,15) - \text{area}(9,13,15)) + (\text{area}(13,19,21) - \text{area}(15,19,21)))$$
$$= 4 \cdot \left(\left(\frac{1}{40} - \frac{1}{60}\right) + \left(\frac{1}{80} - \frac{1}{120}\right)\right) = 4 \cdot \left(\frac{1}{120} + \frac{1}{240}\right) = \frac{1}{20},$$

$$a_{11} = 8 \cdot \text{area}(2,13,21) = \frac{8}{240} = \frac{1}{30},$$

$$a_{12} = \text{area}(U_1) - 4 \cdot \text{area}(9,13,21) = \frac{1}{10} - \frac{4}{240} = \frac{1}{12}.$$

The region whose area is $\sum_{i=4}^{12} a_i$ consists of U and 8 triangles outside U. Therefore,

$$\sum_{i=4}^{12} a_i = \text{area}(U) + 8 \cdot \text{area}(2,5,11) = 1 + 2/3 = 5/3.$$

Recall that $\lambda_i(m)$ denote the number of i-wise crossings where each bundle consists of m lines. Note that $\lambda_i(m)$ is proportional to a_i, for $i = 7, 8, \ldots, 12$. Indeed, $\lambda_i(m)$ is equal to the number of grid vertices, i.e., intersection points of the axis-parallel lines that lie in a region covered by i strips, which is roughly equal to the ratio $\frac{a_i}{\text{area}(\sigma_0)}$, for $i = 7, 8, \ldots, 12$. More precisely, taking also the boundary effect of the relevant regions

into account, we obtain

$$\lambda_7(m) = \frac{a_7}{\text{area}(\sigma_0)} - O(m) = \frac{11m^2}{105} - O(m),$$
$$\lambda_8(m) = \frac{a_8}{\text{area}(\sigma_0)} - O(m) = \frac{13m^2}{105} - O(m),$$
$$\lambda_9(m) = \frac{a_9}{\text{area}(\sigma_0)} - O(m) = \frac{4m^2}{105} - O(m),$$
$$\lambda_{10}(m) = \frac{a_{10}}{\text{area}(\sigma_0)} - O(m) = \frac{m^2}{20} - O(m),$$
$$\lambda_{11}(m) = \frac{a_{11}}{\text{area}(\sigma_0)} - O(m) = \frac{m^2}{30} - O(m),$$
$$\lambda_{12}(m) = \frac{a_{12}}{\text{area}(\sigma_0)} - O(m) = \frac{m^2}{12} - O(m).$$

Estimating the number of crossings that are not at grid vertices. For $i = 3, 4, 5, 6$, not all the i-wise crossings are at grid vertices. It can be exhaustively verified (by hand) that there are 29 types of such crossings in total; see Figs. 3.20 to 3.22. To list the coordinates of crossing points, we rescale the grid cells to the unit square $[0, 1]^2$. The bundles intersecting at each of these 29 types of vertices are listed in Table 3.6. For $j = 1, 2, \ldots, 29$, let w_j denote the weighted area containing all crossings of type j; where the weight is the number of crossings per grid cell. To complete the estimates of $\lambda_i(m)$ for $i = 3, 4, 5, 6$, we calculate w_j for all j from the bundles intersecting at type j crossings. The values are listed in Table 3.9.

j	Bundles intersecting at type j vertices	j	Bundles intersecting at type j vertices	j	Bundles intersecting at type j vertices
1	$\mathcal{L}_2, \mathcal{L}_6, \mathcal{L}_{10}$	12	$\mathcal{L}_3, \mathcal{L}_8, \mathcal{L}_{10}$	21	$\mathcal{L}_3, \mathcal{L}_7, \mathcal{L}_9, \mathcal{L}_{11}$
2	$\mathcal{L}_4, \mathcal{L}_8, \mathcal{L}_{12}$	13	$\mathcal{L}_2, \mathcal{L}_8, \mathcal{L}_{11}$	22	$\mathcal{L}_1, \mathcal{L}_3, \mathcal{L}_5, \mathcal{L}_9$
3 & 4	$\mathcal{L}_1, \mathcal{L}_6, \mathcal{L}_{11}$	14	$\mathcal{L}_1, \mathcal{L}_4, \mathcal{L}_{10}$	23	$\mathcal{L}_1, \mathcal{L}_4, \mathcal{L}_7, \mathcal{L}_{10}$
5	$\mathcal{L}_3, \mathcal{L}_7, \mathcal{L}_9$	15	$\mathcal{L}_2, \mathcal{L}_5, \mathcal{L}_8$	24	$\mathcal{L}_2, \mathcal{L}_5, \mathcal{L}_8, \mathcal{L}_{11}$
6	$\mathcal{L}_3, \mathcal{L}_5, \mathcal{L}_9$	16	$\mathcal{L}_4, \mathcal{L}_7, \mathcal{L}_{10}$	25	$\mathcal{L}_1, \mathcal{L}_3, \mathcal{L}_7, \mathcal{L}_9, \mathcal{L}_{11}$
7	$\mathcal{L}_3, \mathcal{L}_9, \mathcal{L}_{11}$	17	$\mathcal{L}_1, \mathcal{L}_5, \mathcal{L}_9$	26	$\mathcal{L}_1, \mathcal{L}_3, \mathcal{L}_5, \mathcal{L}_9, \mathcal{L}_{11}$
8	$\mathcal{L}_1, \mathcal{L}_3, \mathcal{L}_9$	18	$\mathcal{L}_3, \mathcal{L}_7, \mathcal{L}_{11}$	27	$\mathcal{L}_3, \mathcal{L}_5, \mathcal{L}_7, \mathcal{L}_9, \mathcal{L}_{11}$
9 & 10	$\mathcal{L}_5, \mathcal{L}_7, \mathcal{L}_{12}$	19	$\mathcal{L}_3, \mathcal{L}_5, \mathcal{L}_7, \mathcal{L}_9$	28	$\mathcal{L}_1, \mathcal{L}_3, \mathcal{L}_5, \mathcal{L}_7, \mathcal{L}_9$
11	$\mathcal{L}_2, \mathcal{L}_4, \mathcal{L}_9$	20	$\mathcal{L}_1, \mathcal{L}_3, \mathcal{L}_9, \mathcal{L}_{11}$	29	$\mathcal{L}_1, \mathcal{L}_3, \mathcal{L}_5, \mathcal{L}_7, \mathcal{L}_9, \mathcal{L}_{11}$

Table 3.6.: Bundles intersecting at type j vertices for $j = 1, 2, \ldots, 29$.

For $\lambda_6(m)$, all the 6-wise crossings that are not at grid vertices, are at the centers of

grid cells, see Fig. 3.20; we have

$$w_{29} = \text{area}(\Gamma_1 \cap \Gamma_3 \cap \Gamma_5 \cap \Gamma_7 \cap \Gamma_9 \cap \Gamma_{11}) = \text{area}(\Gamma_1 \cap \Gamma_5 \cap \Gamma_7 \cap \Gamma_{11}) = a_{12}.$$

It follows that

$$\lambda_6(m) = \frac{a_6 + w_{29}}{\text{area}(\sigma_0)} - O(m) = \frac{a_6 + a_{12}}{\text{area}(\sigma_0)} - O(m) = \frac{2m^2}{15} + \frac{m^2}{12} - O(m) = \frac{13m^2}{60} - O(m).$$

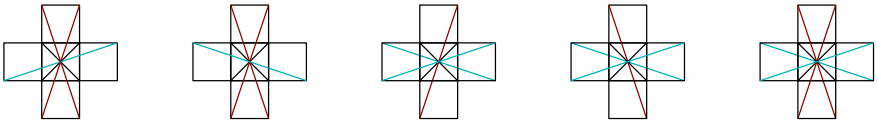

type 25 type 26 type 27 type 28 type 29

Figure 3.20.: Types 25 through 28 are 5-wise crossings that are not at grid vertices. Similarly type 29 is the only type of 6-wise crossings that are not at grid vertices.

Similarly for $\lambda_5(m)$, all the 5-wise crossings that are not at grid vertices, i.e., types 25 through 28, are at the centers of grid cells (see Fig. 3.20) contained in eight small triangles inside U. For example,

$$w_{28} = \text{area}(\Gamma_1 \cap \Gamma_3 \cap \Gamma_5 \cap \Gamma_7 \cap \Gamma_9 - \Gamma_{11}) = \text{area}(1, 14, 22) + \text{area}(2, 13, 21) = 1/120.$$

Observe that sum of the areas of these eight small triangles equals to a_{11}. It follows that

$$\lambda_5(m) = \frac{a_5 + \sum_{j=25}^{28} w_j}{\text{area}(\sigma_0)} - O(m) = \frac{a_5 + a_{11}}{\text{area}(\sigma_0)} - O(m) = \frac{11m^2}{30} + \frac{m^2}{30} - O(m) = \frac{2m^2}{5} - O(m).$$

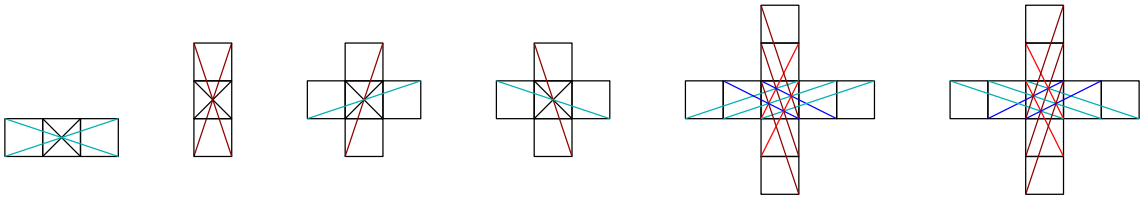

type 19 type 20 type 21 type 22 type 23 type 24

Figure 3.21.: Types 19 through 24 are 4-wise crossings that are not at grid vertices.

To estimate $\lambda_4(m)$, note that besides 4-wise crossings at grid vertices, there are six types of 4-wise crossings i.e., types 19 through 24, in the interiors of grid cells, see Fig. 3.21.

- For types 19 and 20, there is one crossing per grid cell, are at the centers of grid cells; and

$$\begin{aligned} w_{19} &= \text{area}(\Gamma_3 \cap \Gamma_5 \cap \Gamma_7 \cap \Gamma_9 - \Gamma_1 - \Gamma_{11}) \\ &= (\text{area}(2, 10, 13) - \text{area}(2, 10, 21)) + (\text{area}(9, 14, 22) - \text{area}(1, 14, 22)) = 1/15. \end{aligned}$$

  Type 20 is a 90° rotation of type 19; therefore by symmetry,

$$w_{19} = w_{20} = 1/15.$$

- For types 21 and 22, there is one crossing per grid cell, are at the centers of grid cells; and

$$\begin{aligned} w_{21} &= \text{area}(\Gamma_3 \cap \Gamma_7 \cap \Gamma_9 \cap \Gamma_{11} - \Gamma_1 - \Gamma_5) \\ &= (\text{area}(2, 14, 21) - \text{area}(2, 10, 21)) + (\text{area}(1, 13, 22) - \text{area}(1, 9, 22)) = 1/40. \end{aligned}$$

  Type 22 is the reflection in a vertical line of type 21; therefore by symmetry,

$$w_{21} = w_{22} = 1/40.$$

- For types 23 and 24, there are four crossings per grid cell. So

$$w_{23} = 4 \cdot \text{area}(\Gamma_1 \cap \Gamma_4 \cap \Gamma_7 \cap \Gamma_{10}) = 4 \cdot \text{area}(\Gamma_1 \cap \Gamma_7) = 4 \cdot \text{area}(U_1) = 2/5.$$

  Type 24 is the reflection in a vertical line of type 23; therefore by symmetry,

$$w_{23} = w_{24} = 2/5.$$

Type	Co-ordinates of the crossings
23	$\left(\frac{1}{5},\frac{2}{5}\right), \left(\frac{2}{5},\frac{4}{5}\right), \left(\frac{4}{5},\frac{3}{5}\right), \left(\frac{3}{5},\frac{1}{5}\right)$
24	$\left(\frac{1}{5},\frac{3}{5}\right), \left(\frac{3}{5},\frac{4}{5}\right), \left(\frac{4}{5},\frac{2}{5}\right), \left(\frac{2}{5},\frac{1}{5}\right)$

Table 3.7.: Co-ordinates of types 23 and 24 crossings.

Consequently, we have

$$\lambda_4(m) = \frac{a_4 + \sum_{j=19}^{24} w_j}{\text{area}(\sigma_0)} - O(m) = \left(\frac{11}{15} + \frac{2}{15} + \frac{1}{20} + \frac{4}{5}\right)m^2 - O(m) = \frac{103m^2}{60} - O(m).$$

Lastly, we estimate $\lambda_3(m)$. Besides 3-wise crossings at grid vertices, there are 18 types of 3-wise crossings i.e., types 1 through 18, in the interior of grid cells, see Fig. 3.22.

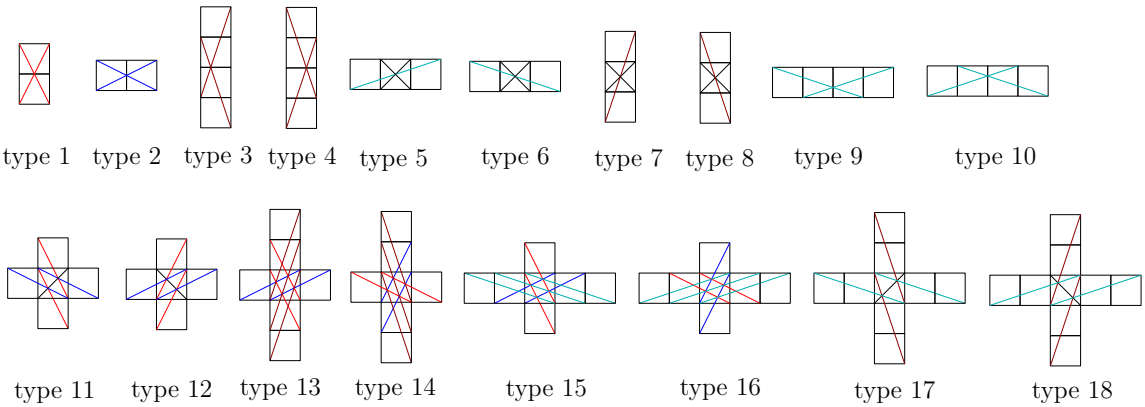

Figure 3.22.: Types 1 through 18 are 3-wise crossings that are not at grid vertices.

- For types 1 and 2, there is one crossing per grid cell at the midpoint of the horizontal and the vertical grid edges respectively; and

$$w_1 = \text{area}(\Gamma_2 \cap \Gamma_6 \cap \Gamma_{10}) = \text{area}(\Gamma_2 \cap \Gamma_{10}) = \text{area}(P(3,4,19,20)) = 1/4.$$

Type 2 is a 90° rotation of type 1; therefore by symmetry,

$$w_1 = w_2 = 1/4.$$

- For types $3, 4, 9, 10$, there is one crossing on the boundary of each grid cell. For

types 3 and 4, the crossings are on horizontal grid edges at distance 1/3 and 2/3 from the vertical line on the left, respectively. For types 9 and 10, the crossings are on vertical grid edges at height 1/3 and 2/3 from the horizontal line below, respectively; and

$$w_3 = \text{area}(\Gamma_1 \cap \Gamma_6 \cap \Gamma_{11}) = \text{area}(\Gamma_1 \cap \Gamma_{11}) = \text{area}(P(1, 2, 21, 22)) = 1/6.$$

Type 4 is the reflection in a horizontal line of type 3, and types 9 and 10 are 90° rotations of types 3 and 4, respectively. Therefore by symmetry,

$$w_3 = w_4 = w_9 = w_{10} = 1/6.$$

- For types $5, 6, 7, 8$, there is one crossing at the centers of grid cells per grid cell; and

$$w_5 = \text{area}(\Gamma_3 \cap \Gamma_7 \cap \Gamma_9 - \Gamma_1 - \Gamma_5 - \Gamma_{11}) = \text{area}(5, 9, 22) + \text{area}(6, 10, 21)) = 1/20.$$

Type 6 is the reflection in a vertical line of type 5, and types 7 and 8 are 90° rotations of types 6 and 5, respectively. Therefore by symmetry,

$$w_5 = w_6 = w_7 = w_8 = 1/20.$$

- For types 11 and 12, there are two crossings per grid cell. Type 11 crossings are at $(1/3, 1/3)$ and $(2/3, 2/3)$, type 12 crossings are at $(1/3, 2/3)$ and $(2/3, 1/3)$; and

$$\begin{aligned} w_{11} &= 2 \cdot (\text{area}(\Gamma_2 \cap \Gamma_4 \cap \Gamma_9)) \\ &= 2 \cdot (\text{area}(P(3, 4, 7, 8)) - \text{area}(3, 8, 18) - \text{area}(4, 7, 17)) = 1/2. \end{aligned}$$

Type 12 is the reflection in a vertical line of type 11; therefore by symmetry,

$$w_{11} = w_{12} = 1/2.$$

- For types $13, 14, 15$, and 16, there are four crossings per grid cell. Thus

$$w_{13} = 4 \cdot (\text{area}(\Gamma_2 \cap \Gamma_8 \cap \Gamma_{11} - \Gamma_5)) = 4 \cdot (\text{area}(3, 9, 13) + \text{area}(4, 10, 16)) = 1/5.$$

  Type 14 is the reflection in a vertical line of type 13, and types 15 and 16 are 90° rotations of types 13 and 14, respectively. Therefore by symmetry,

$$w_{13} = w_{14} = w_{15} = w_{16} = 1/5.$$

Type	Co-ordinates of the crossings
13	$\left(\frac{1}{5}, \frac{3}{5}\right), \left(\frac{3}{5}, \frac{4}{5}\right), \left(\frac{4}{5}, \frac{2}{5}\right), \left(\frac{2}{5}, \frac{1}{5}\right)$
14	$\left(\frac{1}{5}, \frac{2}{5}\right), \left(\frac{2}{5}, \frac{4}{5}\right), \left(\frac{4}{5}, \frac{3}{5}\right), \left(\frac{3}{5}, \frac{1}{5}\right)$
15	$\left(\frac{1}{5}, \frac{3}{5}\right), \left(\frac{3}{5}, \frac{4}{5}\right), \left(\frac{4}{5}, \frac{2}{5}\right), \left(\frac{2}{5}, \frac{1}{5}\right)$
16	$\left(\frac{1}{5}, \frac{2}{5}\right), \left(\frac{2}{5}, \frac{4}{5}\right), \left(\frac{4}{5}, \frac{3}{5}\right), \left(\frac{3}{5}, \frac{1}{5}\right)$

Table 3.8.: Co-ordinates of types $13, 14, 15$, and 16 crossings.

- For types 17 and 18, there are two crossings per grid cell. Type 17 crossings are at $(1/4, 1/4)$, $(3/4, 3/4)$, and type 18 crossings are at $(1/4, 3/4)$, $(3/4, 1/4)$; and

$$w_{17} = 2 \cdot (\text{area}(\Gamma_1 \cap \Gamma_5 \cap \Gamma_9)) = 2 \cdot (\text{area}(\Gamma_1 \cap \Gamma_5)) = 2 \cdot \text{area}(P(1, 2, 9, 10)) = 1/4.$$

  Type 18 is the reflection in a vertical line of type 17; therefore by symmetry,

$$w_{17} = w_{18} = 1/4.$$

Consequently, we have

$$\begin{aligned}\lambda_3(m) &= \frac{a_3 + \sum_{j=1}^{18} w_j}{\text{area}(\sigma_0)} - O(m) = \Big(\frac{4}{3} + \frac{1}{2} + \frac{2}{3} + \frac{1}{5} + 1 + \frac{4}{5} + \frac{1}{2}\Big)m^2 - O(m) \\ &= 5m^2 - O(m).\end{aligned}$$

j	w_j
1	1/4
2	1/4
3 & 4	1/3
5	1/20
6	1/20
7	1/20
8	1/20

j	w_j
9 & 10	1/3
11	1/2
12	1/2
13	1/5
14	1/5
15	1/5
16	1/5

j	w_j
17	1/4
18	1/4
19	1/15
20	1/15
21	1/40
22	1/40
23	2/5

j	w_j
24	2/5
25	1/120
26	1/120
27	1/120
28	1/120
29	1/12

Table 3.9.: Values of w_j for $j = 1, \ldots, 29$.

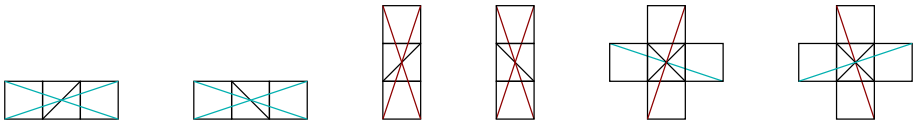

Figure 3.23.: These incidence patterns cannot occur.

The values of $\lambda_i(m)$, for $i = 3, 4, \ldots, 12$, are summarized in Table 3.10; for convenience the linear terms are omitted. Since $m = n/12$, λ_i can be also viewed as a function of n.

i	3	4	5	6	7	8	9	10	11	12
$\lambda_i(m)$	$5m^2$	$\frac{103m^2}{60}$	$\frac{2m^2}{5}$	$\frac{13m^2}{60}$	$\frac{11m^2}{105}$	$\frac{13m^2}{105}$	$\frac{4m^2}{105}$	$\frac{m^2}{20}$	$\frac{m^2}{30}$	$\frac{m^2}{12}$
$\lambda_i(n)$	$\frac{5n^2}{144}$	$\frac{103n^2}{60\cdot144}$	$\frac{2n^2}{5\cdot144}$	$\frac{13n^2}{60\cdot144}$	$\frac{11n^2}{105\cdot144}$	$\frac{13n^2}{105\cdot144}$	$\frac{4n^2}{105\cdot144}$	$\frac{n^2}{20\cdot144}$	$\frac{n^2}{30\cdot144}$	$\frac{n^2}{12\cdot144}$

Table 3.10.: The asymptotic values of $\lambda_i(m)$ and $\lambda_i(n)$ for $i = 3, 4, \ldots, 12$.

The multiplicative factor in Eq. (3.4) is bounded from below as follows:

$$F(n) \geq \prod_{i=3}^{12} B_i^{\lambda_i(n)} \geq 2^{\frac{5n^2}{144}} \cdot 8^{\frac{103n^2}{60\cdot144}} \cdot 62^{\frac{2n^2}{5\cdot144}} \cdot 908^{\frac{13n^2}{60\cdot144}} \cdot 24698^{\frac{11n^2}{105\cdot144}}$$
$$\cdot 1232944^{\frac{13n^2}{105\cdot144}} \cdot 112018190^{\frac{4n^2}{105\cdot144}} \cdot 18410581880^{\frac{n^2}{20\cdot144}}$$
$$\cdot 5449192389984^{\frac{n^2}{30\cdot144}} \cdot 2894710651370536^{\frac{n^2}{12\cdot144}} \cdot 2^{-O(n)}.$$

We prove by induction on n that $T(n) \geq 2^{cn^2 - O(n \log n)}$ for a suitable constant $c > 0$. It

suffices to choose c (using the values of B_i for $i = 3, \ldots, 12$ in Table 3.2) so that

$$\frac{1}{144}\Big(5 + \frac{103}{60}\log 8 + \frac{2}{5}\log 62 + \frac{13}{60}\log 908 + \frac{11}{105}\log 24698 + \frac{13}{105}\log 1232944 + \frac{4}{105}\log 112018190 + \frac{1}{20}\log 18410581880 + \frac{1}{30}\log 5449192389984 + \frac{1}{12}\log 2894710651370536\Big) \geq \frac{11c}{12}.$$

The above inequality holds if we set

$$c = \frac{1}{132}\Big(5 + \frac{103}{60}\log 8 + \frac{2}{5}\log 62 + \frac{13}{60}\log 908 + \frac{11}{105}\log 24698 + \frac{13}{105}\log 1232944 + \frac{4}{105}\log 112018190 + \frac{1}{20}\log 18410581880 + \frac{1}{30}\log 5449192389984 + \frac{1}{12}\log 2894710651370536\Big) > 0.2053. \tag{3.8}$$

3.5. Hexagonal construction with 12 slopes

We next describe and analyze a hexagonal construction with lines of 12 slopes, which provides our main result in Theorem 3.1. Consider 12 bundles of parallel lines whose slopes are $0, \infty, \pm\sqrt{3}/5, \pm 1/\sqrt{3}, \pm\sqrt{3}/2, \pm\sqrt{3}, \pm 3\sqrt{3}$. Let H be a regular hexagon whose side has unit length. The axes of the 12 strips containing the bundles of lines are incident to the center of H; see Figs. 3.24 and 3.25. This construction yields the lower bound $b_n \geq 0.2083\, n^2$ for large n.

i	α_i	β_i	γ_i
1	$3\sqrt{3}$	1	$-\sqrt{3}$
2	$3\sqrt{3}$	1	$-3\sqrt{3}$
3	$\sqrt{3}$	1	0
4	$\sqrt{3}$	1	$-2\sqrt{3}$
5	$\sqrt{3}$	2	$-\sqrt{3}$
6	$\sqrt{3}$	2	$-2\sqrt{3}$
7	1	$\sqrt{3}$	-1
8	1	$\sqrt{3}$	-3

i	α_i	β_i	γ_i
9	$\sqrt{3}$	5	$-2\sqrt{3}$
10	$\sqrt{3}$	5	$-4\sqrt{3}$
11	0	1	0
12	0	1	$-\sqrt{3}$
13	$-\sqrt{3}$	5	$-\sqrt{3}$
14	$-\sqrt{3}$	5	$-3\sqrt{3}$
15	-1	$\sqrt{3}$	0
16	-1	$\sqrt{3}$	-2

i	α_i	β_i	γ_i
17	$-\sqrt{3}$	2	0
18	$-\sqrt{3}$	2	$-\sqrt{3}$
19	$-\sqrt{3}$	1	$\sqrt{3}$
20	$-\sqrt{3}$	1	$-\sqrt{3}$
21	$-3\sqrt{3}$	1	$2\sqrt{3}$
22	$-3\sqrt{3}$	1	0
23	-1	0	1
24	-1	0	0

Table 3.11.: Coefficients of the 24 lines.

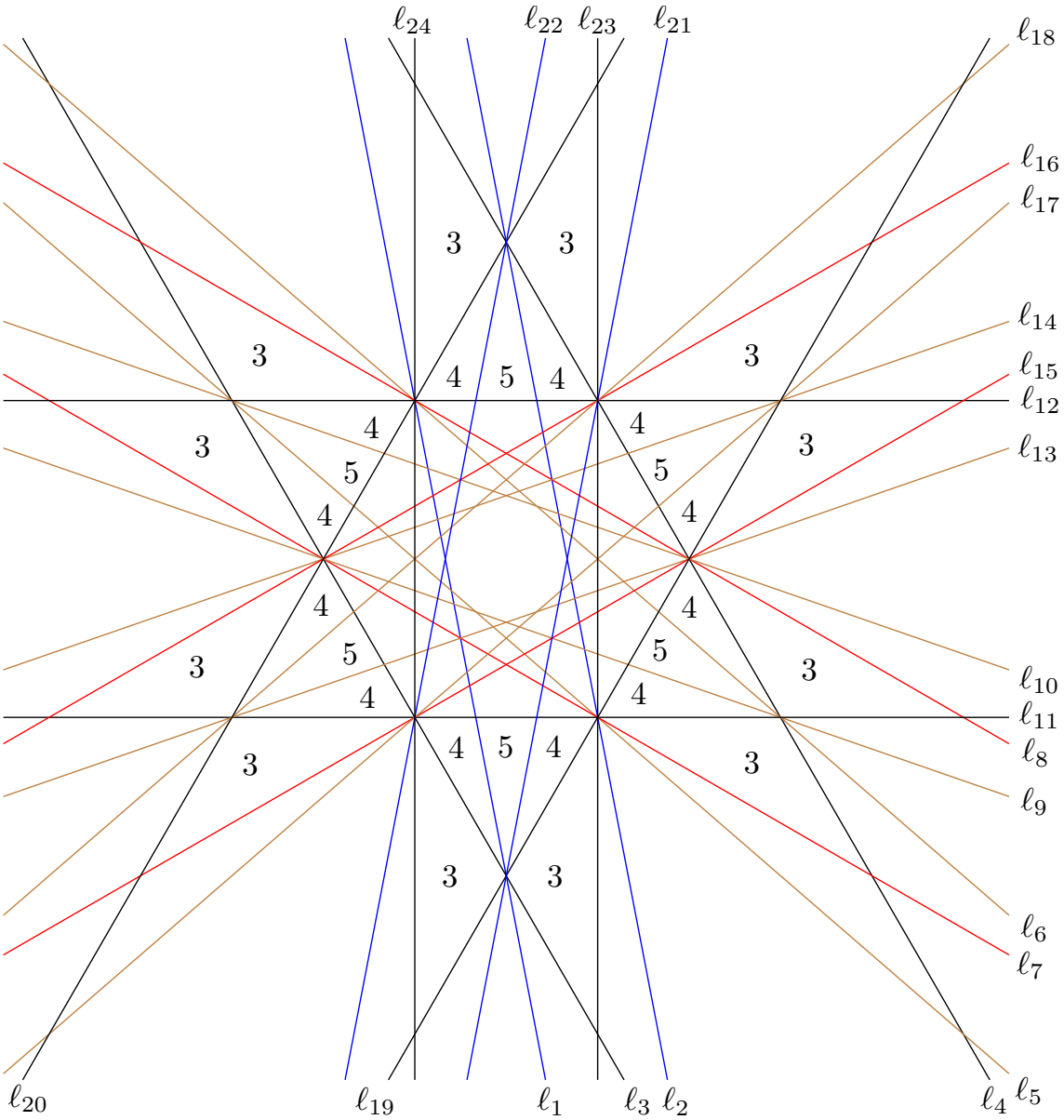

Figure 3.24.: Construction with 12 slopes shows the twelve strips and the corresponding covering multiplicities. These numbers only reflect incidences at the grid vertices made by the primary lines. The numbers inside the hexagon H (drawn in black lines) are shown in Fig. 3.25.

Assume a coordinate system where the lower left corner of H is at the origin, and the lower side of H lies along the x-axis. Let $\mathcal{L} = \mathcal{L}_1 \cup \ldots \cup \mathcal{L}_{12}$ be the partition of the lines into twelve bundles of parallel lines. The m lines in $\mathcal{L}_i$ are contained in the strip Γ_i bounded by the two lines ℓ_{2i-1} and ℓ_{2i}, for $i = 1, \ldots, 12$. The equation of line ℓ_i is $\alpha_i x + \beta_i y + \gamma_i = 0$, with $\alpha_i, \beta_i, \gamma_i$, for $i = 1, \ldots, 24$, given in Table 3.11.

Γ_2, Γ_6 and Γ_{10} are bounded by the pairs of lines supporting opposite sides of H, while Γ_4, Γ_8 and Γ_{12} are bounded by the pairs of lines supporting opposite short diagonals

of H. Therefore $H = \Gamma_2 \cap \Gamma_6 \cap \Gamma_{10}$. We refer to lines in $\mathcal{L}_2 \cup \mathcal{L}_6 \cup \mathcal{L}_{10}$ as the *primary* lines, to lines in $\mathcal{L}_4 \cup \mathcal{L}_8 \cup \mathcal{L}_{12}$ as the *secondary* lines, and to the rest of the lines as the *tertiary* lines. Note that the distance between consecutive lines in any of the bundles of

- primary lines is $\frac{\sqrt{3}}{m}\left(1 - O\left(\frac{1}{m}\right)\right)$;
- secondary lines is $\frac{1}{m}\left(1 - O\left(\frac{1}{m}\right)\right)$;
- tertiary lines is $\sqrt{\frac{3}{7}}\frac{1}{m}\left(1 - O\left(\frac{1}{m}\right)\right)$.

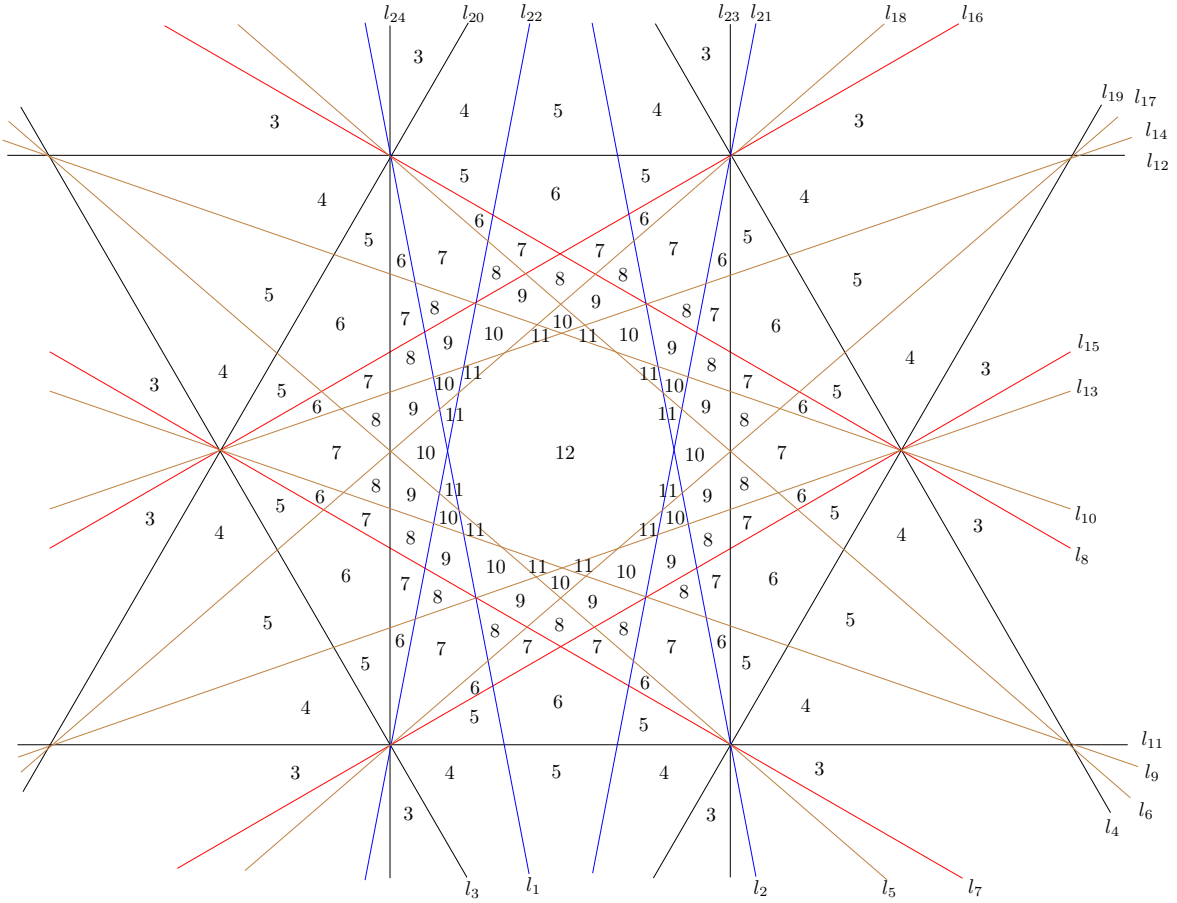

Figure 3.25.: Detail of the construction with 12 slopes depicts the covering multiplicities inside the hexagon H. These numbers only reflect incidences at the grid vertices made by the primary lines.

We refer to the intersection points of the primary lines as *grid vertices*. There are two types of grid vertices: the grid vertices in H are intersection of 3 primary lines and the ones outside H are intersection of 2 primary lines.

Let $\sigma_0 = \sigma_0(m)$ and $\delta_0 = \delta_0(m)$ denote the basic parallelogram and triangle respectively, determined by the primary lines (i.e., lines in $\mathcal{L}_2 \cup \mathcal{L}_6 \cup \mathcal{L}_{10}$) in all three possible

orientations. The side length of $\sigma_0(m)$ and δ_0 is $\frac{2}{m}\left(1-O\left(\frac{1}{m}\right)\right)$. We refer to these basic parallelograms as *grid cells*. Recall that (i) the area of an equilateral triangle of side s is $\frac{s^2\sqrt{3}}{4}$; and (ii) the area of a regular hexagon of side s is $\frac{s^2 3\sqrt{3}}{2}$; as such, we have

$$\begin{aligned}
\text{area}(H) &= \frac{3\sqrt{3}}{2},\\
\text{area}(\delta_0) &= \frac{4}{m^2}\frac{\sqrt{3}}{4}\left(1-O\left(\frac{1}{m}\right)\right) = \frac{\sqrt{3}}{m^2}\left(1-O\left(\frac{1}{m}\right)\right),\\
\text{area}(\sigma_0) &= 2\cdot\text{area}(\delta_0) = \frac{2\sqrt{3}}{m^2}\left(1-O\left(\frac{1}{m}\right)\right).
\end{aligned}$$

Estimating the number of crossings at grid vertices. For $i=3,\ldots,12$, let a_i denote the area of the (not necessarily connected) region covered by exactly i of the 12 strips. Recall that $\text{area}(i,j,k)$ denotes the area of the triangle made by ℓ_i, ℓ_j and ℓ_k.

Observe that a_{12} is the area of the 12-gon $\bigcap_{i=1}^{12}\Gamma_i$. This 12-gon is not regular, since consecutive vertices lie on two concentric cycles of radii $\frac{1}{3}$ and $\frac{\sqrt{3}}{5}$ centered at $(\frac{1}{2},\frac{\sqrt{3}}{2})$. So a_{12} is the sum of the areas of 12 congruent triangles; each with one vertex at the center of H and other two as the two consecutive vertices of the 12-gon. Each of these triangles has area $\frac{\sqrt{3}}{60}$. Therefore,

$$\begin{aligned}
a_{12} &= 12\cdot\frac{\sqrt{3}}{60} = \frac{\sqrt{3}}{5},\\
a_{11} &= 12\cdot\text{area}(1,5,9) = 12\cdot\frac{1}{140\sqrt{3}} = \frac{\sqrt{3}}{35},\\
a_{10} &= 6\cdot(\text{area}(1,5,13)-\text{area}(1,5,9)) + 6\cdot(\text{area}(5,9,22)-\text{area}(1,5,9))\\
&= 6\cdot\left(\frac{\sqrt{3}}{70}-\frac{1}{140\sqrt{3}}\right)+6\cdot\left(\frac{1}{56\sqrt{3}}-\frac{1}{140\sqrt{3}}\right) = \frac{13\sqrt{3}}{140},\\
a_9 &= 12\cdot(\text{area}(1,7,22)-\text{area}(1,9,22)) = 12\cdot\left(\frac{1}{20\sqrt{3}}-\frac{1}{56\sqrt{3}}\right) = \frac{9\sqrt{3}}{70},\\
a_8 &= 6\cdot(\text{area}(9,22,24)-\text{area}(7,22,24)) + 12\cdot\text{area}(7,13,22)\\
&= 6\cdot\left(\frac{\sqrt{3}}{40}-\frac{1}{20\sqrt{3}}\right)+12\cdot\frac{\sqrt{3}}{140} = \frac{19\sqrt{3}}{140},\\
a_7 &= 12\cdot(\text{area}(7,22,24)-\text{area}(13,22,24)) + 6\cdot(\text{area}(1,17,22)-\text{area}(1,13,22))
\end{aligned}$$

$$= 12 \cdot \left(\frac{1}{20\sqrt{3}} - \frac{\sqrt{3}}{140} \right) + 6 \cdot \left(\frac{5}{28\sqrt{3}} - \frac{1}{14\sqrt{3}} \right) = \frac{23\sqrt{3}}{70},$$

$$a_6 = 12 \cdot (\text{area}(13, 22, 24)) + 6 \cdot (\text{area}(7, 11, 15) - 2 \cdot \text{area}(1, 11, 15))$$
$$= 12 \cdot \frac{\sqrt{3}}{140} + 6 \cdot \left(\frac{1}{4\sqrt{3}} - 2 \cdot \frac{1}{20\sqrt{3}} \right) = \frac{27\sqrt{3}}{70},$$

$$a_5 = 12 \cdot (\text{area}(1, 11, 15)) + 6 \cdot (\text{area}(1, 11, 21)) = 12 \cdot \frac{1}{20\sqrt{3}} + 6 \cdot \frac{1}{4\sqrt{3}} = \frac{7\sqrt{3}}{10},$$

$$a_4 = 12 \cdot (\text{area}(1, 3, 11)) = 12 \cdot \frac{1}{4\sqrt{3}} = \sqrt{3},$$

$$a_3 = 12 \cdot (\text{area}(4, 7, 11)) = 12 \cdot \frac{\sqrt{3}}{4} = 3\sqrt{3}.$$

The region whose area is $\sum_{i=5}^{12} a_i$ consists of the hexagon H and 6 triangles outside H. Therefore,

$$\sum_{i=5}^{12} a_i = \text{area}(H) + 6 \cdot \text{area}(1, 11, 21) = \frac{3\sqrt{3}}{2} + 6 \cdot \frac{1}{4\sqrt{3}} = 2\sqrt{3}.$$

Recall that $\lambda_i(m)$ denotes the number of i-wise crossings where each bundle consists of m lines. Note that $\lambda_i(m)$ is proportional to a_i, for $i = 5, 6, \ldots, 12$. Indeed, $\lambda_i(m)$ is equal to the number of grid vertices that lie in a region covered by i strips, which is roughly equal to the ratio $\frac{a_i}{\text{area}(\sigma_0)}$, for $i = 5, 6, \ldots, 12$. More precisely, taking also the boundary effect of the relevant regions into account, we obtain

$$\lambda_{12}(m) = \frac{a_{12}}{\text{area}(\sigma_0)} - O(m) = \frac{\sqrt{3}}{5} \frac{m^2}{2\sqrt{3}} - O(m) = \frac{m^2}{10} - O(m),$$
$$\lambda_{11}(m) = \frac{a_{11}}{\text{area}(\sigma_0)} - O(m) = \frac{m^2}{70} - O(m),$$
$$\lambda_{10}(m) = \frac{a_{10}}{\text{area}(\sigma_0)} - O(m) = \frac{13m^2}{280} - O(m),$$
$$\lambda_9(m) = \frac{a_9}{\text{area}(\sigma_0)} - O(m) = \frac{9m^2}{140} - O(m),$$
$$\lambda_8(m) = \frac{a_8}{\text{area}(\sigma_0)} - O(m) = \frac{19m^2}{280} - O(m),$$
$$\lambda_7(m) = \frac{a_7}{\text{area}(\sigma_0)} - O(m) = \frac{23m^2}{140} - O(m),$$
$$\lambda_6(m) = \frac{a_6}{\text{area}(\sigma_0)} - O(m) = \frac{27m^2}{140} - O(m),$$

$$\lambda_5(m) = \frac{a_6}{\text{area}(\sigma_0)} - O(m) = \frac{7m^2}{20} - O(m).$$

Estimating the number of crossings that are not at grid vertices. For $i = 3, 4$, not all the i-wise crossings are at grid vertices. It can be exhaustively verified (by hand) that there are 21 types of crossings; see Figs. 3.26–3.31. Types 1 through 3 are 4-wise crossings and types 4 through 21 are 3-wise crossings. The bundles intersecting at each of these 21 types of vertices are listed in Table 3.12. The relative positions of all these crossings are shown in Fig. 3.32. For $j = 1, 2, \ldots, 21$, let w_j denote the weighted area containing all the crossings of type j; where the weight is the number of crossings per grid cell. To complete the estimates of $\lambda_i(m)$ for $i = 3, 4$, we calculate w_j for all j from the bundles intersecting at type j crossings. The values are listed in Table 3.16. Observe that $\Gamma_i \cap \Gamma_j$ is a parallelogram defined by the two pairs of parallel lines ℓ_{2i-1}, ℓ_{2i} and ℓ_{2j-1}, ℓ_{2j}, respectively, thus $\text{area}(\Gamma_i \cap \Gamma_j) = \text{area}(P(2i-1, 2i, 2j-1, 2j))$.

j	Bundles intersecting at type j vertices
1	$\mathcal{L}_6, \mathcal{L}_{12}, \mathcal{L}_3, \mathcal{L}_9$
2	$\mathcal{L}_2, \mathcal{L}_8, \mathcal{L}_{11}, \mathcal{L}_5$
3	$\mathcal{L}_{10}, \mathcal{L}_4, \mathcal{L}_1, \mathcal{L}_7$
4	$\mathcal{L}_2, \mathcal{L}_7, \mathcal{L}_9$
5	$\mathcal{L}_6, \mathcal{L}_{11}, \mathcal{L}_1$
6	$\mathcal{L}_{10}, \mathcal{L}_3, \mathcal{L}_5$
7	$\mathcal{L}_{12}, \mathcal{L}_5, \mathcal{L}_7$

j	Bundles intersecting at type j vertices
8	$\mathcal{L}_4, \mathcal{L}_{11}, \mathcal{L}_9$
9	$\mathcal{L}_8, \mathcal{L}_1, \mathcal{L}_3$
10	$\mathcal{L}_1, \mathcal{L}_5, \mathcal{L}_9$
11	$\mathcal{L}_{11}, \mathcal{L}_3, \mathcal{L}_7$
12	$\mathcal{L}_{12}, \mathcal{L}_3, \mathcal{L}_9$
13	$\mathcal{L}_4, \mathcal{L}_1, \mathcal{L}_7$
14	$\mathcal{L}_8, \mathcal{L}_{11}, \mathcal{L}_5$

j	Bundles intersecting at type j vertices
15	$\mathcal{L}_4, \mathcal{L}_8, \mathcal{L}_{12}$
16	$\mathcal{L}_6, \mathcal{L}_{12}, \mathcal{L}_3$
17	$\mathcal{L}_6, \mathcal{L}_{12}, \mathcal{L}_9$
18	$\mathcal{L}_2, \mathcal{L}_8, \mathcal{L}_{11}$
19	$\mathcal{L}_2, \mathcal{L}_8, \mathcal{L}_5$
20	$\mathcal{L}_{10}, \mathcal{L}_4, \mathcal{L}_1$
21	$\mathcal{L}_{10}, \mathcal{L}_4, \mathcal{L}_7$

Table 3.12.: Bundles intersecting at type j vertices for $j = 1, 2, \ldots, 21$.

- To estimate $\lambda_4(m)$, note that all the 4-wise crossings that are not at grid vertices, are at the centers of the grid cells (see Fig. 3.26); we have

$$w_1 = \text{area}(\Gamma_6 \cap \Gamma_{12} \cap \Gamma_3 \cap \Gamma_9) = \text{area}(\Gamma_3 \cap \Gamma_9) = \text{area}(P(5, 6, 17, 18)) = \frac{\sqrt{3}}{4}.$$

Types 2 and 3 are 120° and 240° rotations of type 1, respectively; therefore by symmetry,

$$w_1 = w_2 = w_3 = \frac{\sqrt{3}}{4}.$$

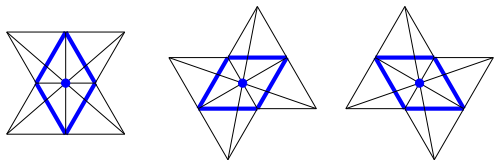

Figure 3.26.: Types 1–3 are incidences of 4 lines (4-wise crossings) that are not at grid vertices.

Consequently, we have

$$\lambda_4(m) = \frac{a_4 + \sum_{j=1}^{3} w_j}{\text{area}(\sigma_0)} - O(m) = \left(\frac{1}{2} + \frac{3}{8}\right) m^2 - O(m) = \frac{7m^2}{8} - O(m).$$

Lastly, we estimate $\lambda_3(m)$. Besides 3-wise crossings at grid vertices in H (whose number is proportional to a_3), there are 18 types of 3-wise crossings i.e., types 4 through 21, on the boundary or in the interior of the grid cells in H. To list the coordinates of the crossing points (shown as blue dots), we set the leftmost vertex of the grid cell (shown in blue lines) at $(0, 0)$ and the length of the sides of each grid cell as 1.

- For types $4, 5$, and 6, there are two crossings per grid cell at $\frac{1}{3}$rd and $\frac{2}{3}$rd of the short diagonal (see Fig. 3.27); and

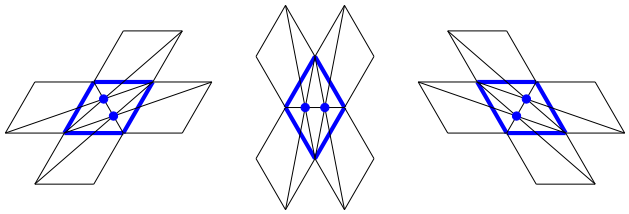

Figure 3.27.: Types 4–6 are incidences of 3 lines (3-wise crossings) that are not at grid vertices.

$$\begin{aligned} w_4 &= 2 \cdot \text{area}(\Gamma_2 \cap \Gamma_7 \cap \Gamma_9) \\ &= 2 \cdot (\text{area}(P(3, 4, 17, 18)) - \text{area}(3, 13, 17) - \text{area}(4, 14, 18)) \\ &= 2 \cdot \left(\frac{2}{\sqrt{3}} - \frac{1}{4\sqrt{3}} - \frac{1}{4\sqrt{3}}\right) = \sqrt{3}. \end{aligned}$$

Types 5 and 6 are 120° and 240° rotations of type 4, respectively; therefore by symmetry,

$$w_4 = w_5 = w_6 = \sqrt{3}.$$

- For types $7, 8$, and 9, there are four crossings per grid cell, see Fig. 3.28.

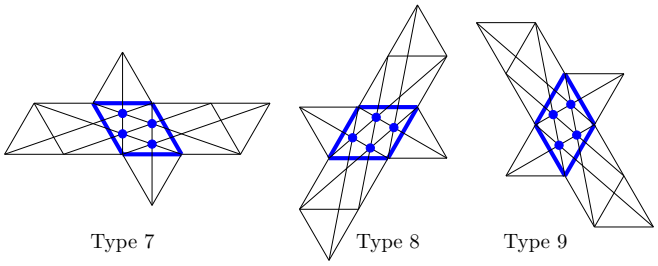

Figure 3.28.: Types 7–9 are incidences of 3 lines (3-wise crossings) that are not at grid vertices.

Type	Co-ordinates of the crossings
7	$\left(\frac{1}{2}, \frac{-\sqrt{3}}{10}\right), \left(\frac{1}{2}, \frac{-3\sqrt{3}}{10}\right), \left(1, \frac{-\sqrt{3}}{5}\right), \left(1, \frac{-2\sqrt{3}}{5}\right)$
8	$\left(\frac{2}{5}, \frac{\sqrt{3}}{5}\right), \left(\frac{7}{10}, \frac{\sqrt{3}}{10}\right), \left(\frac{4}{5}, \frac{2\sqrt{3}}{5}\right), \left(\frac{11}{10}, \frac{3\sqrt{3}}{10}\right)$
9	$\left(\frac{3}{10}, \frac{\sqrt{3}}{10}\right), \left(\frac{2}{5}, \frac{-\sqrt{3}}{5}\right), \left(\frac{3}{5}, \frac{\sqrt{3}}{5}\right), \left(\frac{7}{10}, \frac{-\sqrt{3}}{10}\right)$

Table 3.13.: Co-ordinates of types $7, 8$, and 9 crossings.

$$\begin{aligned} w_7 &= 4 \cdot \text{area}(\Gamma_{12} \cap \Gamma_5 \cap \Gamma_7) \\ &= 4 \cdot (\text{area}(P(9, 10, 13, 14)) - \text{area}(10, 13, 23) - \text{area}(9, 14, 24)) \\ &= 4 \cdot \left(\frac{2\sqrt{3}}{5} - \frac{\sqrt{3}}{20} - \frac{\sqrt{3}}{20}\right) = \frac{6\sqrt{3}}{5}. \end{aligned}$$

Types 8 and 9 are $120°$ and $240°$ rotations of type 7, respectively; therefore by symmetry,

$$w_7 = w_8 = w_9 = \frac{6\sqrt{3}}{5}.$$

- For types $10, 11$, there are six crossings per grid cell, (see Fig. 3.29); and

$$\begin{aligned} w_{10} &= 6 \cdot \text{area}(\Gamma_1 \cap \Gamma_5 \cap \Gamma_9) \\ &= 6 \cdot (\text{area}(P(1, 2, 17, 18)) - \text{area}(1, 9, 17) - \text{area}(2, 10, 18)) \\ &= 6 \cdot \left(\frac{2\sqrt{3}}{7} - \frac{\sqrt{3}}{28} - \frac{\sqrt{3}}{28}\right) = \frac{9\sqrt{3}}{7}. \end{aligned}$$

Type	Co-ordinates of the crossings
10	$\left(\frac{5}{14}, \frac{-\sqrt{3}}{14}\right), \left(\frac{5}{7}, \frac{-\sqrt{3}}{7}\right), \left(\frac{15}{14}, \frac{-3\sqrt{3}}{14}\right), \left(\frac{3}{7}, \frac{-2\sqrt{3}}{7}\right), \left(\frac{11}{14}, \frac{-5\sqrt{3}}{14}\right), \left(\frac{8}{7}, \frac{-3\sqrt{3}}{7}\right)$
11	$\left(\frac{8}{7}, \frac{3\sqrt{3}}{7}\right), \left(\frac{11}{14}, \frac{5\sqrt{3}}{14}\right), \left(\frac{3}{7}, \frac{2\sqrt{3}}{7}\right), \left(\frac{15}{14}, \frac{3\sqrt{3}}{14}\right), \left(\frac{5}{7}, \frac{\sqrt{3}}{7}\right), \left(\frac{5}{14}, \frac{\sqrt{3}}{14}\right)$

Table 3.14.: Co-ordinates of types 10 and 11 crossings.

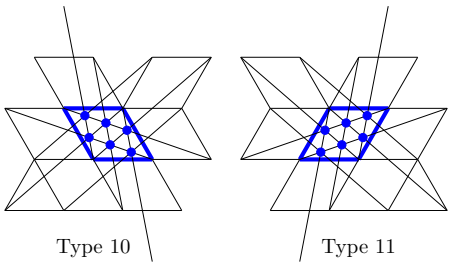

Figure 3.29.: Types 10, 11 are incidences of 3 lines (3-wise crossings) that are not at grid vertices.

Type 11 is the reflection in a vertical line of type 10; therefore by symmetry,

$$w_{10} = w_{11} = \frac{9\sqrt{3}}{7}.$$

- For types 12, 13, and 14, there are two crossings per grid cell.

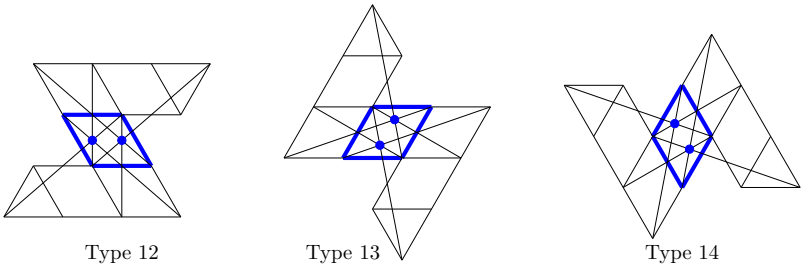

Figure 3.30.: Types 12–14 are incidences of 3 lines (3-wise crossings) that are not at grid vertices.

$$w_{12} = 2 \cdot \text{area}(\Gamma_{12} \cap \Gamma_3 \cap \Gamma_9) = 2 \cdot \text{area}(\Gamma_3 \cap \Gamma_9) = 2 \cdot \text{area}(P(5, 6, 17, 18)) = \frac{\sqrt{3}}{2}.$$

Types 13 and 14 are 120° and 240° rotations of type 12, respectively; therefore by symmetry,

$$w_{12} = w_{13} = w_{14} = \frac{\sqrt{3}}{2}.$$

- For type 15, there are two crossings at $\frac{1}{3}$rd and $\frac{2}{3}$rd of the long diagonal per grid

Type	Co-ordinates of the crossings
12	$\left(\frac{1}{2}, \frac{-\sqrt{3}}{4}\right), \left(1, \frac{-\sqrt{3}}{4}\right)$.
13	$\left(\frac{5}{8}, \frac{\sqrt{3}}{8}\right), \left(\frac{7}{8}, \frac{3\sqrt{3}}{8}\right)$.
14	$\left(\frac{3}{8}, \frac{\sqrt{3}}{8}\right), \left(\frac{5}{8}, \frac{-\sqrt{3}}{8}\right)$

Table 3.15.: Co-ordinates of types 12, 13, and 14 crossings.

cell (see Fig. 3.31); and

$$\begin{aligned} w_{15} &= 2 \cdot \text{area}(\Gamma_4 \cap \Gamma_8 \cap \Gamma_{12}) \\ &= 2 \cdot (\text{area}(P(15, 16, 23, 24)) - \text{area}(7, 15, 24) - \text{area}(8, 16, 23)) \\ &= 2 \cdot \left(\frac{2}{\sqrt{3}} - \frac{1}{4\sqrt{3}} - \frac{1}{4\sqrt{3}}\right) = \sqrt{3}. \end{aligned}$$

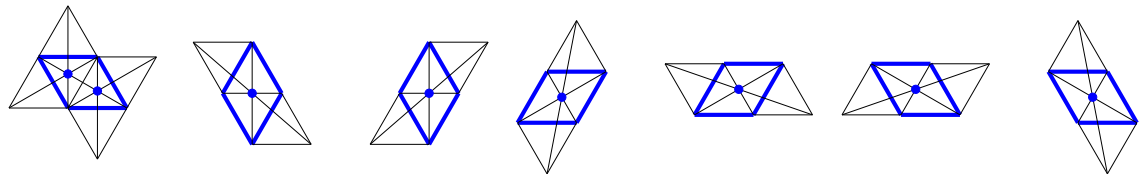

Figure 3.31.: Types 15–21 are incidences of 3 lines (3-wise crossings) that are not at grid vertices.

- For types 16 through 21, there is one crossing per grid cell at the center of the parallelogram and can be obtained from types 1 through 3 by losing one of the tertiary bundles (see Fig. 3.31); and

$$\begin{aligned} w_{16} &= \text{area}(\Gamma_6 \cap \Gamma_{12} \cap \Gamma_3 - \Gamma_9) = \text{area}(\Gamma_{12} \cap \Gamma_3) - \text{area}(\Gamma_{12} \cap \Gamma_3 \cap \Gamma_9) \\ &= \text{area}(P(5, 6, 23, 24)) - \text{area}(P(5, 6, 17, 18)) = \frac{\sqrt{3}}{2} - \frac{\sqrt{3}}{4} = \frac{\sqrt{3}}{4}. \end{aligned}$$

Type 17 is the reflection in a vertical line of type 16, types 18 and 20 are 120° and 240° rotations of type 16, respectively. Types 19 and 21 are 120° and 240° rotations of type

17, respectively. Therefore by symmetry,

$$w_{16} = w_{17} = w_{18} = w_{19} = w_{20} = w_{21} = \frac{\sqrt{3}}{4}.$$

Consequently, we have

$$\begin{aligned}\lambda_3(m) &= \frac{a_3 + \sum_{j=4}^{21} w_j}{\text{area}(\sigma_0)} - O(m) = \left(\frac{3}{2} + \frac{3}{2} + \frac{9}{5} + \frac{9}{7} + \frac{3}{4} + \frac{1}{2} + \frac{3}{4}\right) m^2 - O(m) \\ &= \frac{283}{35} m^2 - O(m).\end{aligned}$$

j	1	2	3	4	5	6	7	8	9	10	11
w_j	$\frac{\sqrt{3}}{4}$	$\frac{\sqrt{3}}{4}$	$\frac{\sqrt{3}}{4}$	$\sqrt{3}$	$\sqrt{3}$	$\sqrt{3}$	$\frac{6\sqrt{3}}{5}$	$\frac{6\sqrt{3}}{5}$	$\frac{6\sqrt{3}}{5}$	$\frac{9\sqrt{3}}{7}$	$\frac{9\sqrt{3}}{7}$

j	12	13	14	15	16	17	18	19	20	21
w_j	$\frac{\sqrt{3}}{2}$	$\frac{\sqrt{3}}{2}$	$\frac{\sqrt{3}}{2}$	$\sqrt{3}$	$\frac{\sqrt{3}}{4}$	$\frac{\sqrt{3}}{4}$	$\frac{\sqrt{3}}{4}$	$\frac{\sqrt{3}}{4}$	$\frac{\sqrt{3}}{4}$	$\frac{\sqrt{3}}{4}$

Table 3.16.: Values of w_j for $j = 1, \ldots, 21$.

The values of $\lambda_i(m)$, for $i = 3, \ldots, 12$, are summarized in Table 3.17; for convenience the linear terms are omitted. Since $m = n/12$, λ_i can be also viewed as a function of n.

i	3	4	5	6	7	8	9	10	11	12
$\lambda_i(m)$	$\frac{283m^2}{35}$	$\frac{7m^2}{8}$	$\frac{7m^2}{20}$	$\frac{27m^2}{140}$	$\frac{23m^2}{140}$	$\frac{19m^2}{280}$	$\frac{9m^2}{140}$	$\frac{13m^2}{280}$	$\frac{m^2}{70}$	$\frac{m^2}{10}$
$\lambda_i(n)$	$\frac{283n^2}{35\cdot 144}$	$\frac{7n^2}{8\cdot 144}$	$\frac{7n^2}{20\cdot 144}$	$\frac{27n^2}{140\cdot 144}$	$\frac{23n^2}{140\cdot 144}$	$\frac{19n^2}{280\cdot 144}$	$\frac{9n^2}{140\cdot 144}$	$\frac{13n^2}{280\cdot 144}$	$\frac{n^2}{70\cdot 144}$	$\frac{n^2}{10\cdot 144}$

Table 3.17.: The asymptotic values of $\lambda_i(m)$ and $\lambda_i(n)$ for $i = 3, \ldots, 12$.

The multiplicative factor in Eq. (3.4) is bounded from below as follows:

$$\begin{aligned}F(n) \geq \prod_{i=3}^{12} B_i^{\lambda_i(n)} \geq\ & 2^{\frac{283n^2}{35\cdot 144}} \cdot 8^{\frac{7n^2}{8\cdot 144}} \cdot 62^{\frac{7n^2}{20\cdot 144}} \cdot 908^{\frac{27n^2}{140\cdot 144}} \cdot 24698^{\frac{23n^2}{140\cdot 144}} \\ & \cdot 1232944^{\frac{19n^2}{280\cdot 144}} \cdot 112018190^{\frac{9n^2}{140\cdot 144}} \cdot 18410581880^{\frac{13n^2}{280\cdot 144}} \\ & \cdot 5449192389984^{\frac{n^2}{70\cdot 144}} \cdot 2894710651370536^{\frac{n^2}{10\cdot 144}} \cdot 2^{-O(n)}.\end{aligned}$$

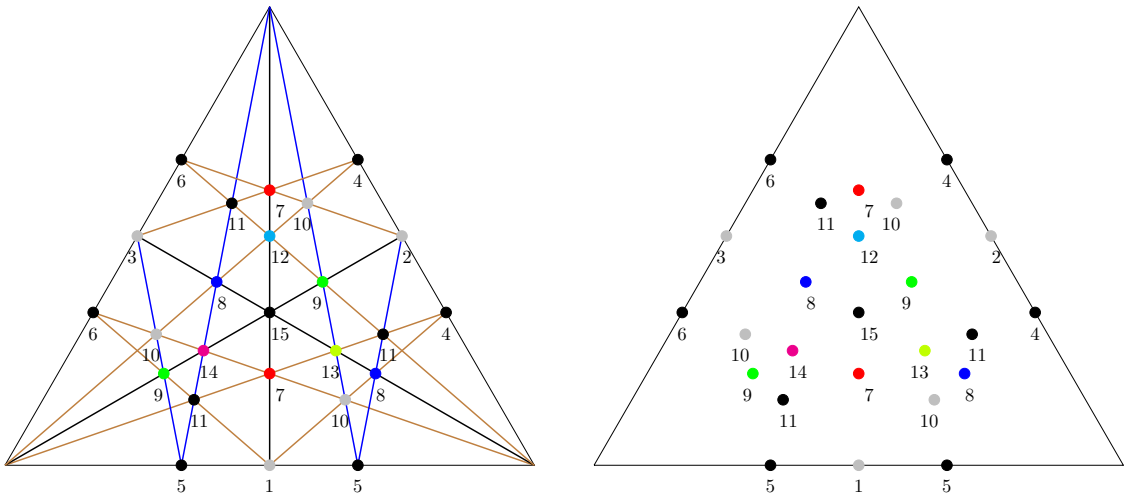

Figure 3.32.: In the 12-gon in the middle of H, all the triangular grid cells contain 3-crossings and 4-crossings of all types 1 through 15. In other grid cells of the construction only some of these types appear.

We prove by induction on n that $T(n) \geq 2^{cn^2 - O(n \log n)}$ for a suitable constant $c > 0$. It suffices to choose c (using the values of B_i for $i = 3, \ldots, 12$ in Table 3.2) so that

$$\frac{1}{144}\Big(\frac{283}{35} + \frac{7}{8}\log 8 + \frac{7}{20}\log 62 + \frac{27}{140}\log 908 + \frac{23}{140}\log 24698 + \frac{19}{280}\log 1232944 + \frac{9}{140}\log 112018190 + \frac{13}{280}\log 18410581880 + \frac{1}{70}\log 5449192389984 + \frac{1}{10}\log 2894710651370536\Big) \geq \frac{11c}{12}.$$

The above inequality holds if we set

$$c = \frac{1}{132}\Big(\frac{283}{35} + \frac{7}{8}\log 8 + \frac{7}{20}\log 62 + \frac{27}{140}\log 908 + \frac{23}{140}\log 24698 + \frac{19}{280}\log 1232944 + \frac{9}{140}\log 112018190 + \frac{13}{280}\log 18410581880 + \frac{1}{70}\log 5449192389984 + \frac{1}{10}\log 2894710651370536\Big) > 0.2083, \tag{3.9}$$

and the lower bound in Theorem 3.1 follows. □

3.6. Conclusion

We analyzed several recursive constructions derived from arrangements of lines with 3, 4, 6, 8, and 12 distinct slopes; in two different styles (rectangular and hexagonal). The

hexagonal construction with 12 slopes yields the lower bound $b_n \geq 0.2083\, n^2$ for large n. We think that increasing the number of slopes will further increase the lower bound, and likely the proof complexity at the same time. The questions of how far can one go and whether there are other more efficient variants remain. We conclude with the following questions.

1. What lower bounds on B_n can be deduced from line arrangements with a higher number of slopes? In particular, hexagonal and rectangular constructions with 16 slopes seem to be the most promising candidates. Note that the value of B_{16} is currently unknown.

2. What lower bounds on B_n can be obtained from rhombic tilings of a centrally symmetric octagon (see 3.33)? Or from those of a centrally symmetric $2k$-gon for some other even $k \geq 5$? No closed formulas for the number of such tilings seem to be available at the time of this writing. However, suitable estimates could perhaps be deduced from previous results; see, e.g., [30, 31, 34, 43].

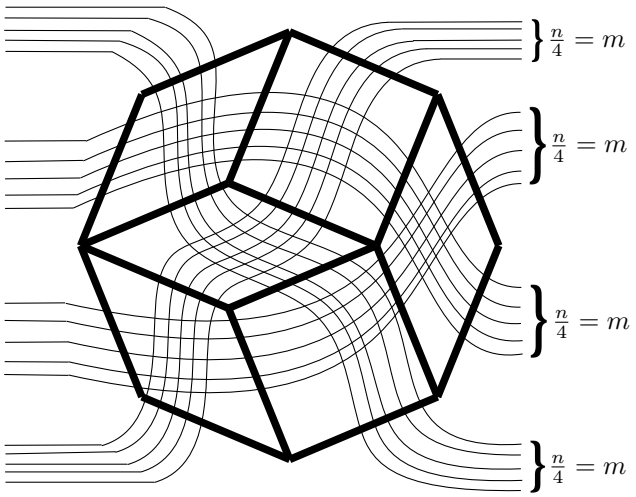

Figure 3.33.: Estimating B_n using the rhombic tilings of a centrally symmetric octagon.

Assuming n to be a multiple of 4 in the recursion step (similar to Eq. (3.3)), this construction yields the recurrence

$$T(n) \geq P^{oct}\left(\frac{n}{4}, \frac{n}{4}, \frac{n}{4}, \frac{n}{4}\right) \cdot \left(T\left(\frac{n}{4}\right)\right)^4.$$

where $\mathcal{P}^{oct}(n,n,n,n)$ denotes the number of rhombic tilings of a centrally symmetric octgon with side lengths n of each side. As per our knowledge, the exact solution of $\mathcal{P}^{oct}(n,n,n,n)$ is still unknown. An exact solution or a good estimate could lead to a sharper lower bounds of the number of pseudoline arrangements.

Bibliography

[30] N. Destainville, R. Mosseri, and F. Bailly. Fixed-boundary octagonal random tilings: a combinatorial approach. *Journal of Statistical Physics*, 102(1-2):147–190, 2001.

[31] N. Destainville, R. Mosseri, and F. Bailly. A formula for the number of tilings of an octagon by rhombi. *Theoretical Computer Science*, 319:71–81, 2004.

[32] A. Dumitrescu and R. Mandal. New lower bounds for the number of pseudoline arrangements. *Proc. 30th ACM-SIAM Symposium on Discrete Algorithms (SODA 2019)*, pp. 410–425.

[33] A. Dumitrescu, R. Mandal, New lower bounds for the number of pseudoline arrangements, *Journal of Computational Geometry* 11(1): pp. 60–92 (2020).

[34] S. Elnitsky. Rhombic tilings of polygons and classes of reduced words in Coxeter groups. *Journal of Combinatorial Theory Ser. A*, 77:193–221, 1997.

[35] V. Elser. Solution of the dimer problem on an hexagonal lattice with boundary. *Journal of Physics A: Mathematical and General*, 17:1509, 1984.

[36] S. Felsner. On the number of arrangements of pseudolines. *Discrete & Computational Geometry*, 18:257–267, 1997.

[37] S. Felsner. *Geometric Graphs and Arrangements*. Advanced Lectures in Mathematics, Vieweg Verlag, 2004.

[38] S. Felsner and J. E. Goodman. Pseudoline arrangements. in *Handbook of Discrete and Computational Geometry* (3rd edition), (J. E. Goodman, J. O'Rourke, C. D. Tóth, editors), CRC Press, Boca Raton, pp. 125–157, 2017.

[39] S. Felsner and P. Valtr. Coding and counting arrangements of pseudolines. *Discrete & Computational Geometry*, 46(4):405–416, 2011.

[40] J. E. Goodman and R. Pollack. A combinatorial perspective on some problems in geometry. *Congressus Numerantium*, 32:383–394, 1981.

[41] J. E. Goodman and R. Pollack. Allowable sequences and order types in discrete and computational geometry. in *New Trends in Discrete and Computational Geometry* (J. Pach, editor), Algorithms and Combinatorics, Vol. 10, Springer, New York, pp. 103–134, 1993.

[42] B. Grünbaum. *Arrangements and Spreads*. Regional Conference Series in Mathematics, Vol. 10, American Mathematical Society, Providence, 1972.

[43] M. Hutchinson and M. Widom. Enumeration of octagonal tilings. *Theoretical Computer Science*, 598:40–50, 2015.

[44] J. Kawahara, T. Saitoh, R. Yoshinaka, and S. Minato. Counting primitive sorting networks by πDDs. Technical Report, Hokkaido University, TCS-TR-A-11-54, 2011. `http://www-alg.ist.hokudai.ac.jp/~thomas/TCSTR/tcstr_11_54/tcstr_11_54.pdf`

[45] D. E. Knuth. *Axioms and Hulls*. Lecture Notes in Computer Science, Vol. 606, Springer, Berlin, 1992.

[46] D. E. Knuth. *The Art of Computer Programming, Vol. 3: Sorting and Searching*. 2nd edition, Addison–Wesley, Reading, MA, 1998.

[47] J. Kynčl. Improved enumeration of simple topological graphs. *Discrete & Computational Geometry*, 50(3):727–770, 2013.

[48] P. A. MacMahon. *Combinatory Analysis*, vol. II. Chelsea, New York, 1960. Reprint of the 1916 edition.

[49] J. Matoušek. *Lectures on Discrete Geometry*. Springer, New York, 2002.

[50] M. L. Orrick, Jr. The area of a triangle formed by three lines. *Pi Mu Epsilon Journal*, 7(5):294–298, 1981.

[51] G. Salmon. *A Treatise on Conic Sections*. Longman, Brown, Green and Longmans, 3rd edition, 27–28, 1855.

[52] N. Sloane and S. Plouffe. The On-Line Encyclopedia of Integer Sequences. `http://oeis.org` (accessed July 22, 2019).

[53] R. Stanley. On the number of reduced decompositions of elements of Coxeter groups. *European Journal of Combinatorics*, 5:359–372, 1984.

[54] K. Yamanaka, S. Nakano, Y. Matsui, R. Uehara, and K. Nakada. Efficient enumeration of all ladder lotteries and its application. *Theoretical Computer Science*, 411(16-18):1714–1722, 2010.

A. Source code for monotone paths

The following C code was compiled with `gcc 4.7.1` in Windows 8.1 in a quad core processor. Following is a correct way of compiling the program.

```
gcc path.c
```

Following is the output from the program.

```
Maximum number of patterns in a group is 201
```

```
/**
 * Input: n (type: Integer) number of vertices in the group
 * Output: Maximum number of patterns in groups of size n
 * This program
 * 1. generates all sides of sizes from 0 to n-1 using divide and conquer
    and stores them in files
 * 2. combine all these pairs of sides to generate all the groups of size n
 * 3. computes number of patterns each group has and output the maximum
    number of patterns
 * @authr: Ritankar Mandal
 * @date: Sep 30, 2016
 */


#define MAXNSQUARE 400
```

```
#define MAXN 20


#include<stdio.h>
#include<math.h>
#include<stdlib.h>
#include<string.h>
#include<time.h>



/// Variables
long long int numSidesOfSize[MAXN];

/// Structures
/// contains a graph in an adjacency matrix
typedef struct _group
{
    long long int index;
    int adjMat[MAXN][MAXN];
    int numV;
} group;

group groupWithMaxNumPaths[500];
int groupWithMaxNumPathsCounter;
int maxNumPathsOfGroupsOfSizen;



/// Functions
void introduction();
long long int generateSidesOfSize(int, int);
long long int generateSidesOfSizeBruteForce(int);
long long int nextPermutaion(long long int);
```

```
int checkPlanarity(group);
long long int generateSidesOfSizeDandC(int, int);
long long int combineSidesOfSize(long long int, FILE*, int, int, int);
long long int generateGroupsOfSize(int);
int checkCompatibility(group, group);
group createTempGroup(group, group);
int computeNumPaths(group);
group reverseSideWithYAxis(group);

void drawMaxGroups(int);
void drawGraph(FILE *fp, group);
void printGraph(FILE *fp, group);
void writePaths(FILE *fp, group);

long long int binCoeff(int, int);
int min(int, int);
void checkSides(int);
int main()
{
    char timebuffStart[100], timebuffFinish[100];
    double timeDiff;
    /// Log the starting time of the experiment
    time_t start = time (0);
    strftime (timebuffStart, 100, "%H:%M:%S on %m-%d-%Y", localtime (&start));
    printf("Experiment started at %s. \n", timebuffStart);

    int n, i;
    long long int numGroupsOfSize;

    printf("Enter the number of vertices in a group: ");
    scanf("%d", &n);
```

```
    introduction();
    for(i=2 ; i<=n-1 ;i++)
        numSidesOfSize[i] = generateSidesOfSize(i, 0);
    numSidesOfSize[n] = generateSidesOfSize(n, 1);
    printf("Number of sides of size %d is %lld.\n", n, numSidesOfSize[n]);

    numGroupsOfSize = generateGroupsOfSize(n);
    printf("Number of groups of size %d is %lld.\n", n, numGroupsOfSize);
    printf("Maximum number of patterns in a group of size %d is %d.\n", n,
        maxNumPathsOfGroupsOfSizen);
    printf("Number of groups of size %d with maximum number of patterns is
        %d.\n", n, groupWithMaxNumPathsCounter);


    /// Log the finishing time of the experiment
    time_t finish = time (0);
    strftime (timebuffFinish, 100, "%H:%M:%S on %m-%d-%Y", localtime
        (&finish));
    printf("Experiment started at %s. \n", timebuffStart);
    printf("Experiment finished at %s. \n", timebuffFinish);
    timeDiff = difftime(finish, start);
    printf("The experiment takes %f seconds to execute.\n", timeDiff);

    drawMaxGroups(n);

    return 0;
}


void introduction()
```

```
{
    int i, j;
    group tempSide;
    FILE *fpSides;

    //fpSides = fopen("./OutputFiles/sides_0.txt", "w");
    if((fpSides = fopen("./OutputFiles/sides_0.txt", "w")) == NULL)
    {
        printf("Can't open the file ./OutputFiles/sides_0.txt\n");
        exit(1);
    }
    tempSide.index = 0;
    tempSide.numV = 0;
    for(i = 0 ; i <= tempSide.numV+1 ; i++)
        for(j = 0 ; j <= tempSide.numV+1 ; j++)
            tempSide.adjMat[i][j] = 0;
    fwrite(&tempSide, sizeof(tempSide), 1, fpSides);
    fclose(fpSides);
    numSidesOfSize[0] = 1;

    //fpSides = fopen("./OutputFiles/sides_1.txt", "w");
    if((fpSides = fopen("./OutputFiles/sides_1.txt", "w")) == NULL)
    {
        printf("Can't open the file ./OutputFiles/sides_1.txt\n");
        exit(1);
    }
    tempSide.index = 0;
    tempSide.numV = 1;
    for(i = 0 ; i <= tempSide.numV+1 ; i++)
        for(j = 0 ; j <= tempSide.numV+1 ; j++)
            tempSide.adjMat[i][j] = 0;
```

```
    fwrite(&tempSide, sizeof(tempSide), 1, fpSides);
    fclose(fpSides);
    numSidesOfSize[1] = 1;
}


long long int generateSidesOfSize(int sideSize, int last)
{
    long long int numPlanarSides = 0;
    if(sideSize <= 8)
        numPlanarSides = generateSidesOfSizeBruteForce(sideSize);
    else
        numPlanarSides = generateSidesOfSizeDandC(sideSize, last);

    return numPlanarSides;
}


/**
  * Input: sideSize (type: int).
  * Output: Number of sides of size sideSize (type: long long int).
  * This function generates all sides of sideSize using brute force.
  */
long long int generateSidesOfSizeBruteForce(int sideSize)
{
    printf("sideSize is %d.\n", sideSize);

    int j, k, l, m, numChords, numPossibleEdges = 0;
    int possibleEdgesSource[MAXNSQUARE], possibleEdgesDestination[MAXNSQUARE];
    group tempSide;
    int sideStructSize = sizeof(tempSide);
```

```
long long int i, v, numSides, numPlanarSides = 0;


for(l = 0 ; l <= sideSize-1 ; l++)
    for(m = l+2 ; m <= sideSize+1 ; m++)
        if( ( ( (m-l) >= 2 ) || (l==0) || ( m==(sideSize+1) ) ) &&
            !((l==0) && ( m==(sideSize+1) )) )
        {
            possibleEdgesSource[numPossibleEdges] = l;
            possibleEdgesDestination[numPossibleEdges] = m;
            numPossibleEdges++;
        }

/// numPossibleEdges = (sideSize^2 + sideSize - 2)/2
printf("For sideSize %d, numPossibleEdges is %d.\n", sideSize,
    numPossibleEdges);

/// Opening the file "./OutputFiles/sides_<sideSize>.txt" to write the
    sides
char sideFileName[100];
FILE *fpSides;
sprintf(sideFileName, "./OutputFiles/sides_%g.txt", (double) sideSize);
//fpSides = fopen(sideFileName, "w");
if((fpSides = fopen(sideFileName, "w")) == NULL)
{
    printf("Can't open the file %s\n", sideFileName);
    exit(1);
}

/// Generating all planar sides

/// Generate the empty side
```

```
tempSide.index = numPlanarSides;
tempSide.numV = sideSize;
for(l = 0 ; l <= sideSize+1 ; l++)
    for(m = 0 ; m <= sideSize+1 ; m++)
        tempSide.adjMat[l][m] = 0;
fwrite(&tempSide, sideStructSize, 1, fpSides);

if(numPlanarSides%100 == 0)
    printf("%lld th planar side of size %d has been generated.\n",
        numPlanarSides, sideSize);
numPlanarSides++;

/// Generate the non-empty sides
for(numChords = 1; numChords <= sideSize-1; numChords++)
{
    numSides = binCoeff(numPossibleEdges, numChords);
    v = pow(2, numChords) - 1;

    /// Generating all planar sides with numChords chords
    for(i = 0 ; i < numSides ; i++)
    {
        tempSide.numV = sideSize;
        for(l = 0 ; l <= sideSize+1 ; l++)
            for(m = 0 ; m <= sideSize+1 ; m++)
                tempSide.adjMat[l][m] = 0;

        for(j = 0 ; j < numPossibleEdges ; j++)
        {
            k = v >> j;
            tempSide.adjMat[possibleEdgesSource[j]][possibleEdgesDestination[j]]
                = (k & 1);
```

```
            }

            /// Checks planarity of tempSide
            if(checkPlanarity(tempSide) == 1)
            {
                tempSide.index = numPlanarSides;
                fwrite(&tempSide, sideStructSize, 1, fpSides);
                if(numPlanarSides%500 == 0)
                    printf("%lld th planar side of size %d has been
                        generated.\n", numPlanarSides, sideSize);
                numPlanarSides++;
            }

            /// Generate the next subset (bit permutation)
            v = nextPermutaion(v);
        }
    }
    printf("Total number of planar sides of size %d is %lld.\n", sideSize,
        numPlanarSides);
    fclose(fpSides);
    return numPlanarSides;
}


/**
  * Input 1: parameter1 (type: int).
  * Input 2: parameter2 (type: int).
  * Output: Binomial Coefficient C(parameter1, parameter2) (type: long long
      int)
  */
long long int binCoeff(int parameter1, int parameter2)
```

```
{
    long long int C[100][100];
    int i, j;

    /// Calculates the value of Binomial Coefficient in bottom up manner
    for (i = 0; i <= parameter1; i++)
    {
        for (j = 0; j <= min(i, parameter2); j++)
        {
            /// Base Cases
            if (j == 0 || j == i)
                C[i][j] = 1;

            /// Calculate value using previously stored values
            else
                C[i][j] = C[i-1][j-1] + C[i-1][j];
        }
    }

    return C[parameter1][parameter2];
}



/**
  * Input: v (type: long long int)
  * Output: next pattern of bits after v (type: long long int).
  * It has same number of 1's in binary as the input.
  * It is taken from the website
    http://graphics.stanford.edu/~seander/bithacks.html#NextBitPermutation
  */
long long int nextPermutaion(long long int v)
```

```
{
    //long long int v; // current permutation of bits
    long long int w; // next permutation of bits

    long long int t = (v | (v - 1)) + 1;
    w = t | ((((t & -t) / (v & -v)) >> 1) - 1);

    return w;
}



int min(int parameter1, int parameter2)
{
    return (parameter1 < parameter2) ? parameter1: parameter2;
}



/**
  * Input: tempGraph (type: group).
  * Output: if the input is planar then returns 1, otherwise returns 0.
  */
int checkPlanarity(group tempSide)
{
    int j, k, l, m, status = 1;

    for(j = 0 ; j <= tempSide.numV ; j++)
        for(k = j+1 ; k <= tempSide.numV+1 ; k++)
            for(l = 0 ; l <= tempSide.numV ; l++)
                for(m = l+1 ; m <= tempSide.numV+1 ; m++)
                    if( (tempSide.adjMat[j][k] == 1) && (tempSide.adjMat[l][m]
                        == 1))
```

```
                    if( ( (j<l) && (l<k) && (k<m) ) || ( (l<j) && (j<m) &&
                        (m<k) ) )
                            status = 0;

    return status;
}


/**
  * Input: sideSize (type: int).
  * Output: Number of sides of size sideSize (type: long long int).
  * This function uses all sides of sizes smaller than sideSize,
  * places them side by side and combines to generate all sides of size
      sideSize
  */
long long int generateSidesOfSizeDandC(int sideSize, int last)
{
    int i;
    long long int numPlanarSides = 0;

    /// Opening the file "./OutputFiles/sides_<sideSize>.txt" to write the
       sides
    char sideFileName[100];
    FILE *fpSides;
    sprintf(sideFileName, "./OutputFiles/sides_%g.txt", (double) sideSize);
    //fpSides = fopen(sideFileName, "w");
    if((fpSides = fopen(sideFileName, "w")) == NULL)
    {
        printf("Can't open the file %s\n", sideFileName);
        exit(1);
    }
```

```
    /// Combine sides
    //for(i=0; i<= sideSize/2; i++)
        //numPlanarSides = combineSidesOfSize(numPlanarSides, fpSides, i,
            sideSize-i-1, last);
    numPlanarSides = combineSidesOfSize(numPlanarSides, fpSides, 5, 5, last);
    numPlanarSides = combineSidesOfSize(numPlanarSides, fpSides, 4, 6, last);
    numPlanarSides = combineSidesOfSize(numPlanarSides, fpSides, 3, 7, last);
    numPlanarSides = combineSidesOfSize(numPlanarSides, fpSides, 2, 8, last);
    //numPlanarSides = combineSidesOfSize(numPlanarSides, fpSides, 1, 9, last);
    //numPlanarSides = combineSidesOfSize(numPlanarSides, fpSides, 0, 10,
        last);

    fclose(fpSides);
    return numPlanarSides;
}


long long int combineSidesOfSize(long long int numPlanarSides, FILE* fpSides,
    int leftSideSize, int rightSideSize, int last)
{
    long long int i, j;
    long long int numLeftSides = numSidesOfSize[leftSideSize];
    long long int numRightSides = numSidesOfSize[rightSideSize];
    char leftSideFilename[200], rightSideFilename[100];
    FILE *fpLeftSides, *fpRightSides;
    group tempLeftSide, tempRightSide, tempSide;
    int l, m, cntr;
    int sideSize = leftSideSize + rightSideSize + 1;
    int sideStructSize = sizeof(tempSide);
```

```
/// Opening the files "./OutputFiles/sides_<leftSideSize>.txt" to read the
    left sides
sprintf(leftSideFilename, "./OutputFiles/sides_%g.txt", (double)
    leftSideSize);
//fpLeftSides = fopen(leftSideFilename, "r");
if((fpLeftSides = fopen(leftSideFilename, "r")) == NULL)
{
    printf("Can't open the file %s\n", leftSideFilename);
    exit(1);
}

for(i = 0; i < numLeftSides ; i++)
{
    /// Read the left side
    fread(&tempLeftSide, sideStructSize, 1, fpLeftSides);

    /// Opening the file "./OutputFiles/sides_<rightSideSize>.txt" to read
        the right sides
    sprintf(rightSideFilename, "./OutputFiles/sides_%g.txt", (double)
        rightSideSize);
    //fpRightSides = fopen(rightSideFilename, "r");
    if((fpRightSides = fopen(rightSideFilename, "r")) == NULL)
    {
        printf("Can't open the file %s\n", rightSideFilename);
        exit(1);
    }

    for(j = 0; j < numRightSides ; j++)
    {
        /// Read the right side
        fread(&tempRightSide, sideStructSize, 1, fpRightSides);
```

```
/// Combine left and right sides
tempSide.numV = sideSize;
/// reset the adjacency matrix
for(l = 0 ; l <= sideSize+1 ; l++)
    for(m = 0 ; m <= sideSize+1 ; m++)
        tempSide.adjMat[l][m] = 0;

/// Copy the left adjacency matrix to the left
for(l = 0 ; l <= leftSideSize+1 ; l++)
    for(m = 0 ; m <= leftSideSize+1 ; m++)
        tempSide.adjMat[l][m] = tempLeftSide.adjMat[l][m];

/// Copy the right adjacency matrix to the right
for(l = 0 ; l <= rightSideSize+1 ; l++)
    for(m = 0 ; m <= rightSideSize+1 ; m++)
        tempSide.adjMat[l + leftSideSize + 1][m + leftSideSize +1]
            = tempRightSide.adjMat[l][m];

/// Add the incoming and outgoing edges incident to vertex at
    leftSideSize+1
for(cntr = 3*last ; cntr < 4 ; cntr++)
{
    if( (cntr == 0) || (cntr == 1) )
        tempSide.adjMat[0][leftSideSize+1] = 1;
    else if( (cntr == 2) || (cntr == 3) )
        tempSide.adjMat[0][leftSideSize+1] = 1;

    if( (cntr == 0) || (cntr == 2) )
        tempSide.adjMat[leftSideSize+1][sideSize+1] = 1;
    else if( (cntr == 1) || (cntr == 3) )
```

```
                tempSide.adjMat[leftSideSize+1][sideSize+1] = 1;

            /// Store the side
            tempSide.index = numPlanarSides;
            fwrite(&tempSide, sideStructSize, 1, fpSides);
            if(numPlanarSides%500 == 0)
                printf("%lld th planar sides of size %d has been
                    generated.\n", numPlanarSides, sideSize);
            numPlanarSides++;
        }//for(cntr) loop ends

    }//for(j) loop ends
    fclose(fpRightSides);
}//for(i) loop ends
fclose(fpLeftSides);
return numPlanarSides;
}


long long int generateGroupsOfSize(int groupSize)
{
    long long int i, j, numGroups = 0;
    int numPaths, maxnumPaths = 0;

    group tempUpperSide, tempLowerSide, tempGroup;
    int sideStructSize = sizeof(tempUpperSide);
    long long int numPlanarSides = numSidesOfSize[groupSize];

    /// Opening the file "./OutputFiles/sides_<sideSize>.txt" to read the
        upper sides
    FILE *fpUpperSides, *fpLowerSides;
```

```
char sideFileName[100];
sprintf(sideFileName, "./OutputFiles/sides_%g.txt", (double) groupSize);
//fpUpperSides = fopen(sideFileName, "r");
if((fpUpperSides = fopen(sideFileName, "r")) == NULL)
{
    printf("Can't open the file %s\n", sideFileName);
    exit(1);
}

groupWithMaxNumPathsCounter = 0;

for(i = 0 ; i < numPlanarSides ; i++)
{
    fread(&tempUpperSide, sideStructSize, 1, fpUpperSides);
    if(i%100 == 0)
        printf("Upper side is (%lld/%lld), with so far maxnumPaths is
            %d.\n", tempUpperSide.index, numPlanarSides-1, maxnumPaths);

    /// Opening the file "./OutputFiles/sides_<sideSize>.txt" to read the
        lower sides
    //fpLowerSides = fopen(sideFileName, "r");
    if((fpLowerSides = fopen(sideFileName, "r")) == NULL)
    {
        printf("Can't open the file %s\n", sideFileName);
        exit(1);
    }

    for(j = 0 ; j < i ; j++)
        fread(&tempLowerSide, sideStructSize, 1, fpLowerSides);

    for(j = i ; j < numPlanarSides ; j++)
```

```
{
    fread(&tempLowerSide, sideStructSize, 1, fpLowerSides);
    //printf("Upper and lower sides are (%lld,%lld) of %lld, with so
        far maxnumPaths is %d\n", tempUpperSide.index,
        tempLowerSide.index, numPlanarSides-1, maxnumPaths);

    if(checkCompatibility(tempUpperSide, tempLowerSide) == 1)
    {
        tempGroup = createTempGroup(tempUpperSide, tempLowerSide);
        tempGroup.index = numGroups;

        /// calculates total number of paths in tempGroup
        numPaths = computeNumPaths(tempGroup);

        if(maxnumPaths < numPaths)
        {
            maxnumPaths = numPaths;
            groupWithMaxNumPathsCounter = 0;
            groupWithMaxNumPaths[groupWithMaxNumPathsCounter] =
                tempGroup;
            groupWithMaxNumPathsCounter++;
        }
        else if(maxnumPaths == numPaths)
        {
            groupWithMaxNumPaths[groupWithMaxNumPathsCounter] =
                tempGroup;
            groupWithMaxNumPathsCounter++;
        }
        numGroups++;
    }//if(checkCompatibility) ends
```

```
    /// reverse the lower side around Y axis
    tempLowerSide = reverseSideWithYAxis(tempLowerSide);

    if(checkCompatibility(tempUpperSide, tempLowerSide) == 1)
    {
        tempGroup = createTempGroup(tempUpperSide, tempLowerSide);
        tempGroup.index = numGroups;

        /// calculates total number of paths in tempGroup
        numPaths = computeNumPaths(tempGroup);

        if(maxnumPaths < numPaths)
        {
            maxnumPaths = numPaths;
            groupWithMaxNumPathsCounter = 0;
            groupWithMaxNumPaths[groupWithMaxNumPathsCounter] =
                tempGroup;
            groupWithMaxNumPathsCounter++;
        }
        else if(maxnumPaths == numPaths)
        {
            groupWithMaxNumPaths[groupWithMaxNumPathsCounter] =
                tempGroup;
            groupWithMaxNumPathsCounter++;
        }
        numGroups++;
    }//if(checkCompatibility) ends

}//for(j) for lowerside ends

fclose(fpLowerSides);
```

```
    }//for(i) for upperside ends

    fclose(fpUpperSides);
    maxNumPathsOfGroupsOfSizen = maxnumPaths;
    printf("Maximum number of patterns in a group of size %d is %d.\n",
        groupSize, maxnumPaths);
    printf("There are total %lld groups of size %d.\n", numGroups, groupSize);

    return numGroups;
}



/**
  * Input 1: tempUpperSide (type: group).
  * Input 2: tempLowerSide (type: group).
  * Output: If both sides have no common inner edge means they are compatible
     returns 1,
  * otherwise returns 0.
  */
int checkCompatibility(group tempUpperSide, group tempLowerSide)
{
    int l, m, status = 1, groupSize = tempUpperSide.numV;

    for(l = 1 ; l <= groupSize+1 ; l++)
        for(m = l+2 ; m <= groupSize ; m++)
            if( (tempUpperSide.adjMat[l][m] == 1) &&
                (tempLowerSide.adjMat[l][m] == 1) )
                status = 0;

    return status;
}
```

```
/// returns a group generated from two sides
group createTempGroup(group tempUpperSide, group tempLowerSide)
{
    int l, m;
    group tempGroup;

    tempGroup.numV = tempUpperSide.numV;
    for(l = 0 ; l <= tempGroup.numV+1 ; l++)
        for(m = 0 ; m <= tempGroup.numV+1 ; m++)
            tempGroup.adjMat[l][m] = 0;

    for(l = 0 ; l <= tempGroup.numV ; l++)
        tempGroup.adjMat[l][l+1] = 1;

    tempGroup.adjMat[0][tempGroup.numV+1] = 1;
    for(m = 2 ; m <= tempGroup.numV ; m++)
    {
        if( (tempUpperSide.adjMat[0][m] == 1) && (tempLowerSide.adjMat[0][m]
            == 0) )
                tempGroup.adjMat[0][m] = 1;
        if( (tempUpperSide.adjMat[0][m] == 0) && (tempLowerSide.adjMat[0][m]
            == 1) )
                tempGroup.adjMat[0][m] = -1;
        if( (tempUpperSide.adjMat[0][m] == 1) && (tempLowerSide.adjMat[0][m]
            == 1) )
                tempGroup.adjMat[0][m] = 2;
    }
    for(l = 1 ; l <= tempGroup.numV-1 ; l++)
    {
```

```
        if( (tempUpperSide.adjMat[l][tempGroup.numV+1] == 1) &&
            (tempLowerSide.adjMat[l][tempGroup.numV+1] == 0) )
                tempGroup.adjMat[l][tempGroup.numV+1] = 1;
        if( (tempUpperSide.adjMat[l][tempGroup.numV+1] == 0) &&
            (tempLowerSide.adjMat[l][tempGroup.numV+1] == 1) )
                tempGroup.adjMat[l][tempGroup.numV+1] = -1;
        if( (tempUpperSide.adjMat[l][tempGroup.numV+1] == 1) &&
            (tempLowerSide.adjMat[l][tempGroup.numV+1] == 1) )
                tempGroup.adjMat[l][tempGroup.numV+1] = 2;
    }
    for(l = 1 ; l <= tempGroup.numV ; l++)
        for(m = l+2 ; m <= tempGroup.numV+1 ; m++)
        {
            if( (tempUpperSide.adjMat[l][m] == 1) &&
                (tempLowerSide.adjMat[l][m] == 0) )
                tempGroup.adjMat[l][m] = 1;
            if( (tempUpperSide.adjMat[l][m] == 0) &&
                (tempLowerSide.adjMat[l][m] == 1) )
                tempGroup.adjMat[l][m] = -1;
        }

    return(tempGroup);
}


/// calculates total number of paths in tempGroup
int computeNumPaths(group tempGroup)
{
        int numVisited[MAXN];
        int j, k;
```

```
        numVisited[0] = 1;
        for(j = 1 ; j <= tempGroup.numV+1 ; j++)
            numVisited[j] = 0;

        for(j = 0 ; j <= tempGroup.numV ; j++)
            for(k = j+1 ; k <= tempGroup.numV+1 ; k++)
                if(tempGroup.adjMat[j][k] != 0)
                    numVisited[k] += numVisited[j];

        return(numVisited[tempGroup.numV+1]);
}


group reverseSideWithYAxis(group tempSide)
{
    int l, m;
    group reverseTempSide;
    reverseTempSide.numV = tempSide.numV;
    /// reverse the adjacency matrix
    for(l = 0 ; l <= tempSide.numV+1 ; l++)
        for(m = 0 ; m <= tempSide.numV+1 ; m++)
            reverseTempSide.adjMat[l][m] =
                tempSide.adjMat[tempSide.numV+1-m][tempSide.numV+1-l];

    return reverseTempSide;
}


void drawMaxGroups(int groupSize)
{
    char textFilename[100], latexFilename[100], timebuff[100],
```

```
    systemCommand[100];
FILE *fptext, *fplatex;
int i;
group tempGroup;

/// Get current time of the experiment
time_t now = time (0);
strftime (timebuff, 100, "\\texttt{%H:%M:%S} on \\texttt{%m-%d-%Y}",
    localtime (&now));

sprintf(latexFilename, "./OutputFiles/Max_Groups_latex_%g.tex", (double)
    groupSize);
//fplatex = fopen(latexFilename, "w");
if((fplatex = fopen(latexFilename, "w")) == NULL)
{
    printf("Can't open the file %s.\n", latexFilename);
    exit(1);
}
fprintf(fplatex, "\\documentclass[12pt]{article} \n");
fprintf(fplatex, "\\usepackage{tikz} \n");
fprintf(fplatex, "\\usepackage[landscape]{geometry} \n");
fprintf(fplatex, "\\begin{document} \n");
fprintf(fplatex, "The number of vertices is {\\color{red} $%d$}.\\\\ \n",
    groupSize);
fprintf(fplatex, "\\hrule \n\\vspace{2mm} \n");

sprintf(textFilename, "./OutputFiles/Max_Groups_text_%g.txt", (double)
    groupSize);
//fptext = fopen(textFilename, "w");
if((fptext = fopen(textFilename, "w")) == NULL)
{
```

```
        printf("Can't open the file %s.\n", textFilename);
        exit(1);
    }

    for(i = 0 ; i < groupWithMaxNumPathsCounter ; i++)
    {
        tempGroup = groupWithMaxNumPaths[i];
        drawGraph(fplatex, tempGroup);
        writePaths(fplatex, tempGroup);
        fprintf(fplatex, "\\hrule \n\\vspace{2mm} \n");
        printGraph(fptext, tempGroup);
    }

    fprintf(fplatex,"File generated at %s.\\\\ \n", timebuff);
    fprintf(fplatex, "\\end{document} \n");
    fclose(fplatex);
    fclose(fptext);

    sprintf(systemCommand, "pdflatex -output-directory=./OutputFiles
        ./OutputFiles/Max_Groups_latex_%g.tex > log", (double) groupSize);
    system(systemCommand);
    sprintf(systemCommand, "gnome-open ./OutputFiles/Max_Groups_latex_%g.pdf",
        (double) groupSize);
    system(systemCommand);
}


/// draws the tempGroup in latex file pointed by FILE pointer fp
void drawGraph(FILE *fp , group tempGroup)
{
    int j,l,m;
```

```
double r;
double leftBoundary, rightBoundary, upBoundary, downBoundary;

leftBoundary = 1 - 0.2;
rightBoundary = tempGroup.numV + 0.2;
upBoundary = ( tempGroup.numV - 1 ) / 2.0 + 0.2;
downBoundary = - ( ( tempGroup.numV - 1 ) / 2.0 + 0.5) ;

fprintf( fp ,"\\begin{tikzpicture} \n");

fprintf( fp ,"\\draw [white] [thick] (%f,%f) -- (%f,%f); \n",
    leftBoundary, upBoundary, rightBoundary, upBoundary);
fprintf( fp ,"\\draw [white] [thick] (%f,%f) -- (%f,%f); \n",
    rightBoundary, upBoundary, rightBoundary, downBoundary);
fprintf( fp ,"\\draw [white] [thick] (%f,%f) -- (%f,%f); \n",
    rightBoundary, downBoundary, leftBoundary, downBoundary);
fprintf( fp ,"\\draw [white] [thick] (%f,%f) -- (%f,%f); \n",
    leftBoundary, downBoundary, leftBoundary, upBoundary);


fprintf( fp ,"\\draw [black] [thick] (1,0) -- (%d,0); \n", tempGroup.numV);
for(j = 1 ; j<= tempGroup.numV ; j++)
    fprintf( fp ,"\\draw [fill] (%d,0) circle [radius=0.05]; \n", j);
for(j = 1 ; j<= tempGroup.numV ; j++)
    fprintf( fp ,"\\node at (%d,-.25) {$u_{%d}$};\n", j, j);


for(m = 2 ; m <= tempGroup.numV ; m++)
{
    r = ( m - 1 ) / 2.0;
    if(tempGroup.adjMat[0][m] == 1)
```

```
        fprintf( fp ,"\\draw [black] [thick] [latex-] (%d,0) to
            [out=90,in=0] (1,%f); \n", m, r);
    else if(tempGroup.adjMat[0][m] == -1)
        fprintf( fp ,"\\draw [black] [thick] [latex-] (%d,0) to
            [out=270,in=0] (1,%f); \n", m, -r);
    else if(tempGroup.adjMat[0][m] == 2)
    {
        fprintf( fp ,"\\draw [black] [thick] [latex-] (%d,0) to
            [out=90,in=0] (1,%f); \n", m, r);
        fprintf( fp ,"\\draw [black] [thick] [latex-] (%d,0) to
            [out=270,in=0] (1,%f); \n", m, -r);
    }
}

for(l = 1 ; l <= tempGroup.numV-1 ; l++)
{
    r = ( tempGroup.numV - l ) / 2.0;
    if(tempGroup.adjMat[l][tempGroup.numV+1] == 1)
        fprintf( fp ,"\\draw [black] [thick] [-latex] (%d,0) to
            [out=90,in=180] (%d,%f); \n", l, tempGroup.numV, r);
    else if(tempGroup.adjMat[l][tempGroup.numV+1] == -1)
        fprintf( fp ,"\\draw [black] [thick] [-latex] (%d,0) to
            [out=270,in=180] (%d,%f); \n", l, tempGroup.numV, -r);
    else if(tempGroup.adjMat[l][tempGroup.numV+1] == 2)
    {
        fprintf( fp ,"\\draw [black] [thick] [-latex] (%d,0) to
            [out=90,in=180] (%d,%f); \n", l, tempGroup.numV, r);
        fprintf( fp ,"\\draw [black] [thick] [-latex] (%d,0) to
            [out=270,in=180] (%d,%f); \n", l, tempGroup.numV, -r);
    }
}
```

```
    for(l = 1 ; l <= tempGroup.numV-1 ; l++)
        for(m = l+2 ; m <= tempGroup.numV ; m++)
        {
            if(tempGroup.adjMat[l][m] == 1)
                fprintf( fp ,"\\draw [black] [thick] [-latex] (%d,0) to
                    [out=90,in=90] (%d,0); \n", l, m);
            else if(tempGroup.adjMat[l][m] == -1)
                fprintf( fp ,"\\draw [black] [thick] [-latex] (%d,0) to
                    [out=270,in=270] (%d,0); \n", l, m);
        }

    fprintf( fp ,"\\end{tikzpicture} \n\n");
}


/// writes all the paths of the tempGroup in the FILE pointed by pointer fp
void writePaths(FILE *fp, group tempGroup)
{
    int i, j, k, status;
    int temp[20];
    int prev, next, pathCount = 1;
    int t = pow(2, tempGroup.numV);

    fprintf( fp, "The paths are\\\\\n");
    fprintf( fp, "{\\color{red} $1$}: $\\emptyset$ ");

    for(i = t-1 ; i >= 1 ; i--)
    {
        status = 1;
        for(j = tempGroup.numV-1 ; j >= 0 ; j--)
```

```
{
    k = i >> j;
    temp[tempGroup.numV-j] = (k & 1);
}

prev = 0;
j = 1;
while(j <= tempGroup.numV)
{
    if(temp[j] == 1)
    {
        next = j;
        if(tempGroup.adjMat[prev][next] != 0)
            prev = next;
        else
            status = 0;
    }
    j++;
}

if(tempGroup.adjMat[prev][tempGroup.numV+1] == 0)
    status = 0;

if(status == 1)
{
    pathCount++;
    fprintf( fp, "\\hspace{5mm} ");
    fprintf( fp, "{\\color{red} $%d$}: ", pathCount);

    for(j = 1 ; j <= tempGroup.numV ; j++)
        if(temp[j] == 1)
```

```
                fprintf( fp, "%d ", j);
        }
    }

    fprintf( fp ,"\\\\ \n");
}


/// Prints the tempGroup in a text file pointed by FILE pointer fp
void printGraph(FILE *fp , group tempGroup)
{
    int l , m;

    fprintf( fp, "    ");
    for(l = 0 ; l <= tempGroup.numV+1 ; l++)
        fprintf( fp, "v%d, ", l);
    fprintf( fp, "\n");
    fprintf( fp, "    ");
    for(l = 0 ; l <= tempGroup.numV+1 ; l++)
        fprintf( fp, "-----");
    fprintf( fp, "\n");

    for(l = 0 ; l <= tempGroup.numV+1 ; l++)
    {
        fprintf( fp, "v%d | ", l);
        for(m = 0 ; m <= tempGroup.numV+1 ; m++)
            fprintf( fp, "%d, ", tempGroup.adjMat[l][m]);
        fprintf( fp, "\n");
    }
}
```

```
void checkSides(int sideSize)
{
    group tempSide;
    FILE *fp;
    char sideFileName[100];
    sprintf(sideFileName, "./OutputFiles/sides_%g.txt", (double) sideSize);
    fp = fopen(sideFileName, "r");
    int sideStructSize = sizeof(tempSide);
    long long int i, numSides = numSidesOfSize[sideSize];

    for(i = 0; i < numSides ; i++)
    {
        fread(&tempSide, sideStructSize, 1, fp);
    }
    fclose(fp);
    printf("checked all sides of size %d.\n", sideSize);
}
```

Ritankar Mandal

Email: rmandal@uwm.edu

Research interests

Combinatorial and Computational Geometry, Graph Theory and Combinatorics, Approximation Algorithms, Randomized Algorithms.

Education

University of Wisconsin-Milwaukee
PhD in Computer Science — 2013 – Present

Indian Statistical Institute
Master of Technology in Computer Science — 2011 – 2013

West Bengal University of Technology
Bachelor of Technology in Computer Science — 2007 – 2011

Awards and scholarships

CEAS Dean's Scholarship (UWM) — 2014
Chancellor's Graduate Student Award (UWM) — 2013

Journal Publications

New lower bounds for the number of pseudoline arrangements
A. Dumitrescu, R. Mandal.
J. Comput. Geom. 11(1): 60-92 (2020).

Monotone paths in geometric triangulations
A. Dumitrescu, R. Mandal, and Cs. D. Tóth.
Theory Comput. Syst. 62(6): 1490-1524 (2018).

On representing a simple polygon perceivable to a blind person
S. Banerjee, B. B. Bhattacharya, B. Bhattacharya, A. Biswas, S. Das, R. Mandal, and S. Roy.
Inf. Process. Lett. 120: 1–5 (2017)

Conference Proceedings

New lower bounds for the number of pseudoline arrangements
A. Dumitrescu and R. Mandal.
Proceedings of the 30th ACM-SIAM Symposium on Discrete Algorithms (SODA 2019), San Diego, January 2019.

Monotone paths in geometric triangulations
A. Dumitrescu, R. Mandal, and Cs. D. Tóth.
Proceedings of the 27th International Workshop on Combinatorial Algorithms, (IWOCA 2016), Helsinki, Finland, August 2016, LNCS 9843.

Research experience

Pseudoline arrangements
Advisor: Professor Adrian Dumitrescu (UWM)

Let B_n be the number of nonisomorphic arrangements of n pseudolines. We show that $B_n \geq 2^{cn^2 - O(n \log n)}$ for some constant $c > 0.2083$. Further, our constructions are likely to spur new developments and improved lower bounds for related problems, such as in topological graph drawings. The work is available here.

Monotone paths
Advisor: Professor Adrian Dumitrescu (UWM)
A directed path in a graph is monotone in direction of **u** if every edge in the path has a positive inner product with **u**. A path is monotone if it is monotone in some direction. We prove that the (maximum) number of monotone paths in a geometric triangulation of n points in the plane is $O(1.7864^n)$. The journal paper is available here.

Polygon reconstruction from point sets
Advisor: Professor B. B. Bhattacharya (ISI)
Algorithm for generating points on an arrangement of axis-parallel polygons to reconstruct each polygon separately using nearest point rule. The journal paper is available here.

Teaching experience

Instructor, Department of Computer Science (UWM) Fall 17, Spring 20, Spring 21
CS 317: Discrete Information Structures
Logic, Proof Techniques, Set Theory, Functions, Combinatorics, Probability, and Graph Theory.

Teaching assistant, Department of Computer Science (UWM)
CS 250: Introductory Computer Programming
Problem solving using an Object-oriented Programming language (JAVA), including control structures, functions, arrays, vectors, and pre-defined objects.

Industry experience

Strand Life Sciences India
Internship Summer 2012
Implementation three modules in NGS Genespring for statistical modeling and visualization of large multivariate data.

Skills

Programming
Proficient in: C.
Familiar with: JAVA, R.